THE REPORT OF STUDY RESULT BY SUBSIDY

助 成 研 究 成 果 報 告 書

第27回

The Watanabe Foundation
公益財団法人 渡邉財団

助 成 研 究 成 果

報 告 書

第27回

（研究期間：令和3年4月1日～令和4年3月31日）

30周年記念特別助成2018

（研究期間：平成31年4月1日～令和4年3月31日）

公益財団法人 渡邉財団

目　　次

巻　頭　言

公益財団法人 渡邉財団

理事長　小　谷　　誠

今から45年程前に私は米国のマサチューセッツ工科大学（MIT）に留学して、人間の身体から発生する微弱な磁気を計測して、病気の診断に役立てようとする研究を2年間行い、帰国後も生体磁気計測の研究を続けてきた。

人間の心臓や脳からは微弱な磁気が発生していることは以前から推定されていたが、この微弱な磁気を計測できる磁束計がなかった。ところが、1970年代に超伝導技術を応用した超高感度のSQUID磁束計が米国立研究所とMITの共同研究で開発された。

MITではこのSQUID磁束計を用いて、心臓から発生する磁気の計測に成功し、更に心臓磁気の千分の1程度の脳から発生する磁気計測に挑戦している頃、私はMITに留学した。

私がMITに留学した頃、MITの研究所では大変なことが起っていた。それは、米国の著名な医師が、「MITのグループは心臓や脳の神経活動に伴って発生する磁気を計測していると言っているが、それは間違いである。彼らの計測している磁気は血液の中の鉄分が地磁気を乱している磁気を計測しているのにすぎない」と新聞で批判された。その結果、MITの生体磁気計測の研究への米国の公的研究費は大幅に削減されていた。

私は、この医師の意見は理にかなっていると思って、十数名の健常者の血液を採取してSQUID磁束計で計測したが、血液は全く磁性がないことがわかった。

その理由は、鉄自体は常に磁性を持っているが、鉄が酸素と結合する仕方によって強い磁性を持ったり、全く磁性を持たなくなる。血液中の鉄は全く磁性を持たないように酸素と結合しているのである。

人間の祖先がこの世に登場し、立って歩き、言葉を交わすようになったのは、今から200万年程前と云われている。この間に、地磁気の大きさと方向が10回ほど変わっている。このように地磁気の大きさや方向が大きく変わる環境の中で人間は進化してきたので、地磁気の影響はあまり受けないように人体はできている。

ところが、人間が電気を使うようになったのは、僅か200年ほど前からである。そのため、人体は電気に対しては防衛能力が進化しておらず、大変敏感に反応する。例えば、心臓の表面に数ボルトの電圧を加えると心臓は正常に働かなくなる。ところが、外部から心臓に磁気を加えて心臓を止めることは大変困難である。

このような人体の特徴から電気治療器は即効性があるが、取り扱いを間違えると大変危険である。それに対して、磁気治療器は危険性は少ないが、時間をかけてじっくり治療する必要性があると思われる。

本財団は生体磁気現象を通して国民の医療と健康に貢献することを目的として、学術研究を助成し、講演会を開催するなど、社会に向けた活動をしている。しかし、磁気の作用は、基礎的現象から始まり、体内の複雑な相互作用への関与を通して生じるものであり、短期間の実験試行ではなく、長期間腰を落ち着けて追求して初めて明らかにされることが多い。

いっぽう昨今の学界においては、短期間に成果を挙げ、学位や業績に結びつけようとする雰囲気が強く、原因結果の関係が明白な現象や、客観的に説明できる現象に関心が集中するように見受けられる。これに対して本財団は、性急に成果を求めようとするよりも、長期間にわたる努力を覚悟して特定の問題に取り組む学究の徒を支援したいと考えている。

この報告書は、令和2年度に助成した研究の報告書を、原文のままにまとめたものである。基礎面から実際の応用にいたる広い範囲の研究が含まれているが、いずれもこの領域に新しい道を拓くことを目指している。この報告書が契機になって、志を同じくする研究者の間に連絡が始まり、磁気健康科学の発展に貢献することを期待している。

光線力学療法における磁場効果

Magnetic Field Effects on Photodynamic Therapy

米村弘明
Hiroaki Yonemura

崇城大学工学部，〒860-0082　熊本県熊本市西区池田 4-22-1
Faculty of Engineering, Sojo University
4-22-1 Ikeda, Nishi-ku, Kumamoto 860-0082, Japan

Abstract

The magnetic field effects on the generation of singlet oxygen ($^1O_2^*$) in photodynamic therapy (PDT type II) using fullerene derivatives (such as C_{70}) as photosensitizers were investigated in CCl_4 solution of fullerene derivatives. $^1O_2^*$ generation was evaluated by directly observing the phosphorescence of $^1O_2^*$ obtained around 1275 nm due to the photoexcitation of fullerene derivatives. The phosphorescence intensity of $^1O_2^*$ varied with magnetic fields as compared to that without a magnetic field. The magnetic field effects on the generation of $^1O_2^*$ due to PDT type II were observed for the first time. The magnetic field effects can be explained in terms of triplet-triplet pair mechanism.

Keywords: photodynamic therapy, singlet oxygen, phosphorescence, magnetic field effect, triplet-triplet pair

1. 目的

光線力学療法（PDT）は，光励起によって活性酸素種を生成する薬物（Sen：図 1）を投与し，がんのような体内の有害組織および感染症，皮膚病などの疾病を治療する方法である．光増感剤によって最初に生成される活性酸素種が一重項酸素（$^1O_2^*$）であるタイプⅡが現代の PDT の主流である（図 1）．

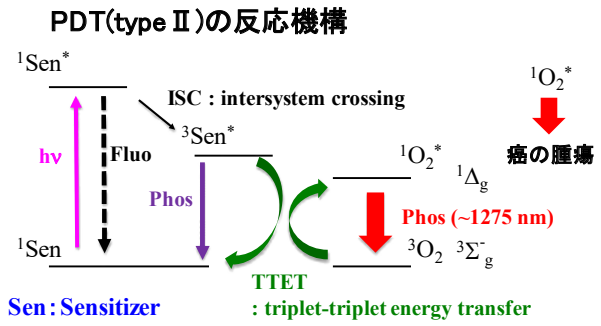

図 1 Sen による PDT（タイプⅡ）の反応機構

我々はタイプⅡの治療機構において最も重要な役割を果たす$^1O_2^*$に注目した．ここで，$^1O_2^*$を最も直接的に観測する方法は，$^1O_2^*$の発光（りん光）を観測する手段である．しかしながら，$^1O_2^*$のりん光は近赤外光領域である 1270 nm 付近に発光ピークがあり，かつ非常に弱いために検出が困難である．また，我々は磁場に影響を受ける中間体（ラジカルやラジカル対，３重項や３重項 - ３重項対）を経る光反応に及ぼす磁場の影響に関する基礎研究や，これらの磁場効果を活用した光機能材料の展開という応用研究も行ってきた．

すでに，我々は本研究と関連する PDT についての研究結果として，金属ナノ粒子の光特性である局在表面プラズモン共鳴（LSPR）（共鳴する波長の光を照射した時に，ナノ粒子の周りに照射した光より強い光が発生する現象）を活用して研究を行った．その研究成果として，光増感剤としてロ

ーズベンガル（有機色素）を用いて，PDT に及ぼす銀ナノ粒子（AgNP）の LSPR 効果を検討した結果として，$^1O_2^*$の生成が効率的に起こっている事を見出した．

また，最近，我々は反応中間体を生じる PDT と類似の光反応である光誘起電子移動反応（光によって物質間で電子が移動する反応）や光アップコンバージョン（エネルギーの低い長波長の光をエネルギーの高い短波長の光に変換する現象）や光ダウンコンバージョンである励起子 1 重項分裂（エネルギーの高い短波長の光をエネルギーの低い長波長の光に変換し励起状態にある物質を増加させる現象）に及ぼす磁場効果を報告している．[1),2)]

そこで, 本研究では PDT の反応機構によって発生する活性酸素種（$^1O_2^*$）の発生効率に対する磁場効果を検討する．

2. 方法

PDT のタイプⅡ機構における光増感剤としてフラーレン誘導体（C_{70} 等）を用い，フラーレン誘導体の四塩化炭素（CCl_4）及び二硫化炭素（CS_2）溶液（20 μM）を調整した．サンプル溶液を電磁石中に置き, 外部磁場強度を変化させながら, CW DPSS レーザー(450 nm)を励起光として用いて，光ファイバーを介して近赤外光領域で観測される 1275 nm 付近をピークとする$^1O_2^*$のりん光によって$^1O_2^*$の発生を評価した．また，$^1O_2^*$の発生量に関してはりん光の強度によって評価を行った．

3. 結果

C_{70} の CCl_4 溶液を可視光（450 nm）で励起すると，近赤外光領域において，1275 nm 付近に$^1O_2^*$のりん光が観測された. また, この発光（1275 nm）の励起スペクトルは C_{70} の吸収と対応した．従って，C_{70} を光増感剤として PDT のタイプⅡ機構によって$^1O_2^*$が発生している事がわかった．次に，セルを電磁石中に置き, 450 nm のレーザーによって光励起すると，近赤外光領域において，同様に 1275nm 付近に$^1O_2^*$のりん光が観測された．さらに，磁場印加（0.8 T）すると$^1O_2^*$のりん光強度が増加した（図 2）．この磁場応答は可逆的であった．以上より，PDT のタイプⅡ機構によって発生する

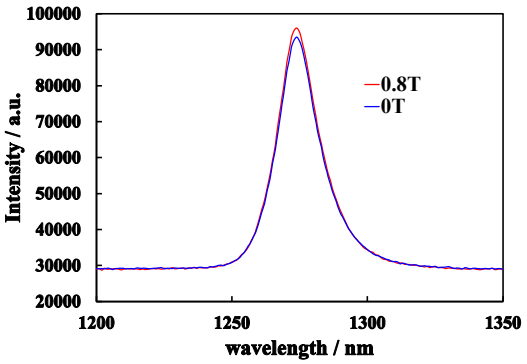

図 2 $^1O_2^*$のりん光スペクトルに対する磁場効果（λ_{ex}=450 nm）

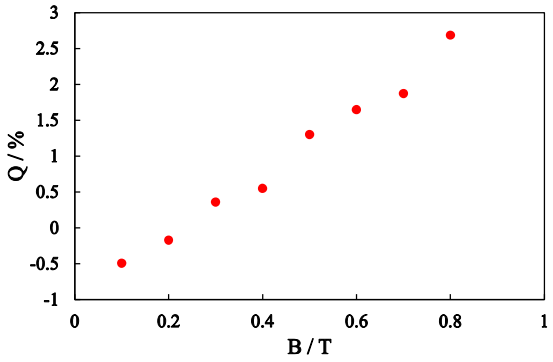

図 3 Q 値の磁場強度依存性

$^1O_2^*$が磁場印加によって変化することを初めて観測した．

次に，磁場強度を変化させながら，$^1O_2^*$のりん光スペクトルを測定した．磁場強度を増加させるにつれ，$^1O_2^*$のりん光強度は変化した．式（1）で表す Q 値によって，磁場効果を評価した．

$$Q(\%) = \frac{I(B) - I(0)}{I(0)} \times 100 \qquad (1).$$

$I(B)$:磁場強度（B T）の 1275 nm における$^1O_2^*$のりん光強度，$I(0)$:磁場強度（0 T）の 1275 nm における $^1O_2^*$のりん光強度を示す．

Q 値は低磁場領域（B = 0.1, 0.2 T）では負になり，その後高磁場領域（0.3 ≦ B ≦ 0.8 T）では Q 値は磁場強度が増加するにつれて増加した（図 3）．

C_{70} の他にフラーレン誘導体（C_{70}PCBM，C_{60},

C_{60}PCBM)についても同様にPDTのタイプⅡ機構によって発生する $^1O_2^*$のりん光に対する磁場効果を観測した.

4. 結果

この磁場効果は，PDT のタイプII機構における三重項-三重項エネルギー移動（TTET）反応で $^3Sen^*$（$^3C_{70}^*$）から $^1O_2^*$が生成する際の中間状態であるT-T 対が磁場の影響を受けるため観測されたと考えられる（式（2））.

$$^3C_{70}^*+{}^3O_2 \rightarrow {}^l(TT)\rightarrow {}^1C_{70}+{}^1O_2^* \quad (l = 1, 3, 5) \quad (2).$$

言い換えれば，低磁場領域で観測される負の磁場効果は hfc 機構によって，高磁場領域で観測される正の磁場効果はT-T 対機構によって観測されたと考えられる.

今後は，フラーレン誘導体以外の光増感剤についても同様な磁場効果の検討を行うと共，様々の溶媒や反応場を用いて同様な磁場効果の検討を行うつもりである．さらに，実際に癌に対するPDT 機構に対する磁場効果に展開する予定である.

謝辞

本研究は公益財団法人渡邉財団の助成を受けて実施したものであり，厚く御礼申し上げます.

本論文の内容は 202 年 11 月 15 日 - 17 日に稲盛会館（鹿児島大学郡元キャンパス），オンライン(ハイブリッド開催)で開催された『第 15 回日本磁気科学会』で報告したものを一部含むものである.

参考文献

1) Y. Noda, F. Shibata, S. Fukuda, G. S. Y. Lee, H. Sakaguchi, H. Yonemura, *Jpn. J. Appl. Phys.*, **59**, SDDB04 (2020).
2) H. Yonemura, D. Aira, N. Asakura, K. Ezoe, H. Sakaguchi, *Jpn. J. Appl. Phys.*, **59**, SDDB03 (2020).

超低周波変動する超微弱磁場が誘導するマイトファジーによる病態制御

Amelioration of pathological states by mitophagy induced by extremely low frequency fluctuation of extremely weak magnetic fields

大野欽司*
Kinji Ohno*

*名古屋大学医学系研究科神経遺伝情報学，〒466-8550　名古屋市昭和区鶴舞町 65
*Neurogenetics, Graduate School of Medicine, Nagoya University
65 Tsurumai-cho, Showa-ku, Nagoya 466-8550 Japan

Abstract

The molecular mechanisms of the effects of weak magnetic fields have not been well dissected. We found that extremely low frequency fluctuation (1-8 Hz) of extremely weak magnetic field (100 mG) (ELF-WMF) provokes the mitochondrial quality-assurance system, mitophagy, and reduces the amount of mitochondrial to two thirds of that before stimulation. The mitochondrial membrane potential was similarly reduced. ELF-WMF later induces mitochondrial neogenesis, which increases the amount of mitochondria and the mitochondrial membrane potential. Exposure of ELF-WMF to wild-type mice showed increased basal oxygen consumption, increased mitochondrial membrane potential, and increased mitochondrial electron transport complex activities in the liver. The mice showed increased voluntary activities, which, however, were not quantitatively evaluated. We expect that the hormetic effects of ELF-WMF could be applied to human diseases, and the studies are currently under progress.

Keywords: weak magnetic field, mitophagy, mitochondrial neogenesis

1. 目的

日本の地磁気約 460 mG よりも微弱な磁束密度は、現在健康機器や医学研究で多く用いられる千数百 G の磁束密度に比べて 1 万倍以上微弱であり、生活環境中にも多く存在すると思われる。この超微弱な磁気刺激の生体・組織・細胞・細胞内小器官・タンパク質に与える正ならびに負の影響はあまり解明されておらず、その分子作用機構も不明である。本研究の目的は、このような超微弱磁場の生体に対する影響を明らかにすることにある。

2. 方法

8 秒間で 1-8 Hz に漸増する 4 ms・100 mG のパルス磁場がリンゲル液の電気抵抗の温度ヒステリシスを最小化することを見出した [1]。マウス肝臓由来 AML12 培養細胞を用いて ELF-WMF 刺激 3 時間後にミトコンドリア量を最小化する条件を MitoTracker Green を用いて決定した。同時に TMRM を用いてミトコンドリア膜電位を計測した。ELF-WMF の標的を明らかにする目的で AML12 細胞のホモジェネートに 8 分間 ELF-WMF 照射を行いミトコンドリア電子伝達系 I-IV の酵素活性の測定を行なった。さらに電子伝達系 II のサブユニット間の酵素活性を行なった。マイトファジーを確認する目的で PINK1, Parkin, LC3-II をウエスタンブロットにて定量した。加えてミトコンドリア電子-電子伝達系タンパク質 7 種類とミトコンドリア外膜タンパク質 VDAC1 の定量を行なった。ミトコンドリア新生の活性化を確認する目的で PGC-1α,

PPARα, TFAM をウエスタンブロットにて定量した。正常の C57BL/6J マウスを ELF-WMF 環境下で 4 週間飼育し、肝臓の酸素消費量・ミトコンドリア膜電位・ミトコンドリア電子伝達系酵素活性を測定した。

3. 結果

リンゲル液の電気抵抗の温度ヒステリシスを最小化する 8 秒間で 1-8 Hz に漸増する 4 ms・100 mG のパルス磁場(extremely low frequency weak magnetic field, ELF-WMF)[1)]が 3 時間でマウス肝臓由来 AML12 培養細胞のミトコンドリア量を 63%まで低下させることを見出した**(図 1)**。

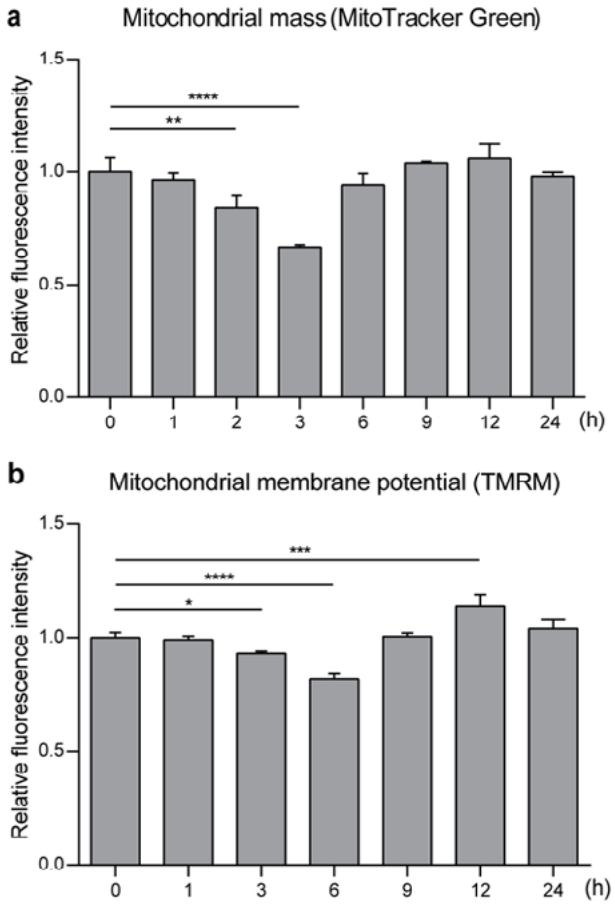

図 1. ELF-WMF は 3 時間で AML12 細胞のミトコンドリア量を低下させ**(a)**、6 時間でミトコンドリア膜電位を低下させる**(b)**。平均と標準偏差を示す($n = 3$)。$^{*}p < 0.05$, $^{**}p < 0.01$, $^{***}p < 0.001$, $^{****}p < 0.0001$ (One-way ANOVA と Dunnett ポストホックテスト)。

ELF-WMF の最適条件を探る目的で 30-3000 mG の磁場強度, 1-16 ms のパルス、各種周波数変動を AML12 細胞に与えミトコンドリア量の現象を測定したところリンゲル液の温度ヒステリシスを最小化する条件がもっとも効果的にミトコンドリア量を減少させた。加えてマウス骨格筋由来 C2C12 細胞・マウス神経由来 Neuro2a 細胞・ヒト iPS 細胞・ヒト腎臓由来 HEK293 細胞・ヒト子宮頸がん由来 HeLa 細胞においても同様の効果を認めた。

AML12 細胞のホモジェネートに 8 分間 ELF-WMF 照射を行いミトコンドリア電子伝達系複合体活性を測定したところ、ELF-WMF はミトコンドリア電子伝達系複合体 II の酵素活性のみを 84%まで低下させた**(図 2)**。電子伝達系 II は 4 つのサブユニット(SDHA, SDHB, SDHC, SDHD)から構成される。(i) SDHA, (ii) SDHA-SDHB, (iii) SHDA-SDHB-SDHC-SDHD, (iii) SHDA-SDHB-SDHC-SDHD-CoQ-CytC の 4 つのサブユニット間の酵素活性測定を行なったところ、ELF-WMF は 8 分間でいずれの酵素活性も 85-95%に低下させた。活性測定の電子受容体として CoQ を用いており CoQ における電子の受け渡しを ELF-WMF は阻害する可能性が示された。

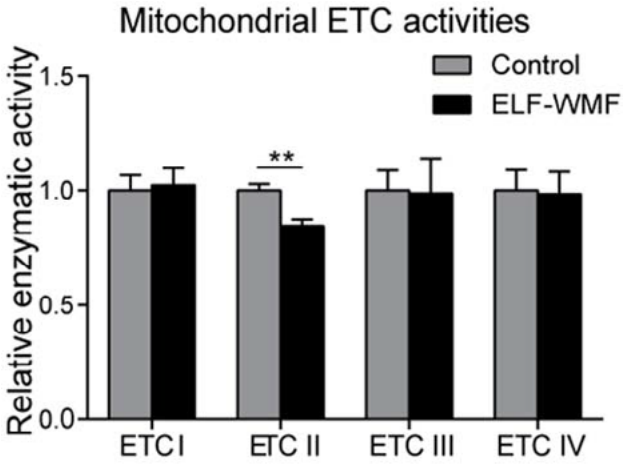

図 2. AML12 細胞ホモジェネートに ELF-WMF を 8 分間照射した後のミトコンドリア電子伝達系酵素活性。平均と標準偏差を示す($n = 3$~6)。$^{**}q < 0.01$ (多重 t 検定)。

AML12 細胞に ELF-WMF 刺激を与えたところ 1.5 時間で PINK1 の発現が上昇し、2 時間で Parkin のミトコンドリアへの誘導がピークになり、2.5 時間で LC3-II の発現が誘導され、マイトファジーの誘導が明らかになった。事実、ELF-WMF 照射 3 時間後に AML12

細胞のミトコンドリア電子電子伝達系タンパク質 7 種類とミトコンドリア外膜タンパク質 VDAC1 が顕著に低下していた。

AML12 細胞に ELF-WMF 暴露 12 時間後には PGC-1α, PPARα, TFAM の発現が誘導されミトコンドリア新生が活性化されることを確認した。

正常 C57BL/6J マウスを ELF-WMF 環境下で 4 週間飼育を行い肝臓の酸素消費量・ミトコンドリア膜電位・ミトコンドリア電子伝達系酵素活性がいずれも有意に上昇することを確認した**(図 3)**。

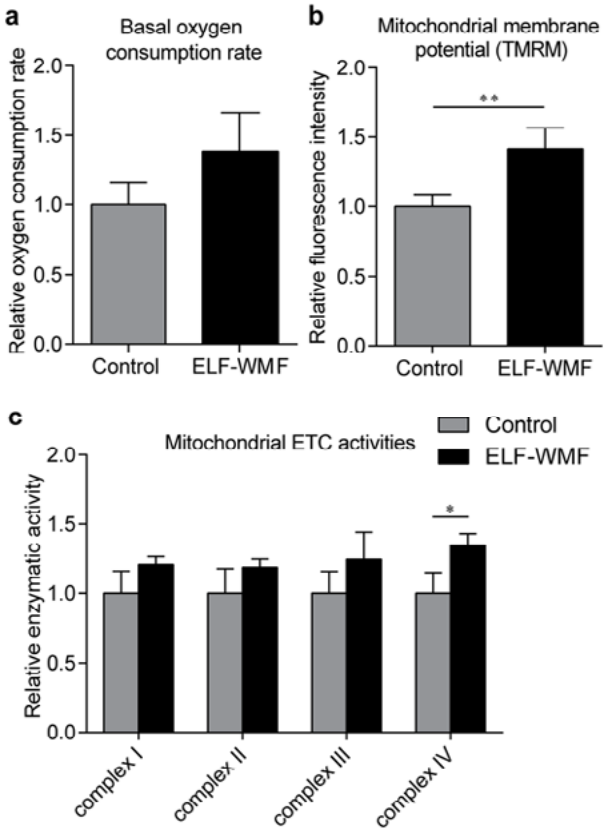

図 3. 正常 C57BL/6J マウスを 4 週間 ELF-WMF 環境下で飼育し、**(a)**肝臓のミトコンドリアの基礎酸素消費量、**(b)**ミトコンドリア膜電位、**(c)**ミトコンドリア電子伝達系酵素活性を測定した。平均と標準偏差を示す($n = 4$)。**(b)** $^{**}p < 0.01$ (t 検定)。**(c)** $^{*}q < 0.05$ (多重 t 検定)。

4. 考察

環境中に存在し、日本の地磁気の 4.5 分の 1 で職業暴露基準[2]の 1/100 の超微弱な磁場が顕著なマイトファジーを誘導することは我々にとっても大きな驚きであり、本研究成果の論文報告を行なった[3]。ELF-WMF のミトコンドリア電子伝達系複合体 II に対する効果はシグナル伝達機構が働かないホモジェネートを用いた実験結果であり、ELF-WMF の直接的な標的がミトコンドリア電子伝達系複合体 II であることを示しており今後量子生物学レベルでの標的の同定を行う。加えて、ELF-WMF によるマイトファジーとミトコンドリア新生はミトコンドリア機能障害を呈する数多くの疾患に対して ELF-WMF が有効であることを示唆しており、現在各種モデル動物・モデル細胞に対する効果を検証している。本研究においてその詳細な分子作用機構を解明するとともに、ミトコンドリア病とパーキンソン病に対する ELF-WMF の効果を実証するとともに病態制御作用機構を明らかにする。

謝辞

本研究をご支援くださいました公益財団法人渡邉財団関係者各位に深く感謝申し上げます。

参考文献

1) Mohri K, Fukushima M: Gradual decreasing characteristics and temperature stability of electric resistivity in water triggered with milligauss AC field. *Ieee Transactions on Magnetics* 38: 3353-3355 (2002).
2) International Commission on Non-Ionizing Radiation P: Guidelines for limiting exposure to time-varying electric and magnetic fields (1 Hz to 100 kHz). *Health Phys* 99: 818-836 (2010).
3) Toda T, Ito M, Takeda JI, Masuda A, Mino H, Hattori N, Mohri K, Ohno K: Extremely low-frequency pulses of faint magnetic field induce mitophagy to rejuvenate mitochondria. *Commun Biol* 5: 453 (2022).

磁場刺激による細胞配向特性を応用した人工骨組織の作製

Fabrication of artificial bone substitute applied to cell orientation characteristics by magnetic stimulation

荒平高章*
Takaaki Arahira*

*九州情報大学経営情報学部，〒818-0117　福岡県太宰府市宰府 6-3-1
*Faculty of Management and Information Sciences, Kyushu Institute of Information Sciences
6-3-1, Saifu, Dazaifu, Fukuoka 818-0117 Japan

Abstract

We developed a magnetic field stimulation device for constructing artificial bone-like tissue in previous Watanabe Foundation. In this study, we fabricated the scaffold material using a 3D printer and fabricated the scaffold material using the molds. The fabricated scaffolds were evaluated by cell experiments to see whether the scaffolds have any effect on cells or not.

Keywords: magnetic stimulus, 3D printer, scaffold, osteoblast

1. はじめに

近年，骨・軟骨再生分野では足場材と細胞による人工組織を生体外で構築し，患部に再生培養骨・軟骨組織を移植する再生療法が臨床応用されている [1),2)]．しかし，未だ生体外での人工組織構築には時間を要するのが現状であり，いかに短期間で人工組織を構築できるかが重要である．また，先行研究において，再生培養骨・軟骨組織移植に関する報告はあるものの，周囲組織の力学特性と同様の組織を構築するには至っておらず，周囲組織との力学的適合性を有する人工組織の構築も大きな課題となっている．これら 2 つの問題を解決するためには，組織工学における 3 要素「足場材」，「細胞」，「成長因子」に対するアプローチが考えられる．特に，足場材の高機能化と細胞の高活性化に関する研究は非常に多くなされており，その一方で「成長因子」に関する研究の歴史は浅い．近年，足場材や細胞に「刺激」を与える研究などが盛んに行われている．

本研究では，この「刺激」に着目した．骨・軟骨細胞を活性化させる刺激としては，圧縮・引張といった力学刺激に対して有用性が示されている．しかし，力学刺激は足場材や細胞に一様に与えることが困難であり，構築した組織の均一性が懸念される．また，力学刺激によって足場材が破壊してしまうことも考えられる．そこで，平成２７年度に貴財団に応募させて頂いた際に，磁場による刺激を提案し，人工骨ー軟骨組織構築のための磁場刺激装置の開発を実施した．その際，磁場刺激が人工骨や人工軟骨を作製する際の骨芽細胞や軟骨細胞を活性化させる結果の他に，骨芽細胞において，磁場の方向に細胞が配向して増殖するという結果が得られた．この磁場に対して配向するという現象は他の研究者による先行研究で神経細胞については報告されているが，骨芽細胞に関しては新たな知見である．この骨芽細胞に関する磁場方向への配向特性を利用して，より配向性のある人工骨組織を作製し，人工骨組織の高機能化を実現させる．

以上より，本稿では，3D プリンターを用いて，足場材の鋳型を作製し，鋳型を用いて足場材の作製を行った．また，作製した足場材に関して細胞

に影響がないかどうかを細胞実験によって評価したので報告する．

2. 方法

2.1 鋳型の作製

3D プリンターダヴィンチ 1.0pro（XYZ プリンティング）を用いて鋳型を作製した．鋳型の大きさは直径約 15mm の円筒で，中央に直径約 2mm の円柱が設置されている（図 1）．

2.2 足場材の作製

作製した鋳型を用いてコラーゲン足場材を凍結乾燥法により作製した [3]．具体的には，コラーゲン溶液を鋳型に填入し，-60℃で凍結後，-50℃で凍結乾燥を行い，グルタルアルデヒド飽和蒸気下で 4 時間化学架橋し，グリシン溶液にてブロッキングを行った．

2.3 鋳型で作製した足場材の毒性評価

鋳型による細胞への影響を検討した．作製した足場材 1 個を 50ml の培地に 24h 浸漬させ，その培地と通常培地の 2 種類を用いて，骨芽細胞様細胞 MC3T3-E1 を 24 ウェルプレートで 24h 培養した．培養後，Cell counting Kit を用いて 450nm の吸光度をプレートリーダで計測した．

2.4 コラーゲン足場材と細胞による磁場刺激実験

鋳型を用いずに作製した柱状のコラーゲン足場材を用いて磁場刺激実験を実施した．磁場刺激装置は自作した装置を用いた [4]．足場材 1 個あたり MC3T3-E1 を 10 万 cell 播種し，一日間前培養をした後，磁場刺激を与えた．刺激条件は，1mT を 30 秒作用させた後，30 分間休止するサイクルを繰り返し実施した．培養 7 日目の細胞数を測定した．

3. 結果および考察

図 2 に鋳型を用いて作製したコラーゲン足場材の画像を示す．鋳型の形状を反映させた足場材となっていた．今回は足場材作製の際に使用した鋳型が細胞へネガティブな影響を与えないかを細胞実験によって確認した．図 3 に 2 次元培養による細胞増殖アッセイによる吸光度の結果を示す．Control は通常培地で培養したもの，Collagen scaffold は足場材を浸漬させた培地で培養したものである．どちらの群も同程度の吸光度を示しており，細胞における毒性などはないと考えられる．したがって，本鋳型を用いて作製したコラーゲン足場材は細胞配向特性を考慮した足場材として機能することが期待できる．

図 4 に基礎的検討として鋳型を用いずに作製した柱状のコラーゲン足場材において磁場刺激を与えて細胞培養を行った際の細胞増殖アッセイによる吸光度を示す．細胞増殖は足場材に対して垂直に磁場を作用させた方が水平に作用させた場合に比べて優れていた．したがって，本研究で作製に成功した図 2 に示す足場材を用いて磁場刺激を与えた場合，中央の中空部分に細胞が進入し組織化を行っていくことが期待できる．

謝辞

この研究は公益財団法人渡邊財団の補助を受けて実施したものである．

参考文献

1) Morishita T et al.: Tissue engineering approach to the treatment of bone tumors: Three cases of cultured bone grafts derived from patients' mesenchymal stem cells. Artif Organs 30: 115-118, 2006.
2) Ichinose S et al.: Comparative sequential morphological analyses during in vitro chondrogenesis and osteogenesis of mesenchymal stem cells embedded in collagen gels. Medical Molecular Morphology 46: 24-33, 2013.
3) Arahira T et al: Effects of proliferation and differentiation of mesenchymal stem cells on compressive mechanical behavior of collagen/β-TCP composite scaffold. J Mech Behav Biomed Mater 39: 218-230, 2014.
4) 荒平高章 他：臨床バイオメカニクス 41(2020).

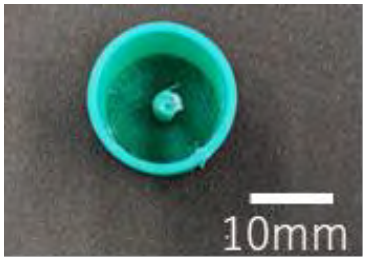

Fig.1 Photograph of mold by 3D printer.

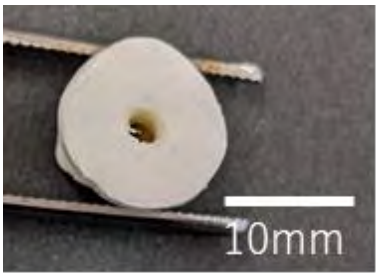

Fig.2 Image of collagen scaffold.

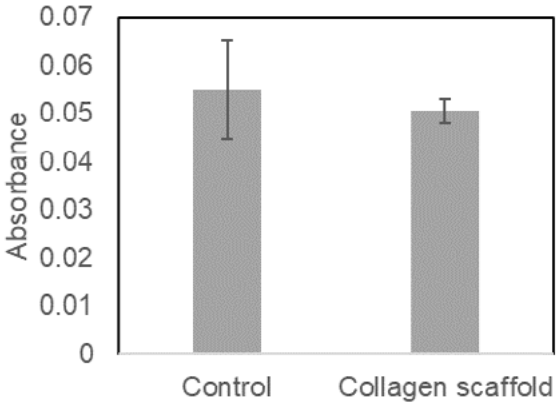

Fig.3 Cell proliferation assay of 2D culture.

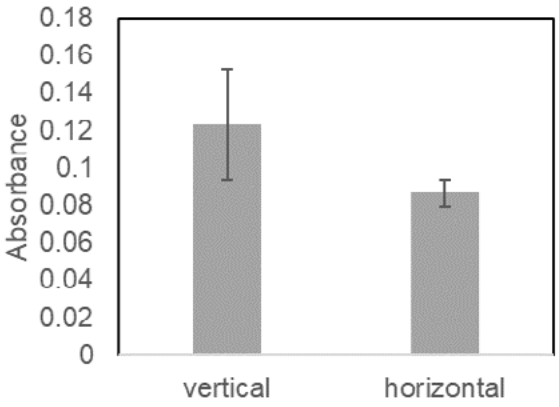

Fig.4 Cell proliferation assay of 3D culture.

ベージュ脂肪の分布位置による形態および代謝特性の比較

Morphological and metabolic characteristics of browning of white adipose tissue in inguinal and epididymal adipose tissues

小川　まどか*　田村　優樹**　畑　純一***
Madoka Ogawa* Yuki Tamura** Junichi Hata***

*京都産業大学 現代社会学部 健康スポーツ社会学科，〒603-8555　京都府京都市北区上賀茂本山
**日本体育大学 体育学部 体育学科，〒158-0081 東京都世田谷区深沢 7-1-1
***東京都立大学 健康福祉学部 放射線学科，〒116-8551　東京都荒川区東尾久 7-2-10
** Kyoto Sangyo University, Motoyama, Kamigamo, Kita-ku, Kyoto 603-8555, Japan
** Nippon Sport Science University, 7-1-1, Fukazawa, Setagaya-ku, Tokyo 158-0081, Japan
*** Tokyo Metropolitan University 7-2-10, Higashiogu, Arakawa-ku, Tokyo 116-8551, Japan

Abstract

The aim of this study was to clarify the morphological characteristics by T2* and diffusion tensor image (DTI) and metabolism products by ^{1}H-MRS in inguinal adipose tissue (iWAT) and epididymal adipose tissue (epiWAT) of the mice, that with and without β3-adrenoceptor agonist. We confirmed the anatomical location and position in relation to other organs and iWAT and epiWAT in vivo were identified from T2* and DTI images. ^{1}H-MRS were 1) more spectral peaks were observed in epiWAT than in iWAT; 2) the administration of β3-adrenoceptor agonists increased the spectral peaks observed in iWAT, whereas not observed that in epiWAT.

Keywords: browning, adipose tissue, inguinal, epididymal, T2*, DTI, ^{1}H-MRS

1. 背景および目的

脂肪組織は，主に皮下と臓器の周囲に分布している．一般的に皮下の脂肪組織は“皮下脂肪”と呼ばれ，心臓や肝臓をはじめとする各臓器の周囲に蓄積する脂肪組織は“内臓脂肪”と呼ばれる．脂肪組織の分布位置による発生の過程や遺伝子の発現パターンの差が示されており,[1] 脂肪組織間には機能的な違いがあると考えられるが，その詳細は不明な点が多い．

脂肪組織は，主に脂肪細胞がその大部分を占める．典型的な脂肪細胞は白色脂肪細胞と呼ばれ，それ以外に褐色脂肪細胞とベージュ脂肪細胞がある.[2] 褐色脂肪細胞とベージュ脂肪細胞には多房性脂肪滴とミトコンドリアが多く存在しており，脱共役タンパク質（UCP-1）を発現し，熱発生を通してエネルギー恒常性の維持を担う.[3] 褐色脂肪細胞は褐色脂肪組織（brown adipose tissue; BAT）内に存在する．一方，ベージュ脂肪細胞は，寒冷，運動，β3 アドレナリン受容体作動薬投与などの環境条件や外部からの刺激に応じてマウスの白色脂肪組織（white adipose tissue; WAT）内に発現する.[4] これらの現象は，脂肪の褐色化（browning）と呼ばれ，新たな肥満対策として注目されている．

生体内における褐色・ベージュ脂肪の評価は FDG-PET, MRI や ^{1}H-MRS によって行われてきた.[5-6] 一方，脂肪の褐色化を捉えるイメージング方法は確立されておらず,[7] その点が生体内のベージュ脂肪の生理学的刺激に対する機能制御機構の解明を妨げる 1 要因だと考えられる．そのため，本研究ではマウスの鼠径部脂肪（iWAT）と精巣上体脂肪（epiWAT）を対象とし，1）T2*および拡散テンソルイメージング（DTI）による形態的な特徴と

^{1}H-MRS による代謝性物質の特徴を明らかにし，2）β3 アドレナリン受容体作動薬投与によって褐色化した脂肪（ベージュ脂肪）と WAT 間で評価指標に差がみられるか否かを明らかにすることを目的とした．本実験を終えているが，画像解析の途中であるため，本報告書ではデータの代表例を示す.

2. 方法

本研究は，京都産業大学動物生命倫理委員会の承認を受けて実施した（承認番号 2021-45）.

2.1. 対象

7 週齢雄性の野生型マウス（C57BL/6J）を対象とし，対照群および β3 群を 6 匹ずつ飼育した.

2.2. 飼育方法

室温 22℃内で 3 日間の予備飼育後，7 日間の飼育を実施した．なお，両群のマウスは餌および水ともに自由摂取とし, 餌は固形飼料 (CREA Rodent Diet CE-2）を用いた．β3 群は，脂肪の褐色化が確認されている実験モデル [4] を元に，β3 アドレナリン受容体作動薬（CL316,243）1 mg・kg^{-1} を腹腔内へ 7 日間投与した．β3 群の N=1 は投与 1 日目に死亡したため，N=5 となった.

2.3. 撮像方法

マウスは撮像開始 10 分前から麻酔ガス（イソフルラン 1.5～3%）を吸入し，室温 20℃内に設置された 86 mm の送信コイルと 18 mm 内径の 4 ch 受信用クライオプローブコイルを備えた 9.4T MR 装置（Bruker Bio Spec）へ固定された．マウスの各脂肪組織を摘出した経験のある共同研究者（Y.T.）と撮影を担当する臨床放射線技師らと共に，解剖学的な位置や他の臓器との位置関係を確認し，iWAT および epiWAT を特定した.

^{1}H-MRS

励起法は PRESS 法を使用した. 詳細なシーケンスは以下に示す．TE＝16.5 ms，TR＝2000 ms，volume of interest＝2 mm×5 mm×8 mm，Average＝128，number of sampling = 2048，acquisition bandwidth = 4401 Hz と設定した．水信号の抑制は解除した.

T2*

詳細なシーケンスは以下に示す．TE= 1.63 ms, 2.96 ms, 4.29 ms, 5.62 ms, 6.95 ms, 8.28ms, 9.61ms, 10.94 ms, 12.27 ms, 13.60 ms, 14.93 ms，TR=800 ms, slice thickness=1 mm, gap=0.2 mm, matrix 214 × 160, number of signal averages=8, acceleration factor=1.6, flip angle=45°, field of view=32 mm×24 mm, number of slices=25.

DTI

詳細なシーケンスは以下に示す．TE=20.583 ms, TR=800, δ/Δ = 5.0/10.5 ms, b-value = 3000 s/mm^2, average = 4, field of view = 32 × 24 mm^2, matrix size = 128 × 96, number of slices = 25, slice thickness = 1.0 mm, slice gap =0.2 mm, motion probing gradient moment = six directions (xy, xz, yz, −xy, −xz, −yz).

2.4. 解析方法

^{1}H-MRS

LC Model (ver. 6.3-1R) の lipid-8 を使用し，各スペクトルを算出した.

T2*および DTI

撮像画像から T2*map および固有ベクトル e1, e2, e3 の画像を作成した．今後，各脂肪組織の T2* 値および e1, e2, e3 方向の見かけの拡散係数（ADC）を算出する.

3. 結果

飼育期間の体重および摂食量は，両群間で有意な差はみられなかった.

図 1 には，両群における各脂肪組織の T2*画像の例を示す.

図 2 には，両群における iWAT および epiWAT の ^{1}H-MRS の例を示す. 両群の epiWAT において，メチレン基（1.3 ppm），α-メチレンからカルボン酸基グループ（2.25 ppm），オレフィン基（5.3 ppm）のピークが確認された．両群の iWAT で確認されたのは，メチレン基（1.3 ppm）と水（4.7 ppm）のピークであった．それに加えて，β3 群の iWAT では，β-メチレンからカルボン酸基グループ（1.5 ppm），グリセロールのバックボーン（4.2 ppm），オレフィン基（5.3 ppm）が確認された.

4. 考察

本研究では, マウス生体の iWAT および epiWAT を対象に, β3 アドレナリン受容体作動薬投与の有無による T2*および DTI による形態的な特徴と

^{1}H-MRS による代謝性物質の特徴を明らかにすることを目的とした. 一部は解析中だが, ^{1}H-MRS による代謝性物質の特徴として，1) iWAT よりも epiWAT で多くのスペクトルのピークが確認された. 2) β3 アドレナリン受容体作動薬の投与によって，iWAT においてスペクトルのピーク数が増加したが，epiWAT でその変化はみられなかった.

蓄積部位によって脂肪内の脂肪酸組成に差があり,[8] その違いは代謝活動の差異を示すとされている.[9] 本研究では，β3 アドレナリン受容体作動薬の投与によって，iWAT でみられるスペクトルのピーク数が増えたが，epiWAT のそれには差がみられなかった．この結果は，β3 アドレナリン受容体作動薬による脂肪の褐色化が epiWAT よりも iWAT の広範囲で確認されたという，生化学解析による報告 [10] を支持していると考えられる.

今後は T2*および DTI の画像解析を進め，β3 アドレナリン受容体作動薬投与の有無による iWAT および epiWAT の形態的な特徴を明らかにする予定である.

謝辞

本研究は渡邊財団研究助成を受けて実施した．また，理化学研究所の機器を使用し，東京都立大学大学院博士課程前期の大城日菜子氏の協力を得て実施された.

参考文献

1) Chanclón, B. et al., Peripancreatic adipose tissue protects against high-fat-diet-induced hepatic steatosis and insulin resistance in mice. Int J Obes, 44, 2323-2334 (2020).
2) Wang, W. et al., Control of brown and beige fat development. Nat Rev Mol Cell Biol, 17, 691-702 (2016).
3) Giralt, M. et al., White, brown, beige/brite: different adipose cells for different functions? Endocrinology, 154, 2992-3000 (2013).
4) Altshuler-Keylin, S. et al., Beige adipocyte maintenance is regulated by autophagy-induced mitochondrial clearance. Cell Metab, 24, 402-419 (2016).
5) Holstila, M. et al., MR signal-fat-fraction analysis and T2* weighted imaging measure BAT reliably on humans without cold exposure. Metabolism, 70, 23-30 (2017).
6) Koskensalo, K. et al., Human brown adipose tissue temperature and fat fraction are related to its metabolic activity. J Clin Endocrinol Metab, 102, 1200-1207 (2017).
7) Hu, H. H., Magnetic resonance of brown adipose tissue: a review of current techniques. Crit Rev Biomed Eng, 43, 161-181 (2015).
8) Machann, J. et al., Intra- and interindividual variability of fatty acid unsaturation in six different human adipose tissue compartments assessed by (1) H-MRS in vivo at 3 T. NMR Biomed, 30, (2017).
9) Hamilton, G. et al., In vivo triglyceride composition of abdominal adipose tissue measured by (1) H MRS at 3T. JMRI, 45, 1455-1463 (2017).
10) Labbé, S. M. et al., Metabolic activity of brown, "beige," and white adipose tissues in response to chronic adrenergic stimulation in male mice. Am J Physiol Endocrinol Metab, 311, E260-268 (2016).

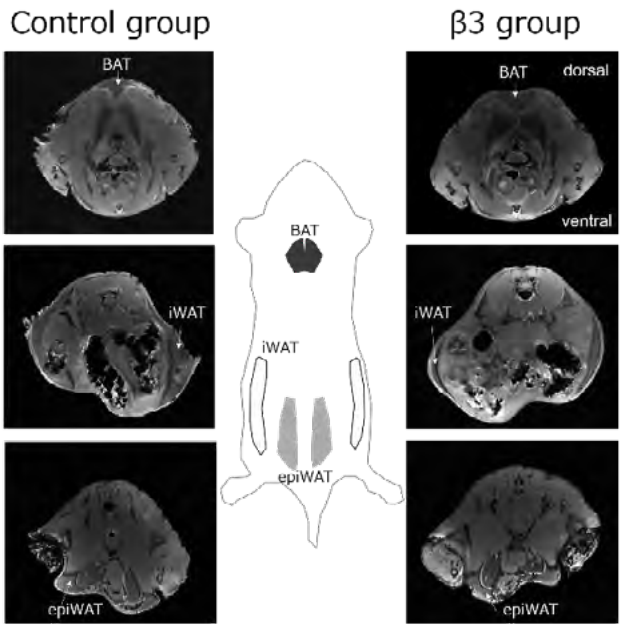

図 1. 褐色脂肪（BAT），鼠径部脂肪（iWAT）および精巣上体脂肪（epiWAT）における T2*map の例

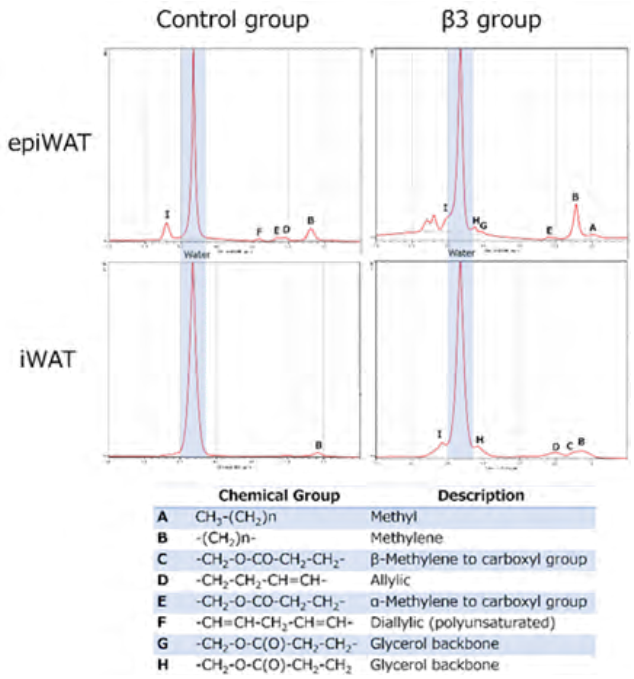

	Chemical Group	Description
A	CH_3-$(CH_2)n$	Methyl
B	-$(CH_2)n$-	Methylene
C	-CH_2-O-CO-CH_2-CH_2-	β-Methylene to carboxyl group
D	-CH_2-CH_2-CH=CH-	Allylic
E	-CH_2-O-CO-CH_2-CH_2-	α-Methylene to carboxyl group
F	-CH=CH-CH_2-CH=CH-	Diallylic (polyunsaturated)
G	-CH_2-O-C(O)-CH_2-CH_2-	Glycerol backbone
H	-CH_2-O-C(O)-CH_2-CH_2	Glycerol backbone

図 2. 両群の鼠径部脂肪（iWAT）および精巣上体脂肪（epiWAT）における ^{1}H-MRS の例

脳波同時記録による新たな経頭蓋磁気刺激法による てんかんの新規バイオマーカー開発

Application of TMS-EEG as a novel biomarker of epilepsy

小玉 聡
Satoshi Kodama

東京大学医学部附属病院　脳神経内科，〒113-8655 東京都文京区本郷 7-3-1
Department of Neurology, The University of Tokyo Hospital
7-3-1 Hongo, Bunkyo-ku, Tokyo 102-0073 Japan

Abstract

TMS (transcranial magnetic stimulation) may be a good candidate for a new diagnostic tool for epilepsy because it can reflect hyperexcitability of the neural cells in brain. TMS-EEG (TMS-electroencephalogram) is a newly developed technique measuring EEG while performing TMS. TMS-EEG may be superior to classic TMS using electromyogram as an indicator of brain function, because it can reflect pure cerebral activity. We evaluated the efficacy of TMS-EEG as a diagnostic measure for epilepsy. Amplitudes of TMS-evoked potentials in myoclonus epilepsy patients tended to be higher in N45, P60, and N100 than in normal subjects, although the sample size was small and the differences were not significant.

Keywords: cortical excitability, TMS-evoked potentials

1. 目的

てんかん患者における脳波同時記録磁気刺激法（TMS-EEG）についての探索的な検討を行った．TMS-EEG とは脳波（electroencephalogram: EEG）を測定しながら TMS （transcranial magnetic stimulation）を行い，TMS に対する脳波反応を計測する方法である (Ref 1, Ref 2)．従来の筋電図による TMS 指標と比較して，TMS-EEG において優れている点は，直接的な脳の反応を記録できるとされる点であり，MEP と異なり脊髄や末梢神経，筋に至るまでの運動経路の影響を受けない点である (Ref 2)．TEP の後期成分は GABA 作動薬やレベチラセタム，ラモトリギンといった抗てんかん薬により振幅が増大することから，何らかの抑制性の機構を反映している可能性が指摘されており，てんかん患者においても一定の変化がみとめられる可能性は十分あり，解明が求められる．

2. 方法

東京大学医学部附属病院にて，磁気刺激法を用いた筋電図検査を，脳波の同時記録とともに施行されたてんかん患者の検査結果を後方視的に収集した．

刺激および表面筋電図記録

TMS は，Magstim 200 Square（Magstim Co. Ltd.）に径 7 cm の 8 の字型コイル（Magstim Co.Ltd.）を接続して，刺激部位を右 FDI に対応する左 M1 とした．

TMS の刺激クリック音による聴性誘発電位を避けるため，患者は耳栓の装着を行った．クリック音は空気伝導だけでなく，頭部に接した TMS コイルからの骨伝導によっても知覚されることから，それを低減させるために，TMS コイルはシリ

コン製シートを介して頭部に置いた．TMS は左 M1 とし，刺激強度は 100%RMT とした．刺激間隔は平均 3.5 s とし，刺激に対する anticipation を避けるために，±500 ms の変動を設け，計 150 回の刺激を行った．

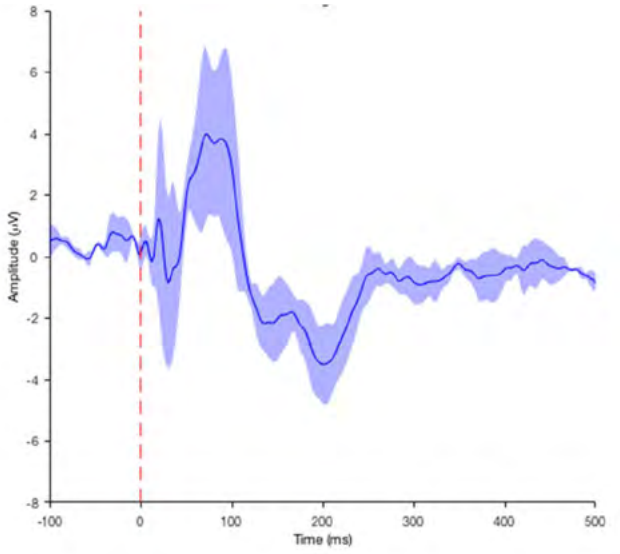

図1A　健常者の平均 TEP

表 1　TEP の潜時･振幅

	健常者		ミオクローヌスてんかん	
	潜時 (ms)	振幅 (μV)	潜時 (ms)	振幅 (μV)
N45	31.8	3.5	33.3	7.5
P60	80.0	5.6	92.4	9.7
N100	136.4	3.4	133.0	6.6
P180	166.7	2.2	197.0	1.3

同時記録脳波

同時記録として行う脳波は，TMS による刺激アーチファクトによる脳波増幅器の飽和を避けることが可能な増幅器 TruScanRE （Deymed Diagnostic, Co. Ltd.）を介して測定した．電極は 32 チャンネルのキャップ型脳波電極を用いて，TMS の刺激部位（左 M1）から離れた右耳朶をレファレンスとして，アナログ信号を 0.16 Hz～1 kHz の通過帯域とする bandpass filter 処理を行った上で，3 kHz のサンプリング周波数にて記録した．電極のインピーダンスは全て 5 kΩ 以下となるように設定した．

脳波のポストプロセシング

脳波のオフライン解析は，MATLAB（ver. R2017b）を用いて行い，以下のパイプラインで行った．1）TMS の前後 1 s にてエポッキング． 2）刺激前 -2 ms ～ 刺激後 10 ms は TMS アーチファクトの

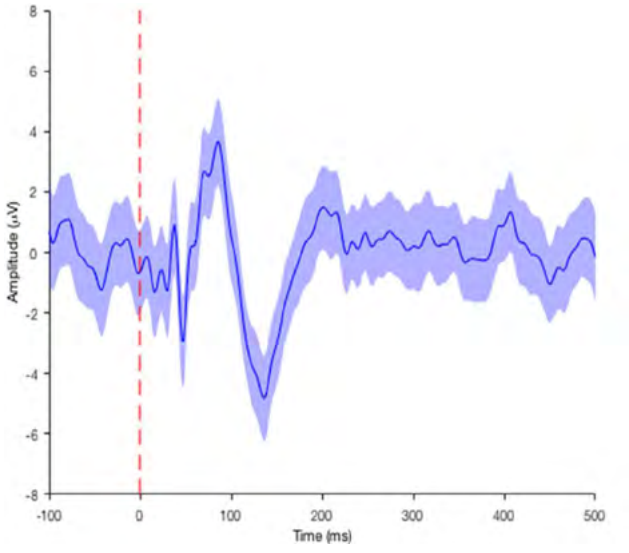

図1B　ミオクローヌスてんかん患者の平均 TEP

混入があるため脳波信号を除去し，除去した部位を三次関数曲線により補間． 3）目視にて明らかな筋電図，体動もしくは眼球運動によるアーチファクト混入が確認できるトライアルを除外． 4）Bandpass filter を 1～500 Hz で設定した上で，Notch filter を 50 Hz で適応． 5）サンプリング周波数を 500 Hz に downsampling． 6）基準誘導を全電極の平均電位へ re-reference する． 7）MATLAB 上で機能するツールボックスの FastICA を用いて，独立成分分析を行い，アーチファクトと考えられる独立成分を除外． 8）関心領域としてあらかじめ設定した誘導（C3, C4, FC5, FC1, FC2, FC6, CP5, CP1, CP2, CP6）の波形を加算平均したものを TEP（TMS evoked potentials）とする．本研究では 30-50 ms に現れる陰性向きピークを N45，50-90 ms に現れる陽性向きピークを P55，90-150 ms に見られる陰性向きピークを N100，150-300 ms に現れる陽性向きピークを P180 と設定した．それぞれの振幅は，前後の 2 つの逆向きのピークからの振幅を平均したものとした．

3. 結果

対象期間中に東京大学医学部附属病院で TMS と脳波の同時記録を施行された 3 名のミオクローヌスてんかんの患者を対象とした．いずれもてんかん外科の手術は受けておらず，検査中もしくは検査後に有害事象を生じた患者はいなかった．

図 1 には，健常者および患者群ごとに加算平均した TEP を示す. 表 1 に加算平均したそれぞれの TEP の成分ごとの潜時と振幅を示す．全般性てんかん患者においては，TEP の潜時はおおむね健常者と一致したが，振幅は N45，P60，N100 において健常者よりも高値となる傾向が認められた．ただし，サンプル数が少なく，有意差は伴わなかった．

4. 考察

本研究ではミオクローヌスてんかんにおいては, 例数が少なく有意差は伴わないものの, N45, P60，N100 の振幅が増大する傾向が見られた．

TEP の各成分の振幅はそれぞれ大脳の神経伝達機構を反映することがこれまでの研究で示唆されている．N45 については GABAA 受容体を介した神経伝達が関与するとされており，それは健常者を対象とした GABAA 受容体アゴニストの投与により N45 の振幅増大が見られた研究に基づく(Ref 3)．同様の研究により，N100 の振幅は GABAB 受容体による抑制性の機構との関連が示唆されている(Ref 3, Ref 4)．本研究で N45，N100 の振幅増大が見られたことは，ミオクローヌスてんかんにおけるこれらの GABA 介在性神経機構の異常を示唆する．ミオクロースてんかんに対して二発刺激を用いた先行研究では，GABAA 系の抑制性神経機構を反映する SICI が減弱しており(Ref 5)，本研究の結果と併せてミオクローヌスてんかんでは同神経機構が十分機能していない可能性が示唆される．

謝辞

この研究は渡辺財団の第 27 回磁気研究助成・岡井治特別助成の補助を受けて実施したものである．

参考文献

1) Ilmoniemi RJ, Virtanen J, Ruohonen J, Karhu J, Aronen HJ, Naatanen R, et al: Neuroreport 8(16)3537-40 (1997).

2) Tremblay S, Rogasch NC, Premoli I, Blumberger DM, Casarotto S, Chen R, et al: Clin Neurophysiol 130(5):802-44 (2019).

3) Premoli I, Castellanos N, Rivolta D, Belardinelli P, Bajo R, Zipser C, et al: J Neurosci. 34(16):5603-12 (2014).

4) Casula EP, Tarantino V, Basso D, Arcara G, Marino G, Toffolo GM, et al: Neuroimage 98:225-32 (2014).

5) Hanajima R, Ugawa Y, Terao Y, Ogata K, Kanazawa I: J Neurol Sci 140(1-2):109-16 (1996).

コンパクトダイヤモンド磁気プローブのための永久磁石形状の最適化手法

Optimization of magnet shape for compact magnetic probe with nitrogen-vacancy center in diamond

桑波田晃弘
Akihiro Kuwahata

東北大学　大学院工学研究科，〒980-8579　宮城県仙台市青葉区荒巻字青葉 6-6-05
Graduate School of Engineering, Tohoku University
6-6-05, Aramaki Aza-Aoba, Aoba-ku, Sendai 980-8579 Japan

Abstract

Cancer cells metastasize through the lymphatic system, so it is necessary to identify and examine the lymph nodes that lymphatic fluid and cancer cells first reach to diagnose metastasis status. A magnetic probe with diamond NV (nitrogen-vacancy) was developed for the detection of sentinel lymph nodes. In order to optimize the performance of diamond NV, in this research, an optimized permanent magnet is developed by the innovative idea (inverse solution), and to be mounted on a compact magnetic probe head to generate a spatially uniform magnetic field, leading to the highly-sensitive magnetic detection.

Keywords: Permanent magnet, diamond nitrogen-vacancy center, inverse problem, optimization

1. 目的

日本における死因第 1 位はがんであり，2020 年に至るまで年推移の死亡率は単調増加している．がんの中でも，日本人女性が罹患する例が多いのが乳房を病巣とする乳がんである．乳がんを治療する際には，がんの転移の有無や転移したがんの数によって治療法が変わることから，がんの転移診断を正確にすることが不可欠である．

ダイヤモンド NV センタ（Diamond Nitrogen-Vacancy Center）を搭載した磁気センサは，磁性ナノ粒子の高感度な検出が可能であり，磁性ナノ粒子法を用いたがんの転移診断など医療分野への応用が期待されている [1,2].

本研究では，ダイヤモンド NV センタの磁気感度を向上するために，目的の磁場一様性から磁石の形状を決定する逆問題的アプローチによって，ダイヤモンド NV センタに特化した，一様な磁場を印加する小型磁石の形状を最適化する手法を開発する．モデルの形状を最適化する逆問題的アプローチによって形状を決定することで，従来の順問題手法にはないユニークな形状の磁石形状の開発を目指す．

2. 方法

従来の磁石形状の設計は順問題の発想に基づいており，最初のステップでは，磁石形状を決定しその磁場分布が一様であるかを検証する．磁場分布が望ましいものでない場合は，再度上記のプロセスを行い，求める磁場分布になるまで繰り返す．このような順問題的設計法では，既知の知見

に基づいた磁石形状のみしか設計できず，革新的な磁石形状を生み出すことは困難である．そこで，本研究では，発想を逆転し，望む磁場分布から磁石の形状を決定する逆問題的手法を開発する．

目標エリアであるダイヤモンドセンサ領域の磁場分布から磁気モーメント 1 つ 1 つの値が求められ，磁気モーメントから磁石形状を決定する．磁気プローブ内に磁石を搭載するできる磁石全体の大きさを決定し，磁石の上部 5 mm にダイヤモンド(3.9 mm×3.9 mm×1 mm)を配置した．磁場の空間一様性が必要な領域は，ダイヤモンド表面である．磁石内部の磁気モーメントは XY 平面に 5 mm 間隔，Z 方向に 6 mm 間隔で計 45 個配置した．逆問題の最適化に関して，チコノフの正則化は，非適切問題に対しても正則パラメータによって近似解を算出できるという特徴を持つ．また，最適な正則化パラメータの判定条件にモロゾフの相変原理を満たす正則化パラメータ決定手法として L-Curve Method を用いた．

3. 結果と考察

最適化問題を解いた結果から得られた磁石形状を図 1 に示す．目標エリアは，XYZ 方向に 50*50*50 分割，計 125000 個の一様性磁場データを入力した最適化結果である．図 1 に示すように，従来の順問題では発想が困難である革新的な磁石形状を得ることに成功した．対象エリアである

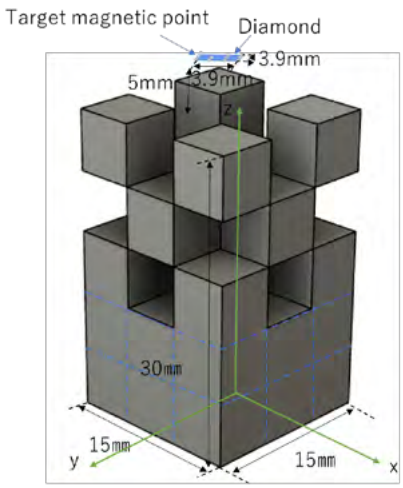

図 1. 最適化磁石形状．最上段は十字型に切り抜かれ，二段目は十字型に磁気モーメントブロックが存在する．三段目は最上段と同じ形状である．

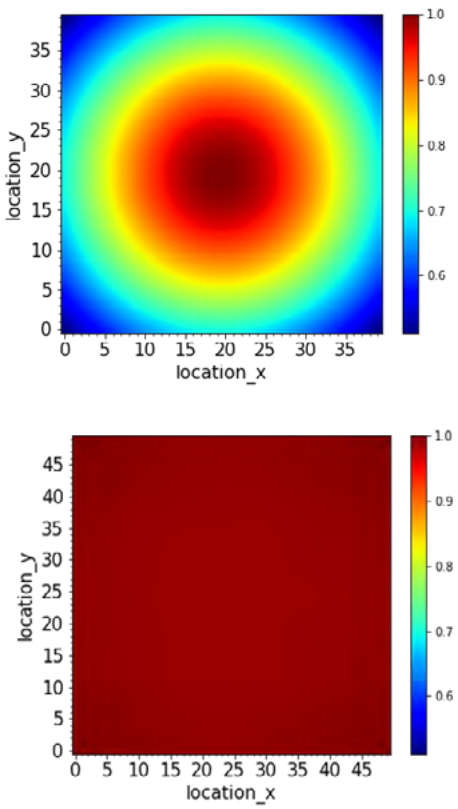

図 2. （上）従来磁石と（下）最適化後の磁石の磁場一様性の評価．

ダイヤモンド領域全体における磁場の最大強度と磁場の最小強度の比率を算出し，磁場一様性を評価した（図 2）．従来磁石では，約 48.1%と磁場一様性は低い．一方，最適化後の磁石形状に置いて，磁場一様性は 99.7%であり，一様性が飛躍的に向上した．

図 3. 小型磁石の組み合わせによる最適化磁石形状の開発．磁気モーメントが存在する部分は永久磁石，磁気モーメントが存在しない部分はアクリルで形成．

約100個の小型磁石とアクリル加工品を組み合わせることで，最適化問題解法によって明らかとなった磁石形状を試作した（図3）．試作した磁石の磁場分布を実測した結果，99.6%の磁場空間一様性であり，数値計算と同等の結果であった．

最適化された磁石形状を用いたダイヤモンド磁気プローブシステムを構築し，マウス動物を模擬した生体ファントムを用いた磁気ナノ粒子検出実験を実施した．磁気コイルシステム，マイクロ波アンテナシステムを構築し，微量の磁性ナノ粒子を検出することに成功した．

4. 結論

磁気モーメント法に基づく逆問題解析手法によって新しい最適化された磁石形状を見出した．磁場一様性は99.7%と高く，生体模擬ファントムを用いた磁性ナノ粒子の検出に成功した．本研究によって，がん診断の精度が向上し，より微小ながんを検出できることが期待できる．

謝辞

本研究は公益財団法人渡邉財団の補助を受けて実施したものである．

本論文の内容は2022年3月に岡山で開催された『令和4年度電気学会全国大会』で報告したものである．

ならびに、本論文の内容は，特開 P202110284，「磁石形状設計方法および最適化設計プログラム」（2022年2月25日）で特許申請したものである．

参考文献

1) M. Sekino, A. Kuwahata, *et al.*, Scientific Reports 8 (2018).
2) A. Kuwahata *et al.*, Scientific Reports 10 (2020).
3) 桑波田晃弘，田中治樹，「磁石形状設計方法および最適化設計プログラム」，特開 P202110284（2022年2月25日）

Na-MRIを用いた全身性強皮症におけるナトリウム代謝異常の解明

Elucidation of Sodium Metabolism Disorders in Systemic Sclerosis using Na-MRI

峯岸　薫
Kaoru Minegishi

横浜市立大学大学附属病院　血液・リウマチ・感染症内科,
〒236-0004　神奈川県横浜市金沢区福浦 3-9
Department of Stem Cell and Immune Regulation,
Yokohama City University Graduate School of Medicine
3-9 Fukuura, Kanazawa-Ku, Yokohama, 236-0004, Japan

Abstract

Systemic sclerosis is an intractable disease of unknown cause that involves progressive fibrosis of the skin and internal organs. Maintaining the homeostasis of water-soluble electrolytes is indispensable to life, and it has been believed that this is maintained by the kidneys. However, it has become clear that metabolism of sodium in our body is controlled in collaboration with the skin, and that abnormal sodium metabolism causes various diseases. Here, we introduced Na-MRI that can measure sodium levels in tissue, in order to elucidate abnormal sodium metabolism in systemic sclerosis as well as its pathology and mechanisms.

Keywords: Na-MRI, sodium metabolism, systemic sclerosis

1. 目的

電解質・体液の恒常性維持は生命維持において不可欠であり，中でもナトリウム(Na)代謝は，脳・心血管・腎疾患など様々な疾患に直結するため，極めて重要である．生体内の Na 調節は，これまで腎臓のみで行われていると考えられてきたが，近年，Na が皮膚，肝臓，筋肉など多臓器と連携して制御されていることが明らかとなり，Na 代謝異常は様々な疾患をもたらすことが判明した．

全身性強皮症は，自己免疫現象を背景に，皮膚や肺など内臓諸臓器の線維化が進行する膠原病であるが，未だ病態の解明が不十分で，有効な治療法の乏しい難治性疾患である．食塩の過剰摂取による皮膚を代表とする組織局所への Na 蓄積は，p38/MAP キナーゼ経路を介する病原性 Th17 細胞へのT細胞の分極による自己免疫疾患増加を導くことが示されており，強皮症患者において①皮膚 Na 量と皮膚硬化の重症度が相関すること，②皮膚に蓄積された Na は皮膚硬化進行の予測因子となることが明らかにされている．

強皮症の病因としては，線維芽細胞の活性化，血管障害，免疫異常が知られている．皮膚硬化は浮腫期，硬化期，萎縮期という経過をとり，浮腫期であれば副腎皮質ホルモンの投与も検討されるが，治療効果は限定的であり，局所の電解質動態は今までに検証されていない．本研究では，「皮膚に蓄積する Na が，強皮症を進展・増悪させるメカニズムを解明し，この調整機構をターゲットとした新規治療法の開発を目指す」ことを目的とする．

この研究を遂行するために，組織 Na 量を評価できるツールとして開発された ^{23}Sodium-magnetic resonance imaging (Na-MRI)を「日本に初導入」したので，結果を報告する．

2. 方法

医療用 MRI は生体を主に構成する ^{1}H 原子を画像化しており，臨床で使用している MRI 装置では ^{23}Na 原子は検出できない．Na-MRI は，^{23}Na が Na 原子の中で唯一の安定同位体で，^{23}Na の陽子数が奇数，中性子数が偶数であり，磁気モーメントが生じることを利用して組織 Na を可視化できる技術で，造影剤を用いずに生体内 Na の検出が可能である．本プロジェクトを遂行するにあたって最も重要である Na-MRI の導入には，Multinuclear Option を搭載した高磁場 MRI 装置が必須であるが，日本国内ではこのオプションを搭載した MRI 装置は限定されている．国立スポーツ科学センター(東京都)は Na-MRI の基礎となるシーメンス社の高磁場 MRI 装置を保有しているため，本研究では，^{1}H 以外の多核種(^{13}C, ^{31}P など)を用いた MR 測定に成功している国立スポーツ科学センターで，シーメンス社製の「MAGNETOM Skyra」を用いて Na-MRI の導入を行った．

3. 結果

3.0 テスラの MRI(MAGNETOM Skyra, Siemens)に，Na 量を測定できる特注コイル(Stark-Contrast, Erlangen, Germany)を搭載し，コイルファイルのインストール，セッティング，撮像シーケンスのパラメータの登録を行った．次に，NaCl 入りのファントムを使用し，テストスキャンを行い，撮像可能な事を確認した(図 1). テストスキャンにおいては，画像の信号雑音比およびノイズの周波数特性を検証し，撮影した画質の精度が良質であることが確認できた(図 2).

さらに，健常人の左下腿で，テストスキャンで設定した撮影条件を用いて，Na-MRI の撮影を実施した．この撮影においては，濃度の異なる NaCl 溶液(10, 20, 30, and 40 mmol/L)を満たしたキャリブレーションチューブを同時に撮影することで，組織 Na 量の定量を行うことができた．今回撮影を行ったのは，50 歳男性と 45 歳男性の 2 症例であるが，Na 量は，それぞれ，皮膚 16.6 mmol/L，筋肉 16.8 mmol/L と，皮膚 13.9 mmol/L，筋肉 16.3 mmol/L であった(図 3).

4. 考察

組織局所における Na 調整機構は，「生体内の Na 量は腎臓によって一定に保たれる」という従来の定説とは異なり，本研究で得られた結果は，当該研究領域においてブレイクスルーとなる発見である．疫学研究をはじめ，世界的な塩分摂取量と各疾患との調査が行われてきたが，これまでの研究は組織局所の Na 蓄積は考慮されておらず，日常臨床で行われている臨床検査では，組織 Na 量の異常を検出することは不可能であり，潜在的に疾患患者の組織 Na・体液バランス異常を見逃している可能性がある．

海外で行われた Na-MRI を用いた臨床研究により，皮膚および筋肉の Na 量には男女差があり，高齢になるほど Na 量が高くなることが示されている [1)]．また，高血圧症患者においては，皮膚および筋肉の Na 量が健常者より高いことも判明している [2)]．本研究においても，45 歳の症例よりも 50 歳の症例の方が皮膚の Na 量が高いことが示された．今後はこの技術を用いて，強皮症の病態解明・新規治療法の開発につながるような臨床研究を展開していく予定である．さらに，Na-MRI の手法は，そのまま他の疾患への臨床応用も可能である．

上述のように, 血清 Na 濃度は体内の総 Na 量の動きを示すものではない．Na-MRI を用いた研究は，画像診断対象外とされてきた疾患の異常を捉える可能性があり，日本での新技術・新産業の創出に貢献できる可能性を秘めており，こうした技術が進化すれば難治性疾患における治療薬の開発もいっそう進むと期待される．

5. 謝辞

本研究をご支援くださいました公益財団法人渡邉財団 関係者各位に深く感謝申し上げます．また，これまでの研究遂行にあたり，多くのご支援を戴きました国立スポーツ科学センターの皆様に厚くお礼申し上げます．

参考文献

1) Kopp C, et al. 23Na magnetic resonance imaging-determined tissue sodium in healthy subjects and hypertensive patients. Hypertension.

2013;61:635-40.
2) Kopp C, et al. (23)Na magnetic resonance imaging of tissue sodium. Hypertension. 2012; 59:167-72.

(図 1)

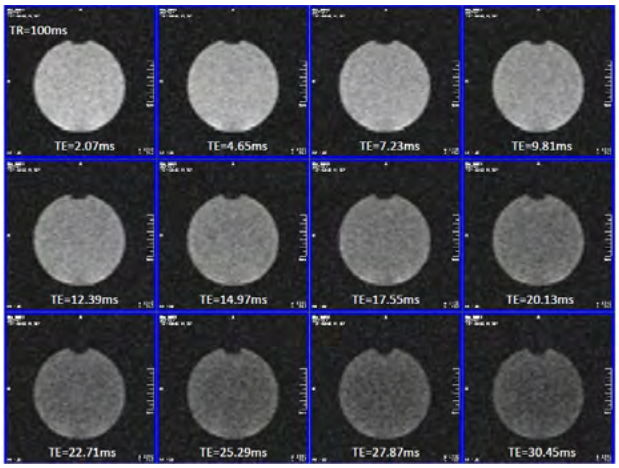

(図 2)

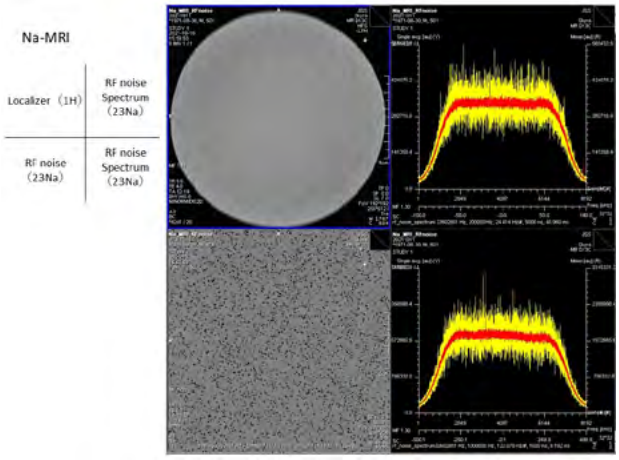

(図 3)

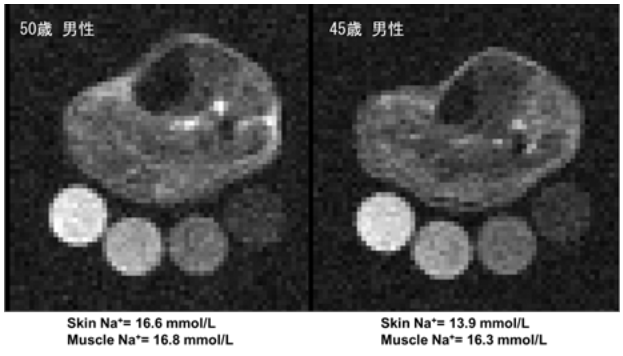

脳の可塑的変化を誘導する磁気刺激と経皮的脊髄刺激の連合性ペア刺激における刺激パラメータの検討

Investigation of stimulation parameters for plastic changes in the central nervous system by paired associative stimulation of magnetic stimulation and transcutaneous spinal cord stimulation

金子直嗣*, **, 佐々木睦*, **, 一寸木洋平*, *, 中澤公孝***

Naotsugu Kaneko*,**, Atsushi Sasaki*,**, Yohei Masugi*,***, and Kimitaka Nakazawa*

*東京大学大学院総合文化研究科，〒153-8902 東京都目黒区駒場 3-8-1

**日本学術振興会，〒102-0083 東京都千代田区麹町 5-3-1

***東京国際大学医療健康学部，〒350-1197 埼玉県川越市的場北 1-13-1

*Department of Life Sciences, Graduate School of Arts and Sciences, The University of Tokyo
3-8-1 Komaba, Meguro-ku Tokyo 153-8902, Japan

**Japan Society for the Promotion of Science
5-3-1 Kojimachi, Chiyoda-ku, Tokyo 102-0083, Japan

***School of Health Sciences, Tokyo International University
1-13-1 Matobakita, Kawagoe-shi Saitama 350-1197, Japan

Abstract

Paired associative stimulation (PAS) method for inducing neural plastic changes involves pairing of peripheral nerve stimulation and transcranial magnetic stimulation (TMS) over the primary motor cortex. The present study aimed to investigate the effect of transcutaneous spinal cord stimulation (TSCS) with TMS for PAS (TSCS-PAS) with different stimulus timings on corticospinal excitability. Our results showed that PAS timed to coincide with the TMS-induced signal arriving at the motor cortex shortly after the TSCS-induced signal, increased corticospinal excitability. We concluded that regulation of stimulus timing is important to induce plastic changes by TSCS-PAS.

Keywords: Paired Associative Stimulation, Transcutaneous Spinal Cord Stimulation, Transcranial Magnetic Stimulation, Corticospinal Excitability.

1. 目的

脳には環境への適応や長期的なトレーニングにより特定の神経回路が機能的に再編する性質（可塑性）がある．例えば，脳卒中患者は，脳神経回路が健常者とは異なることが示されている.[1)] これらの患者における運動機能障害は，長期的なリハビリテーションにより神経回路を再編させることで回復することができる．このような脳の可塑的変化を非侵襲的かつ人為的に誘導することができれば，患者の運動機能を効率よく回復させることが可能になると考えられる．

連合性ペア刺激法(Paired Associative Stimulation: PAS)は脳の可塑的変化を誘導する方法の一つである．この方法は，末梢の感覚神経に対する電気刺激と一次運動野に対する経頭蓋磁気刺激(Transcranial Magnetic Stimulation: TMS)を特定の

タイミングで同期させるペア刺激である．PAS を繰り返し行うことで，皮質脊髄路興奮性を可塑的に変化させることができる.[2] このような PAS による可塑的変化の特徴として，電気刺激した感覚神経に関連する脳領域において特異的に生じることが挙げられる．したがって，複数の感覚神経を同時に電気刺激できる経皮的脊髄刺激法(Transcutaneous Spinal Cord Stimulation: TSCS)[3]と TMS を組み合わせた TSCS-PAS は，より広範な脳領域における可塑的変化を誘導できると考えた．

本研究では，PAS のパラメータの中で重要である刺激タイミングについて着目した．従来の PAS では，電気刺激と TMS のタイミングをわずかにずらすことで，皮質脊髄路興奮性の変化(増大または減少)を操作できることが報告されている.[4] したがって，本研究では，異なる刺激タイミングを用いたそれぞれの TSCS-PAS 介入が皮質脊髄路興奮性に与える影響について明らかにすることを目的とした．

2. 方法

被検者は，重篤な中枢神経疾患を持たない健常成人男性 18 名であった．

実験中，被検者に半座位(膝関節伸展 0 度，股関節屈曲 60 度)で安静状態を保持させ，TSCS-PAS 介入およびその介入効果の評価を行った．

TSCS-PAS は，TSCS と TMS のペア刺激である．TSCS は感覚神経が集まる脊髄後根に刺激する手法であり，被検者の第 1-2 腰椎に陰極，腹部に陽極の表面電極を貼付して電気刺激を与えた．TMS は一次運動野の下肢支配領域に対して行った．介入はこれらのペア刺激を 120 回与えた．

本研究では，TSCS の感覚入力と磁気刺激の入力が一次運動野に到達するタイミングを調節することで，刺激タイミングと興奮性変化について調べた．以下 3 つの異なる刺激タイミングを TSCS-PAS 介入で用いた．

ⅰ．TSCS→TMS 条件: TSCS の感覚入力が一次運動野に到達した直後に TMS を行う(12 名).

ⅱ. TMS→TSCS 条件: TMS 直後に TSCS の感覚入力を一次運動野に到達させる(9 名).

ⅲ. Control 条件: TSCS と TMS の入力を全く違うタイミングで一次運動野に到達させる(12 名).

介入前，介入終了の直後，30 分後において，皮質脊髄路興奮性を TMS により評価した．表面筋電図を前脛骨筋，ヒラメ筋，腓腹筋内側頭，内側広筋，大腿二頭筋長頭の下肢 5 筋に貼付した．一次運動野の下肢支配領域に TMS を行い，各筋の運動誘発電位(Motor evoked potential: MEP)を記録した. MEP の最大振幅値は皮質脊髄路興奮性を反映しており, MEP の変化から TSCS-PAS 介入の効果を調べた．

3. 結果

図 1 に各条件における MEP の変化率を示す．介入前と比較して，TSCS→TMS 条件の TSCS-PAS 介入終了 30 分後，前脛骨筋，ヒラメ筋，大腿二頭筋，腓腹筋の MEP が増大した(Friedman 検定および Wilcoxon の符号順位検定, $p<0.05$). TMS→TSCS 条件と Control 条件ではいずれの筋においても MEP の変化は認められなかった(Friedman 検定，$p>0.05$).

4. 考察

TSCS→TMS 条件における介入は，複数の下肢筋における皮質脊髄路興奮性を増大させた．これは，広範な一次運動野の下肢支配領域における興奮性が増大したことを示唆する．Control 条件と TSCS→TMS 条件では有意な MEP の変化が認められなかったことから，TSCS と TMS の刺激タイミングの調節は一次運動野の可塑的変化を誘導する上で重要であることが示された．

従来の PAS では，刺激タイミングを調節することで皮質脊髄路興奮性を減少させることができる.[4] 今後は，皮質脊髄路興奮性を低下させる TSCS-PAS の刺激パラメータを探索していく．

謝辞

この研究は公益財団法人渡邉財団による第 27 回磁気研究助成の補助を受けて実施したものであり，厚く御礼申し上げます．

本研究の一部内容は，2021 年 9 月に開催された『第 76 回日本体力医学会大会』で報告したものである．また，本研究の一部内容は，国際誌 *Neuroscience* に掲載された.[5]

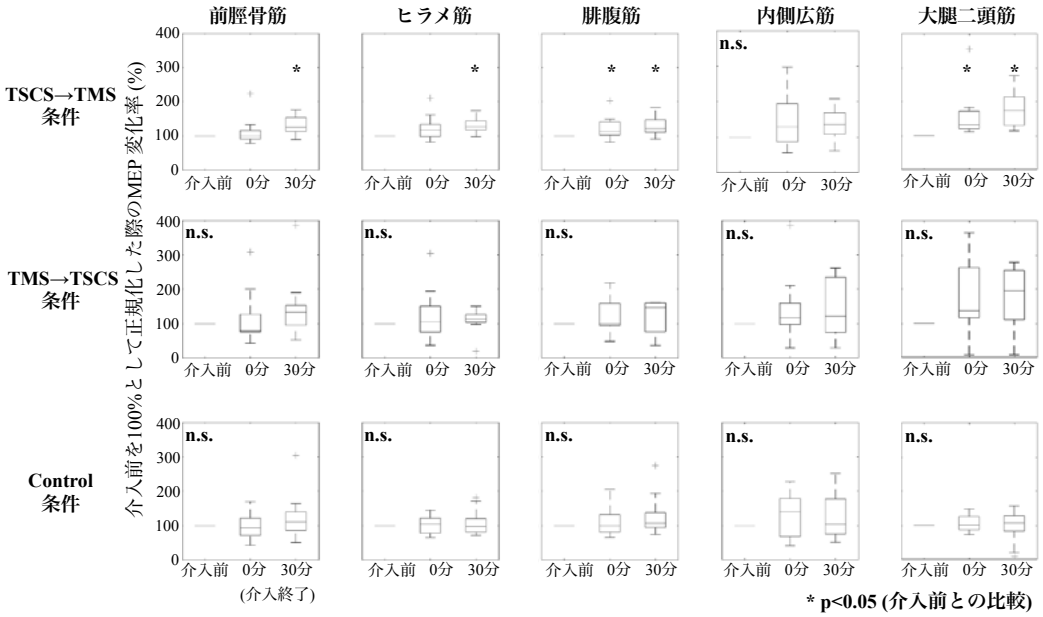

図 1 TSCS-PAS 介入後の MEP 変化率

参考文献

1) Jones, T.A. Motor compensation and its effects on neural reorganization after stroke. *Nat. Rev. Neurosci.* **18**, 267–280 (2017).
2) Stefan, K. et al. Induction of plasticity in the human motor cortex by paired associative stimulation. *Brain* **123**, 572–584 (2000).
3) Courtine, G. et al. Modulation of multisegmental monosynaptic responses in a variety of leg muscles during walking and running in humans. *J. Physiol.* **582**, 1125–1139 (2007).
4) Wolters, A. et al. A temporally asymmetric Hebbian rule governing plasticity in the human motor cortex. *J. Neurophysiol.* **89**, 2339–2345 (2003).
5) Kaneko, N. et al. The Effects of Paired Associative Stimulation with Transcutaneous Spinal Cord Stimulation on Corticospinal Excitability in Multiple Lower-limb Muscles. *Neuroscience.* **476**, 45–59 (2021).

磁気刺激による精神症状発症抑制効果の検討と そのメカニズムの解明

Inhibitory effects of magnetic stimulation on the onset of psychiatric symptoms and elucidation of the mechanism

古賀 農人[*], 戸田 裕之[*], 長峯 正典[**], 浅井 史穂[*], 吉野 相英[*]
Minori Koga[*], Hiroyuki Toda[*], Masanori Nagamine[**], Fumiho Asai[*] and Aihide Yoshino[*]

*防衛医科大学校 精神科学講座, 〒359-8513 埼玉県所沢市並木 3-2
**防衛医科大学校 防衛医学研究センター 行動科学研究部門, 〒359-8513 埼玉県所沢市並木 3-2
*Department of Psychiatry, National Defense Medical College
3-2 Namiki, Tokorozawa, Saitama 359-8513 Japan
** Division of Behavioral Science, National Defense Medical College Research Institute,
3-2 Namiki, Tokorozawa, Saitama 359-8513 Japan

Abstract

The effectiveness of repetitive transcranial magnetic stimulation (rTMS) has not been fully proven, for example, it is still unclear whether rTMS is effective in preventing recurrence and relapse in depression. The molecular mechanism of the effect of rTMS has been poorly understood. We investigated behavioral changes and gene expression changes in mice subjected to water immersion restraint stress, which induces depressive symptom-like behavior, when treated with rTMS. We found that rTMS increased the amount of spontaneous behavior. The results of gene expression analysis suggested that the Myd88 gene, which is involved in signaling innate immune responses, is the mechanism of the antidepressant effect of rTMS therapy.

Keywords: Repetitive transcranial magnetic stimulation, depression, microglia, inflammation

1. 目的

うつ病の生物学的な発症メカニズムは未だに解明されておらず，治療法や予防法の開発や創薬が他の身体疾患と比較して遅れている．最近の多くの研究により，脳における異常な炎症と精神症状との有意な相関が示されており，脳内免疫系は治療や予防におけるターゲットとして期待されている．かねて，抗うつ効果が期待されていた磁気刺激であるが，近年，反復経頭蓋磁気刺激（rTMS）が保険適用となった．しかしながら，現時点で維持療法（再燃・再発予防）に関する有効性は不明であることなど，効果については，明らかになっていない点が多い．また，生物学的な効果のメカニズムについても十分な証拠は得られていない．先行研究では，rTMS による炎症性サイトカインの発現抑制が示されていることなど[1]，磁気刺激には抗炎症作用が示唆されている．このことから，磁気刺激の作用点は脳内免疫系が示唆されているが，磁気刺激による改善効果のある病態や効果に関する詳細なメカニズムに関し

ては不明である．そこで本研究では，うつ病の病態モデルマウスを用いて，磁気刺激により改善する症状やその効果に関わる分子の探索を行った．

2. 方法

水浸拘束ストレスモデルの抑うつ症状様行動の分析

C57BL/6 マウス（8 週齢・オス）を馴化の後，マウスを穴の空いた 25mL のプラスチック製のコニカルチューブにいれ，顔にかからない深さの水を入れた容器に内に置き，3 時間の水浸拘束ストレスを負荷した．これを毎日，2 週間行い，最終のストレス負荷から 5 日後にオープンフィールドテストと強制水泳試験を行った（図 1A）．オープンフィールドテストでは，縦 43cm，横 43cm のフィールドにおけるマウスの 5 分間の自発行動を記録した．強制水泳試験は，直径 11cm，高さ 18cm の円筒に 12.5cm の深さになるように水を入れた容器に，マウスを入れ，6 分間の逃げようともがく行動を記録し，後半 5 分間の行動を分析に用いた．

水浸拘束ストレスが引き起こす抑うつ様行動とマイクログリアとの関係の分析

C57BL/6 マウス（6 週齢・オス）に，Elmore らの方法[2]に従い，PLX3397 を 3 週間投与することでマウスの脳におけるマイクログリアを除去した．その後，水浸拘束ストレスを負荷し，オープンフィールドテストおよび強制水泳試験を行った（図 2A）．マイクログリアの除去を確認するため，3 週間の PLX3397 投与後に，脳を摘出し，4%パラホルムアルデヒドで組織を固定した．固定後の脳から凍結切片を作成し，免疫組織蛍光染色により，マイクログリアのマーカー（IBA1）およびアストロサイトのマーカー（GFAP）を検出した．

rTMS による抗うつ効果の検証

馴化後の C57BL/6 マウス（8 週齢・オス）に水浸拘束ストレスを負荷した後，マグスティムラピッドシステム　MRS1000/50 を用いて，出力 57%に設定し，マウスの前頭部分にコイルをあて，15Hz で 150 パルスの刺激を 1 セットとし，3 セット与えた（各刺激の間隔は 36.5 秒）．これを 5 日間毎日行った後，オープンフィールドテストおよび強制水泳試験を行った（図 3）．行動実験の後，マウスの脳を摘出し，海馬を切り出し，総 RNA を抽出した．また，比較対照用のマウスからも同様に総 RNA を抽出した．総 RNA を cDNA に逆転写したものをテンプレートとして，標的遺伝子のプライマーセットを用いてリアルタイム PCR を行い，実験群間の遺伝子発現量比較を行った．

本研究で計画されている動物実験は，防衛医科大学校　動物実験倫理委員会の承認の下に，適正に実施された．

3. 結果

水浸拘束ストレス負荷を受けたマウスは，自発行動量や探索行動に関しては，対照と比較して差が認められなかったが（図 1C），強制水泳における無動時間の有意な延長が認められた（図 1D）．また，この行動変化にマイクログリアの存在が必要であるかを確認するために，マイクログリアを消去したマウスに強制水泳試験を行ったところ，マイクログリアが消去された状況（IBA1 陽性細胞の減少，図 2B）では，水浸拘束ストレスを負荷しても，無動時間の延長は認められなかった（図 2C）．次に，水浸拘束ストレス負荷マウスに対して，rTMS を与えたところ，強制水泳試験における無動時間の延長を抑制することはできなかった（図 3D）が，自発行動は上昇した（図 3B）．立ち上がり行動は有意ではなかった（図 3C）また，遺伝子発現量比較では，*Il-1β*，*Tnf-α*，*Tspo1* 遺伝子は，対照，ストレス，rTMS 群間に差は認められなかった（図 4A,B,E）．*Iba1*, *Gfap*, *Myd88*, *Tlr4* 遺伝子は水浸拘束ストレスに応答し，対照と比較して有意に発現が低下した（図 4C,D,F,G）．これらのうち，*Myd88* 遺伝子においては，ストレス負荷で有意に低下した発現が磁気刺激により対照群と同じレベルに回復していた．

4. 考察

水浸拘束ストレスにより生じた抑うつ症状様行動に対しては，rTMS による症状改善は認められなかった．これは，rTMS の処置期間が短く，生化学的な変化を反映していなかったのかもし

れない．しかし，磁気刺激の負荷により，自発的な行動に関しては有意な上昇が認められ，部分的ではあるものの，うつ病の一部の症状には有効であることが示唆された．また，生化学的な分析では，水浸拘束ストレスにより発現が低下する *MyD88* 遺伝子が rTMS により回復することが示された. MyD88 は炎症性サイトカインの産生といった自然免疫系の活性制御に関わるシグナル伝達を担う分子である．また，この遺伝子を欠損するマウスは，抑うつ様行動を示すことが報告されている [3]．これらのことから，この経路が，抑うつ症状に対する rTMS 療法の作用点であることが示唆された．最近の多数の研究にて，脳における免疫系の異常が抑うつ症状をはじめとする精神症状の病態形成に関わることが指摘されていることから，rTMS による脳内免疫系のコントロールが抑うつ効果のメカニズムなのかもしれない．MyD88 を介した伝達経路における下流の分子の動態など，さらなる詳細なメカニズムの解明が必要である．

謝辞

本研究は，公益財団法人 渡邉財団　第 27 回研究助成金の補助を受けて実施された（助成番号 02302）.

参考文献

1. Tateishi H, Mizoguchi Y, Kawaguchi A, Imamura Y, Matsushima J, Kunitake H, Murakawa T, Haraguchi Y, Kunitake Y, Maekawa T, Kato TA, Asami T, Monji A. Changes in interleukin-1 beta induced by rTMS are significantly correlated with partial improvement of cognitive dysfunction in treatment-resistant depression: a pilot study. Psychiatry Res. 2020 Jul;289:112995.
2. Elmore MR, Najafi AR, Koike MA, Dagher NN, Spangenberg EE, Rice RA, Kitazawa M, Matusow B, Nguyen H, West BL, Green KN. Colony-stimulating factor 1 receptor signaling is necessary for microglia viability, unmasking a microglia progenitor cell in the adult brain. Neuron. 2014 Apr 16;82(2):380-97.
3. Choudhury ME, Mikami K, Nakanishi Y, Matsuura T, Utsunomiya R, Yano H, Kubo M, Ando R, Iwanami J, Yamashita M, Nagai M, Tanaka J. Insomnia and depressive behavior of MyD88-deficient mice: Relationships with altered microglial functions. J Neuroimmunol. 2022 Feb 15;363:577794.

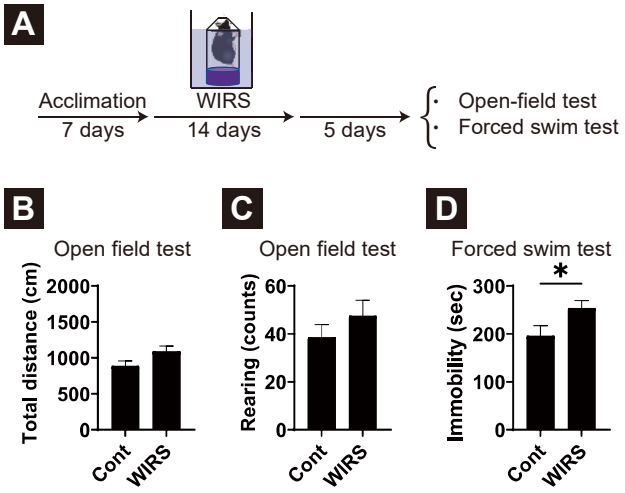

図 1　水浸拘束ストレス負荷マウスの行動
実験工程（A）．オープンフィールドテストによる自発行動量（B）と立ち上がり行動（C）．強制水泳による無動時間（D）．*（p<0.05）は t 検定の結果を示す．

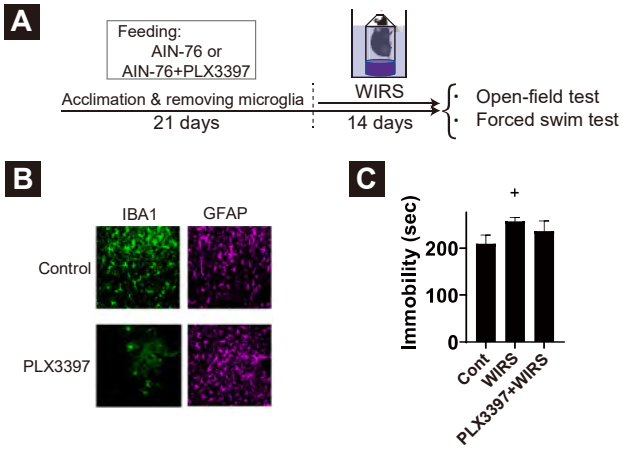

図 2　マイクログリアを消去したマウスのストレスに対する行動変化
実験工程（A）．マイクログリアマーカー（IBA1）とアストロサイトマーカー（GFAP）の免疫組織蛍光染色の結果（B）．強制水泳による無動時間（C）．+（p<0.1）は Dunnett 検定による対照（Cont）との比較の結果を示す．

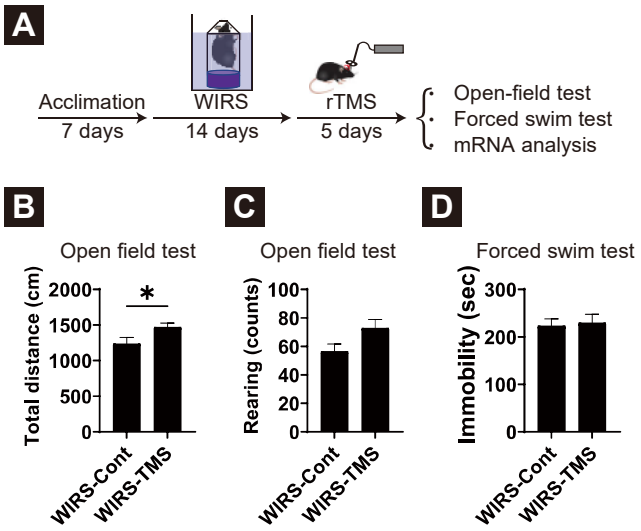

図 3　反復経頭蓋磁気刺激の抑うつ症状様行動に対する効果の検討
実験工程（A）．オープンフィールドテストによる自発行動量（B）と立ち上がり行動（C）．強制水泳による無動時間（D）．*（p<0.05）は t 検定の結果を示す．

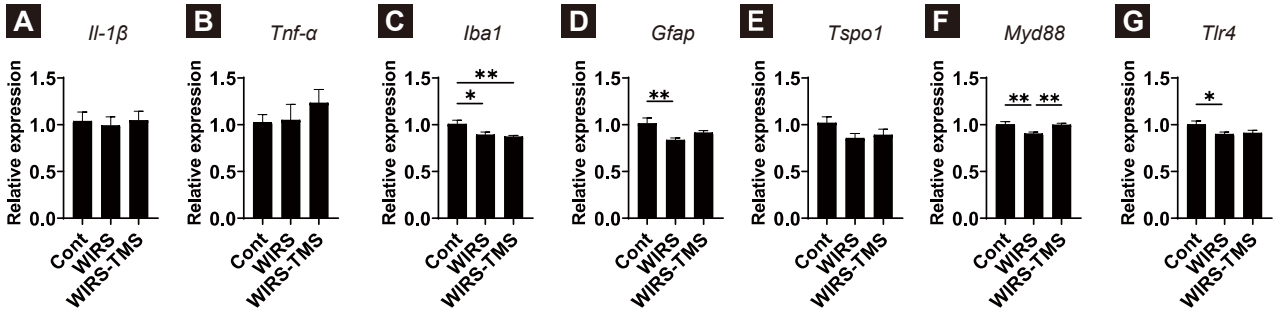

図 4　リアルタイム PCR による遺伝子発現解析の結果
炎症性サイトカイン IL-1β（A），TNF-α（B），マイクログリアのマーカーIBA1（C），アストロサイトのマーカーGFAP（D），活性化型グリアのマーカーTSPO1（E），免疫応答に関わるシグナル伝達分子 MyD88（F）および TLR4（G）をコードする遺伝子発現量比を示す．*(p<0.05)，**(p<0.01)は Tukey 検定の結果を示す．

低頻度磁気刺激による神経ブロック効果

Nerve block effect with low-frequency magnetic stimulation

金田恵理
Eri Kaneda

大阪大学大学院医学系研究科，〒565-0871 大阪府吹田市山田丘 2-2
Department of Cardiovascular Surgery, Graduate of Medicine, Osaka University
2-2 Yamadaoka, Suita-shi, Osaka 565-871 Japan

Abstract

Stellate ganglion block injections for the relief of neuropathic pain and autonomic abnormalities are associated with risks. To ameliorate these problems, there is an attempt to obtain therapeutic effects by applying low-frequency magnetic stimulation to the ganglion and suppressing its function. Using a neodymium magnet, a large magnetic field gradient of 7-9 mT/mm was applied to a rat ganglion for a short time, and the increase in sympathetic nervous system parameters of blood pressure was suppressed. This study confirmed the nerve blocking effect of low-frequency magnetic stimulation.

Keywords: low-frequency magnetic stimulation, sympathetic nervous system

1. 目的

神経障害性疼痛や自律神経異常等の緩和を目的に, 麻酔科やペインクリニックにおいて, 星状神経節ブロック注射という治療が行われている. これは頸部に存在する神経節の１つである星状神経節の近傍に局所麻酔薬を注入することで, 星状神経節の活動を抑制するという侵襲を伴う手技である. この手技は頸動脈の近くに針を刺すリスクがあることや, 眼瞼下垂を代表とするホルネル症候群が高頻度で起こり, 患者にとって好ましくない. 加えて, この施術を受けるためには通院が必須であることも, 継続して治療を受けることへの壁になっている.

一方で, 近年, 同部位への低頻度磁気刺激が星状神経節ブロック注射と同様の作用（以下, ブロック効果と呼ぶ）をもたらす可能性が報告されている [1]. ある研究では, ラットの神経節に対して長期的な磁気刺激を行うことで, アドレナリン作動薬を投与したときの交感神経系パラメータの上昇を抑制できたとの報告もある [2].

そこで, 星状神経節ブロックを非侵襲的に行う手法ならびに装置を確立することを目的に, ラットへの短期的な低頻度磁気刺激によるブロック効果を実証することとした.

2. 方法

2-1. 供試動物に適する磁石の選定

10 週齢雄ヌードラット（体重 220±10g）の解剖学を参考にした磁場シミュレーション解析の結果を元に, 第１頸椎レベルの頸動脈の裏側の位置に 7～9mT/㎜ の磁場勾配を生じるような形状のネオジム磁石を選定した. また, Sham 磁石として同様の形状であり, 磁性をもたない金属を用意した.

2-2. アドレナリン作動薬の投与量決定

交感神経亢進様状態の作出方法として, 血圧を上昇させる作用のあるアドレナリン作動薬を腹腔内投与することとした. 前試験により, 60 分間の間, 血圧を 30-60%の範囲で安定的に維持する投与量を求めた.

2-3. ラットへの磁石装着とブロック効果

麻酔導入後, 尾静脈における非観血的な収縮期血圧測定において, まず 5 分以上の血圧の安定が得られたことを確認する. このときの血圧を Pre 値とする. その後, アドレナリン作動薬を腹腔内投与し, Pre 値の 130%にまで血圧が達したタイミングから磁石またはSham磁石を装着し, 45 分間血圧変化の観察を開始する. 45 分間の経過観察後, それらを取り外し, さらに 15 分間観察を続け, 計 60 分間の観察を完了させる.

3. 結果

3-1. Sham 磁石を装着した個体

麻酔下において, 血圧の Pre 値は 120㎜Hg を安定的に示した. 2-2 で求めた投与量のアドレナリン作動薬を腹腔内投与後, 直ちに血圧が上昇し始めた. 130%の血圧上昇に達した時点で, 2-1 で示した Sham 磁石を適切な部位に装着した. その後 30 分間以上もの間, 血圧は 160㎜Hg (133%) を超えたままであった. 観察開始から 45 分後に Sham 磁石を取り外した後も, 140㎜Hg (117%) のまま推移し, 観察終了後も血圧が Pre 値に近づく傾向はなかった.

3-2. ネオジム磁石を装着した個体

麻酔下において, 血圧 Pre 値 90㎜Hg を安定的に示した. アドレナリン作動薬の腹腔内投与後, Sham 磁石を装着した個体と同様に直ちに血圧が上昇し, 140㎜Hg (156%) にまで達した. ネオジム磁石を適切な部位に装着後, 7 分を経過した頃から血圧が次第に低下し始めた. 装着後 30 分経過した時点で 110㎜Hg (122%), 装着 45 分後には 90㎜Hg を記録した. 観察を終了し, ネオジム磁石を取り外した後も, 若干の血圧低下傾向は止まらず, 観察終了時のラットの収縮期血圧は Pre 値よりも低い 85㎜Hg (94%) であった.

4. 考察

ネオジム磁石を利用したラットにおける低頻度磁気刺激が, 薬剤投与により作出した交感神経亢進様状態の一つである血圧上昇を明らかに抑制した. これは低頻度磁気刺激が神経細胞に作用することでもたらされる電位の変化がイオンチャネルの配向を変え, 神経活動を抑制するという機序に起因することが示唆された.

本研究では, 生体に作用するには比較的大きな磁場勾配を神経節に与えており, 短時間で神経抑制効果が得られた. 結果として収縮期血圧の上昇を強く抑制することが出来た. 低頻度磁気刺激による短時間での神経抑制効果の報告は私の知る限りなく, 実用的な知見を得たことは大きな成果である.

一方で, 医療機器への転用を考えた場合, 安全性と有効性が担保された閾値を求めることは必須である. 例えば, 磁束密度の 37.9mT の静磁場は感覚神経の活動を 80%抑制する[3]との報告があるが, どの程度の神経細胞の活動抑制が機能全体としての神経抑制に結びつくかといったことや, どの範囲の磁場勾配が安全に神経を抑制するかは未知である. 今後, 人体により近いサイズのブタを供しての研究を予定しており, 磁場シミュレーションと連動した低頻度磁気刺激による交感神経抑制効果の検証を行う予定である.

謝辞

本研究は, 公益財団法人渡邉財団による第 27 回岡井治特別研究助成を受けて実施したものである.

参考文献

1) Timothy M. Markman, Roy H. Hamilton, Francis E. Marchlinski, Saman Nazarian. Case series of transcutaneous magnetic stimulation for ventricular tachycardia storm. JAMA 2;323(21):2200-2202 (2020).
2) Hideyuki Okano, Chiyoji Okubo. Effects of 12mT static magnetic field on sympathetic agonist -induced hypertension in wistar rats. Bioelectromagnetics 28:369-378 (2007).
3) Arthur D. Rosen. Thereshold and limits of magnetic field action at the presynaptic membrane. Biochemica et Biophysica Acta, 1193.62-66(1994).

脳磁計測を用いた脳内多感覚統合の動的な理解と直感的な脳-機械インタフェースへの応用

Understanding of multisensory integration of brain by magnetoencephalography and application to multisensory brain-machine interface

小谷潔*
Kiyoshi Kotani*

*東京大学先端科学技術研究センター，〒153-8904 東京都目黒区駒場 4-6-1
*Research Center for Advanced Science and Technology, The University of Tokyo
4-6-1 Komaba, Meguro-ku, Tokyo 153-8904 Japan

Abstract

Brain machine interface (BMI) is an interface that reads the user's intention from the brain activity in real time. In spite of its potential to alter the human interface and communications, there is a disadvantage that the speed of BMI is still slower than other types of interface. In this research, we obtain the brain activity by magnetoencephalograms and investigate the fundamental properties of integrating multi-sensory information in the brain. Then we propose a feasible BMI system with multi-sensory augmented reality technology.

Keywords: Multisensory Integration, Brain Machine Interaction

1. 目的

脳-機械インタフェース(brain-machine interface: BMI) は，ヒトの脳活動による神経電流を制御信号として用いて機器を操作するシステムであり，重度の身体障害を持つ患者の生活を支援するシステムとして期待されている．[1)]実生活に即した BMI として, 拡張現実 (Augmented Reality: AR) 技術を用いた BMI が開発されている．[2)]AR を用いる BMI には, 情報転送速度を向上させるために, 多感覚刺激を提示するものがある．しかし，多感覚刺激の情報が脳内で統合される過程の多くは未解明である．また，近年の脳磁計測において，常温で作動する小型の光ポンピング磁力計 (optically pumped atomic magnetometer: OPM) が開発された．[3)]OPM は，ペーストを用いずに任意の位置に装着可能であり，SQUID-MEG よりも感度が高いため, BMI の精度を向上させる可能性がある．

そこで本研究では，基礎的な研究として，視聴覚刺激に対する応答を高い時空間分解能を持つ脳磁図を用いて計測し，強度と時空間的な局在性の解析を行った．また BMI に OPM-MEG を用いることが可能かの基礎的な検証を行った．さらに, 実用的な BMI の構築に向けた応用研究として, AR を用いて任意の位置および方向に移動と回転が可能な車椅子 BMI と, 環境認識を用いて AR 上で物体選択が可能な BMI の開発を行った.

2. 脳磁図による時空間的な局在性の指標を用いた脳活動の評価

2.1. 方法

計測には 160 チャネルの磁気センサを持つ脳磁計（脳磁計システム RICOH160-1，株式会社リコー）を用いた．視覚と聴覚で選択肢の数が異なる

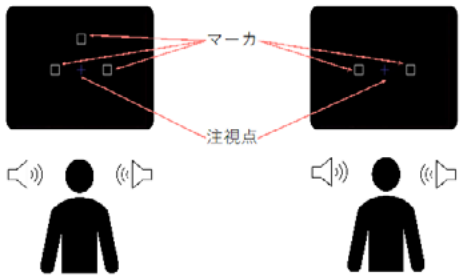

図 1. 視聴覚刺激提示の様子．左側は視覚的選択肢が 3 種類の課題 1，右側は視覚的選択肢が 2 種類の課題 2 である．

2 種類の課題を行った．視覚刺激としてスクリーンに描画したマーカを発光させ，聴覚刺激として 400 Hz の純音を提示した(図 1)． 被験者には，発光したマーカの位置および提示された音の方向が実験前の指示と一致した場合のみボタンを押すよう指示した．

解析では，刺激の種類を標的（ボタンを押すよう指示した刺激），視覚のみ正解の刺激，聴覚のみ正解の刺激，両方不正解の刺激の 4 種類とし，種類ごとに応答波形を加算平均した．160 チャネルの振幅の二乗平均平方根を時間平均した値を反応強度とし，また時空間的な局在性の指標としてチャネルごとの全振幅の 2 乗値の分布から尖度を求めた．

2.2. 結果と考察

課題 1 では，16 回の計測のうち 5 回で標的，9 回で視覚のみ正解の刺激の反応強度が最大となった．多重比較の結果，反応強度について図 2 のように有意差が見られた．

課題 2 では，10 回の計測のうち 6 回で標的，1 回で視覚のみ正解の刺激，2 回で聴覚のみ正解の刺激の反応強度が最大となった．反応強度と尖度に有意差は見られなかった．

視覚的な選択肢が 3 種類あった課題 1 では視覚のみ正解の刺激の反応強度も高い傾向があった．一方，視覚刺激の選択肢が 2 種類あった課題 2 では同様の傾向は見られなかった．したがって、選択肢が多い場合は視覚刺激の情報を優先的に判断しており，視覚優位性の影響が現れたと考えられる．また，どちらの課題についても刺激の種類間で尖度に有意差がなかったことから，時空間的な局在性の違いは観察されなかった．

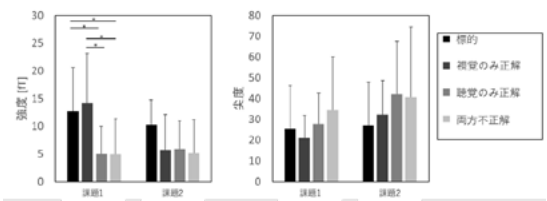

図 2. 振幅の強度および尖度．* p < 0.05

従来の研究では，心理学的手法を用いて視聴覚刺激を提示する実験を行い，視聴覚刺激に対する正答率から，視覚有意性が示されていた [4, 5]．本研究では，脳活動計測により先行研究と同様に視覚優位性が示された．

3. 光ポンピング磁気センサを用いた脳活動の計測

3.1. 方法

計測には，OPM-MEG センサ（QZFM Gen-2, QUSPIN）を 2 個用いた．

実験 1 では，α 波を誘発する課題を行った．OPM-MEG センサを視覚野付近に配置し，被験者は合図の音に合わせて，開眼と閉眼を繰り返した．

実験 2 では，N100m を誘発する課題を行った．OPM-MEG センサを聴覚野付近に配置し，被験者に 400 Hz の純音を 540 回提示した．また，SQUID-MEG を用いて同様の課題を行った．

3.2. 結果と考察

α 波を誘発する実験 1 については, 閉眼時に 10 Hz 付近のスペクトル強度が高くなり， α 波の強度が増加したことが確認された(図 3)．したがって，定常状態視覚誘発磁場を用いる BMI に OPM-MEG を用いることが可能であると考えられる．

N100m を誘発した実験 2 については，刺激提

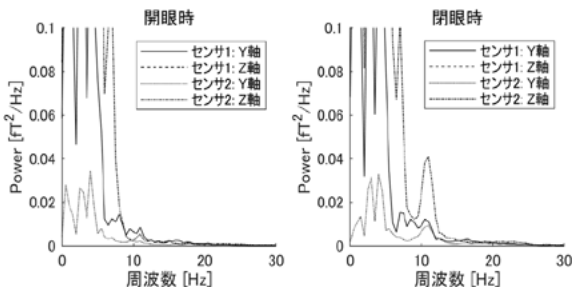

図 3. 開眼時および閉眼時における周波数スペクトル．

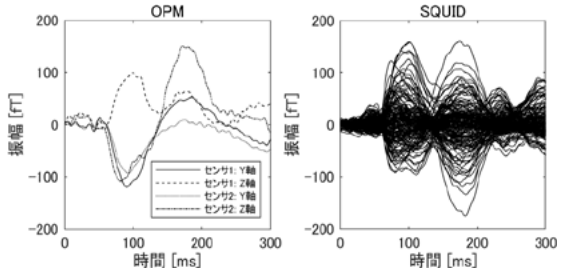

図4.　OPM-MEGおよびSQUID-MEGで観測されたN100mの波形.

示後 100 ms 付近にピークを持つ N100m が SQUID-MEG での計測と同様に，OPM-MEG の計測でも確認された(図 4)．したがって，ミリ秒単位で変化する応答波形を用いてユーザの意図を識別する BMI に OPM-MEG を用いることが可能であると考えられる．

4. 多感覚刺激を用いた車椅子 BMI の開発

4.1 方法

視聴覚刺激の提示には，AR ゴーグル(Microsoft 社製 HoloLens) を用いた．HoloLens を用いて，現実の空間情報を取得し，ディスプレイを通して仮想マーカおよび仮想音源を被験者の周囲に配置した (図 5)．視覚刺激は仮想マーカの発光であり，被験者は車椅子に座り，脳波計と HoloLens を装着した．

車椅子を前進させる課題では，被験者は予め指示されたマーカが発光する回数を数えた．車椅子を回転させる課題では，被験者は予め指示された方向から音が提示される回数を数えた．

4.2. 結果と考察

被験者 4 名について，リーブワンアウト交差検証により識別率を検証した結果，識別率の平均は

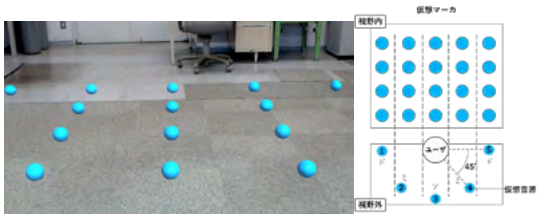

図 5. HoloLens による仮想マーカおよび仮想音源の配置の様子．左はゴーグルから見える視野の様子．右は仮想マーカおよび仮想音源の配置位置.

62.5%であった．仮想マーカおよび仮想音源を合計で 25 個配置したため，チャンスレベルは 4%であり，全被験者の識別率はチャンスレベルを上回った.

空間情報を取得し，仮想マーカや仮想音源を配置することで，任意の位置や方向に移動と回転が可能な BMI の可能性が確認できた.

5. 物体検知と環境認識を用いた AR-BMI の開発

5.1. 方法

AR ゴーグル(Microsoft 社製 HoloLens2)のカメラで撮影した画像から，SSD (Single Shot Multi-box Detector)により物体を検出し，深度センサから生成したマップと組み合わせることで空間内での物体の位置を算出し，AR 空間内の対応する座標に選択肢を表示した．各選択肢を同時に 8~14 Hz で 4 秒間明滅させた際の定常状態視覚誘発電位 (SSVEP)の周波数強度を算出することで，使用者が注目した選択肢を推定した．実用性評価のために被験者 4 名で各 20 回の計測を行い，推定精度を算出した.

5.2. 結果と考察

全被験者で推定精度はチャンスレベルの 25%を上回り，物体検知開始から選択肢の推定終了まで 7 秒以内であった.

シースルー型ディスプレイを用いたことで推

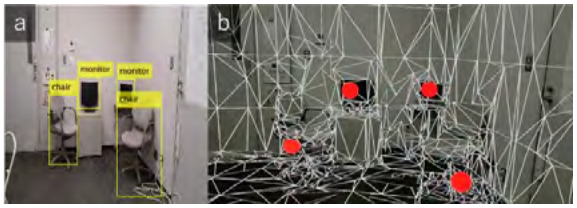

図 6. (a) 実空間内の物体検知の様子. (b) AR 空間上での空間認識と選択肢配置の様子

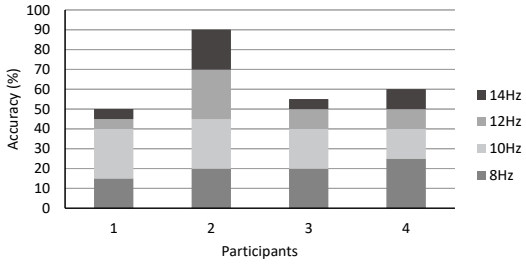

図 7. 被験者毎に算出した推定精度

定精度の低下や個人差が見られたが，機械学習や環境認識を取り入れ動的に選択肢を配置するBCIシステムの可能性が確認できた.

謝辞

この研究は渡邊財団の補助を受けて実施したものである.また，本論文の内容は2021年11月1-5日にオンラインで開催された『43rd Annual International Conference of the IEEE Engineering in Medicine and Biology Society』および2021年9月15-17日にオンラインで開催された『2021年電気学会電子・システム・情報部門大会』および『電気学会論文誌C，2020年7月号』で報告した内容を一部含むものである.

参考文献

1) J. Wolpaw et al. Brain-computer interfaces for communication and control, *Clinical Neurophysiology*, Vol.113, No.6, pp.767-791 (2002).
2) K. Takano et al. Towards intelligent environments: an augmented reality–brain–machine interface operated with a see-through head-mount display, *Frontiers in neuroscience*, Vol. 5, No. 60 (2011).
3) E. Boto et al. Moving magnetoencephalography towards real-world applications with a wearable system. *Nature*, Vol. 555, No. 7698, pp. 657-661 (2018).
4) F.B. Colavita. "Human sensory dominance." *Perception & Psychophysics*, Vol. 16, No. 2, pp. 409-412 (1974):
5) S. Sinnett, et al. "Visual dominance and attention: The Colavita effect revisited." *Perception & Psychophysics*, Vol. 69, No. 5, pp. 673-686, (2007).

令和3年度　研究助成テーマ

令和3年度は、以下のように、第28回 11名（基礎5名・応用4名・テーマ指定2名）30周年記念特別助成2021 1名の研究に対し助成が決定いたしました。

Ⅰ. 基礎研究

Ⅰ-1. 静磁場による脾臓由来IL-10誘導を用いた認知症発症予防の試み
大分大学医学部　内分泌代謝・膠原病・腎臓内科学講座／後藤　孔郎

Ⅰ-2. 生体内局所電磁場と原子核スピンの相互作用計測と新規現象探索
東京大学　大学院工学系研究科／島添　健次

Ⅰ-3. 磁気刺激による内耳前庭系を介した反射機能改善の検証
岐阜医療科学大学　大学院保健医療学研究科／田中　邦彦
＜この研究は岡井治特別研究助成に選ばれました＞

Ⅰ-4. 磁気刺激を用いた神経回路創出法の確立
同志社大学／正水　芳人

Ⅰ-5. がん温熱療法と診断を目指した磁気ナノ微粒子の創製
横浜国立大学／一柳　優子

Ⅱ. 応用研究

Ⅱ-1. 反復経頭蓋磁気刺激併用認知リハビリテーションによる認知機能改善効果の検証
順天堂大学　大学院医学研究科リハビリテーション医学／高倉　朋和

Ⅱ-2. 超小型ナノカプセル19F MRI造影剤の開発
大阪大学　大学院工学研究科／蓑島　維文

Ⅱ-3. 上肢の局所性ジストニアに対する装着型器機を用いた磁気刺激治療
藤田医科大学／藤村 健太

Ⅱ-4. 磁性ナノ粒子を用いた細胞小器官の膜損傷とナノ粒子の細胞外への排出の研究
岩手大学　理工学部　生命コース／芝　陽子

Ⅲ. テーマ指定研究

Ⅲ-1. 統合失調症のガンマ帯域神経振動異常におけるAMPA型グルタミン酸受容体の役割
九州大学　大学院医学研究院　精神病態医学／田村　俊介

Ⅲ-2. 核磁気共鳴エラストグラフィーを用いた肝うっ血評価による心不全の非侵襲リスク層別法の開発
北海道大学　大学院医学研究院　循環病態内科学教室／永井　利幸

Ⅳ. 30周年記念特別助成2021

Ⅳ-1. 治療抵抗性統合失調症に対する最新鋭ニューロモジュレーションの開発
慶応義塾大学　医学部　精神神経科学教室／中島　振一郎

なお、所属は研究助成決定当時のものです。

THE REPORT OF STUDY

RESULT BY SUBSIDY

27TH

(STUDY DURATION : April 1, 2021 - March 31, 2022)

Special Research Grant 2018

(STUDY DURATION : April 1, 2019 - March 31, 2022)

The Watanabe Foundation

CONTENTS

Preface

About 45 years ago, I have been researching feeble magnetic measurements from the human body in order to help diagnose the disease at the Massachusetts Institute of Technology (MIT) in the United States for two years. I have been studying biomagnetism measurement after returning home.

It has been estimated that weak magnetism is generated from human heart and brain, but there was no magnetometer capable of measuring this weak magnetism. However, in the 1970s, an ultra-sensitive SQUID magnetometer using superconducting technology was developed in collaboration between US National Research and MIT.

When the magnetic measurement from heart using this SQUID magnetometer was successful and challenging magnetic measurements from the brain of about 1 / 1,000 of cardiac magnetism, I had been studying at MIT.

MIT laboratory was in big trouble during my study abroad. A prominent doctor in the United States criticized of MIT's research as follows. "They say that they measure the magnetism caused by nerve activity of heart and brain, but that is incorrect. They are only measuring the magnetism that the iron in the blood is disturbing the geomagnetism." As a result, the public research expenditure in the US for MIT biomagnetism research was greatly reduced.

I regarded his theory as correct. Therefore, I measured more than ten blood with SQUID magnetometer, but it turned out that blood had no magnetism at all.
The reason is that iron itself always has magnetism, but it has strong magnetism or no magnetism at all depending on the bonding method of iron and oxygen. Iron in the blood binds to oxygen so that it has no magnetism at all.
The evolution of mankind has progressed from birth to bipedalism to communication through spoken language over 2millions of years. The strength and directions of the geomagnetism have changed about ten times during the years. Since humans have evolved in such magnetic environment, human body have made to have little effect of geomagnetism.

On the other hand, it has been only 200 years or so since humans started using electricity. The humans have not developed full defensive capabilities against it. Therefore, a human body is vulnerable and sensitive to electricity: a heart stops beating once a couple of voltages are applied to the chest, however, it is quite difficult to stop a heart when magnetism is applied externally.
In view of this, it is fair to say that electric medical devices bring an immediate effect. However, they could be dangerous once misused. In contrast, magnetic medical devices are not dangerous, but they must be used for a long time for treatment.

Our foundation intends to contribute to the health and medical care of the nation, by subsidizing scientific research and appealing to the society through seminars. It should be noted, that the effect of the magnetic field is generated from some basic phenomena interacting with the complex mechanism of the body. The effect can only be clarified by a long-term persistent effort, not by short-sighted research.

It is a regrettable tendency in the present scientific sector that researchers are mostly interested in achieving successful results for acquiring a degree or achievement in a short period, focusing on obvious cause-effect relationship or phenomenon which invites quantitative descriptions. In view of such a tendency, our foundation prefers to support researchers who persistently attack a particular problem expecting long-term results rather than those who rush into short-term results.

This report is the summary of research which our foundation supported in the fiscal year 2020 It includes a wide range of topics from basic aspects to practical applications, intending to pave new ways in this area. It is our hope that the report will motivate researchers with similar interests to start communication and contribute to the development of magnetic health science.

Director Makoto Kotani
The Watanabe Foundation

Magnetic Field Effects on Photodynamic Therapy

Hiroaki Yonemura

Faculty of Engineering, Sojo University
4-22-1 Ikeda, Nishi-ku, Kumamoto 860-0082, Japan

Abstract

The magnetic field effects on the generation of singlet oxygen ($^1O_2^*$) in photodynamic therapy (type II of PDT) using fullerene derivatives (such as C_{70}) as photosensitizers were investigated in CCl_4 or CS_2 solution of fullerene derivatives. $^1O_2^*$ generation was evaluated by directly observing the phosphorescence of $^1O_2^*$ obtained around 1275 nm due to the photoexcitation of fullerene derivatives. The phosphorescence intensity of $^1O_2^*$ varied with magnetic fields as compared to that without a magnetic field. The magnetic field effects on the generation of $^1O_2^*$ due to type II of PDT were observed for the first time. The magnetic field effects can be explained in terms of triplet-triplet pair mechanism.

Keywords: photodynamic therapy, singlet oxygen, phosphorescence, magnetic field effect, triplet-triplet pair

1. PURPOSE

Type II of photodynamic therapy (PDT) is a major therapeutic treatment using light and medicine (photosensitizer), which generates singlet oxygen ($^1O_2^*$) as reactive oxygen species due to photoirradiation (Fig. 1). We take notice of the generation of $^1O_2^*$, because the efficiency of the generation of $^1O_2^*$ is important to improve the efficiency of PDT. One of the direct generations of $^1O_2^*$ is measurement of the emission due to $^1O_2^*$. However, it is difficult to detect the emission due to $^1O_2^*$, since the emissions due to $^1O_2^*$ are observed around 1275 nm in infrared wavelength region and the emissions due to $^1O_2^*$ are very weak.

The mechanisms of photochemical reactions in the condensed phase have been explained by considering magnetic field effects (MFEs) on reaction kinetics or yields. Consequently, the magnetic field is expected to provide a novel way to control photochemical reactions and subsequent processes. Previously, we have found the MFEs on photoinduced electron transfer and/or photoelectrochemical reactions in donor–acceptor linked compounds, semiconductor nanoparticles, C_{60} nanoclusters, and conductive polymers. Recently, we have MFEs on photon upconversion based on sensitized triplet–triplet annihilation (PUC-TTA) and the singlet exciton fission (SF) due to triplet-triplet (T-T) pair mechanism.[1,2] Similar T-T pair is generated by triplet–triplet energy transfer reaction (TTET) in type II of PDT (Fig. 1). However, the MFEs on the generation of $^1O_2^*$ in PDT have been reported yet. Therefore, in this study, we examined the MFEs on the generation of $^1O_2^*$ in type II of PDT.

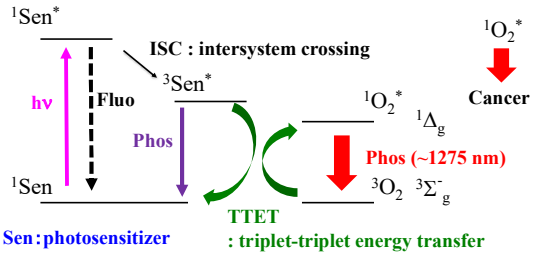

Fig. 1. Reaction mechanism for type II of PDT using photosensitizer (Sen).

2. METHOD

The fullerene derivatives (such as C_{70}) were used as photosensitizers for this measurement of $^1O_2^*$ due to Type II of PDT. The CCl_4 solutions (20 μM) of C_{70} and C_{70}PCBM or CS_2 solutions (20 μM) of C_{70} and C_{60} were prepared. The extinction spectra of the solutions and the sample solutions were recorded on a Shimadzu UV-3150 spectrometer at room temperature. The florescence and the phosphorescence spectra of the sample solutions were recorded on a Horiba Fluorolog-3 (UV-Vis-NIR) spectrometer. The MFEs on the phosphorescence spectra of $^1O_2^*$ for sample solutions of C_{70}, C_{60} and C_{70}PCBM was measured using an electromagnet and a 450 nm continuous-wave (CW) DPSS laser (MDL-III-450-100 mW, Changchun New Industries) in a similar manner to that described in previous paper.[1,2] The sample solutions were placed in the pole gap of an electromagnet. The magnetic field strength was measured by a gauss meter (410 Gaussmeter, Lake Shore).

3. RESULTS

The phosphorescence spectra of $^1O_2^*$ were clearly observed at 1275 nm, when the CCl_4 solution of C_{70} was excited by visible light (450 nm) using from Fluorolog-3 spectrometer. The excitation spectrum for $^1O_2^*$ (1275 nm) was in good agreement with the absorption spectrum in the CCl_4 solution of C_{70}. The results strongly indicate that C_{70} acts as a photosensitizer for Type II of PDT mechanism.

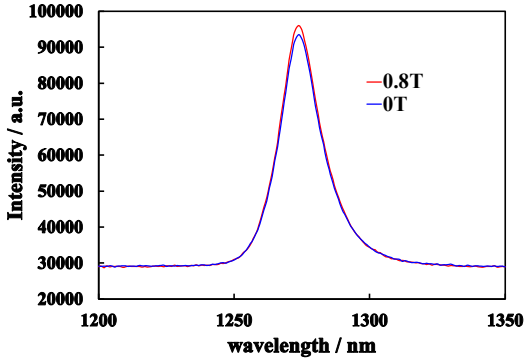

Fig. 2. Magnetic field Effect on phosphorescence spectra of $^1O_2^*$ in CCl_4 solutions of C_{70} under atmospheric pressure without and with magnetic field (0.8 T) (λ_{ex} = 450 nm).

Next, The MFEs on the phosphorescence spectra of $^1O_2$*were measured in the absence and the presence of magnetic field by the combination of the Fluorolog-3 spectrometer with the CW DPSS laser (450 nm) and the electromagnet. Similarly, the phosphorescence spectra of $^1O_2^*$ were clearly observed at 1275 nm in the absence and the presence of magnetic field using the CW DPSS laser (450 nm). The phosphorescence intensity of $^1O_2^*$ in the presence of magnetic field (0.8 T) was larger than that in the absence of magnetic field (Fig. 2). The phosphorescence intensities of $^1O_2^*$ were varied with increasing magnetic field strength.

The magnitude of the MFEs on phosphorescence intensities of $^1O_2^*$ at 1275 nm can be expressed as:

$$Q = (I(B)–I(0))/I(0) \times 100 \qquad (1)$$

where I(0) and I(B) are the phosphorescence intensities of $^1O_2^*$ in the absence and the presence of the magnetic field (B), respectively, as reported previously.

Q became slightly negative in the lower magnetic fields (B = 0.1, 0.2 T) and then Q increased gradually in the higher magnetic fields (0.3 ≦ B ≦ 0.8 T) in the CCl_4 solution of C_{70}, as shown in Fig. 3. Similarly, in the CCl_4 solution of C_{70}PCBM, Q became slightly negative in the lower magnetic field (B = 0.1 T) and then Q increased gradually in the higher magnetic fields (0.2 ≦ B ≦ 0.8 T).

In addition, similar MFEs on phosphorescence intensities of $^1O_2^*$ were observed in the CS_2 solutions of C_{70} and C_{60}.

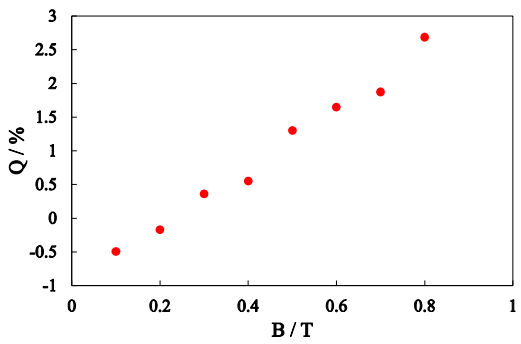

Fig. 3. Magnetic field dependences on the Q-value of the phosphorescence intensities of $^1O_2^*$ at 1275 nm in the CCl_4 solution of C_{70} under atmospheric pressure.

4. DISCUSSION

In this study, the MFEs on phosphorescence intensities of $^1O_2^*$ due to type II of PDT were observed for the first time. These MFEs on phosphorescence intensities of $^1O_2^*$ can be explained in terms of hetero TT pair mechanism in triplet–triplet energy transfer reaction from triplet excited state of photosensitizer ($^3Sen^*$) such as C_{70} to $^3O_2$ as shown in the following equation (2).

$$^3Sen^* + {}^3O_2 \rightarrow {}^l(TT) \rightarrow {}^1Sen + {}^1O_2^* \ (l = 1, 3, 5) \qquad (2)$$

Also, the negative MFEs are most likely attributable to hyperfine coupling mechanism in T-T pair and positive MFEs are most likely responsible for Δg mechanism due to large difference of g-values between $^3Sen^*$ and $^3O_2$ in T-T pair.

Further investigations regarding the mechanism in the MFEs on phosphorescence intensities of $^1O_2^*$ due to type II of PDT including the MFEs using the other photosensitizers are now in progress. We will try to examine the MFEs on PDT in live cells in near future.

ACKNOWLEDGMENT

H.Y. deeply acknowledges Watanabe Foundation to perform this research.

Some parts of this research were reported in the 15th Annual Meeting of the Magneto-Science Society of Japan held on 2021/11/15-17 by hybrid meeting (in Kagoshima University and internet).

REFERENCES

1) Y. Noda, F. Shibata, S. Fukuda, G. S. Y. Lee, H. Sakaguchi, H. Yonemura, *Jpn. J. Appl. Phys.*, **59**, SDDB04 (2020).
2) H. Yonemura, D. Aira, N. Asakura, K. Ezoe, H. Sakaguchi, *Jpn. J. Appl. Phys.*, **59**, SDDB03 (2020).

Amelioration of pathological states by mitophagy induced by extremely low frequency fluctuation of extremely weak magnetic fields

Kinji Ohno*

*Neurogenetics, Graduate School of Medicine, Nagoya University
65 Tsurumai-cho, Showa-ku, Nagoya 466-8550 Japan

Abstract

The molecular mechanisms of the effects of weak magnetic fields have not been well dissected. We found that extremely low frequency fluctuation (1-8 Hz) of extremely weak magnetic field (100 mG) (ELF-WMF) provokes the mitochondrial quality-assurance system, mitophagy, and reduces the amount of mitochondrial to two thirds of that before stimulation. The mitochondrial membrane potential was similarly reduced. ELF-WMF later induces mitochondrial neogenesis, which increases the amount of mitochondria and the mitochondrial membrane potential. Exposure of ELF-WMF to wild-type mice showed increased basal oxygen consumption, increased mitochondrial membrane potential, and increased mitochondrial electron transport complex activities in the liver. The mice showed increased voluntary activities, which, however, were not quantitatively evaluated. We expect that the hormetic effects of ELF-WMF could be applied to human diseases, and the studies are currently under progress.

Keywords: weak magnetic field, mitophagy, mitochondrial neogenesis

1.PURPOSE

The effects and the molecular mechanisms of extremely weak magnetic fields on mammalian cells have been scarcely dissected. The specific aims of this study is to elucidate the effects and the molecular mechanisms of extremely weak magnetic fields.

2. METHODS

The amount of mitochondria and the mitochondrial membrane potential were measured with MitoTracker Green and TMRM, respectively, in mouse liver-derived AML12 cells. Homogenates of AML12 cells were exposed to ELF-WMF for 8 min, and the mitochondrial electron transport complex (ETC) activities were measured to identify the target of ELF-WMF in the absence of cell signaling systems. We also quantified activities between mitochondrial ETC II subunits. Mitophagy was examined by Western blotting of PINK1, Parkin, and LC3-II. In addition, the reduced mitochondrial amount was confirmed by Western blotting of seven mitochondrial ETC proteins and mitochondrial outer membrane protein, VDAC1. Mitochondrial neogenesis was confirmed by Western blotting of PGC-1α, PPARα, and TFAM. Wild-type C57BL/6J mice were kept under ELF-WMF for 4 weeks, and mitochondrial basal oxygen consumption, mitochondrial membrane, and mitochondrial ETC activities were quantified.

3.RESULTS

We first observed that 4 ms pulses of 100 mG magnetic field that were given at 1-8 Hz in 8 sec (extremely low frequency weak magnetic field, ELF-WMF) minimized the temperature hysteresis of electric resistance of modified Ringer solution[1]. ELF-WMF reduced the amount of mitochondrial in mouse liver-

derived AML12 cells in 3 h to 63% **(Figure 1)**.

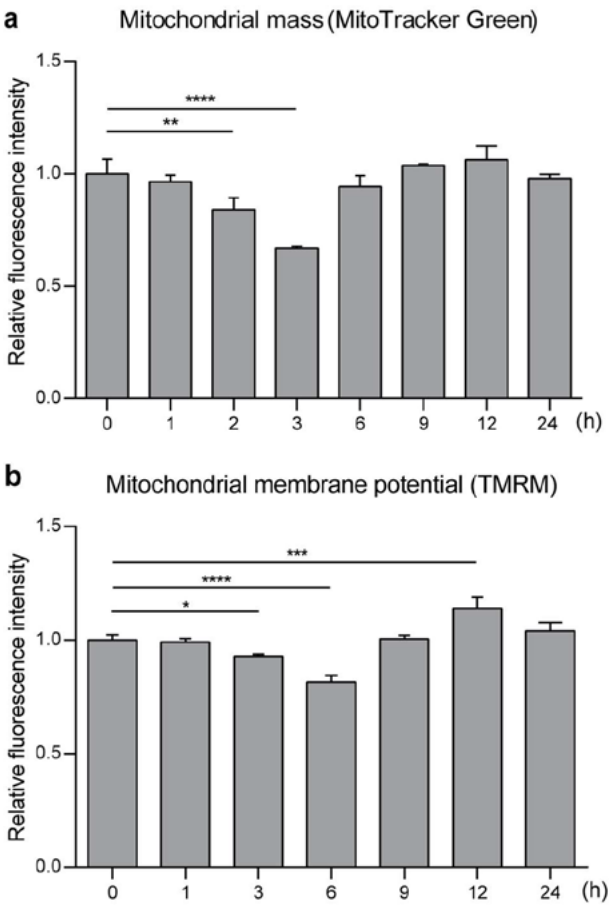

Figure 1. ELF-WMF reduced the amount of mitochondria in 3 h **(a)** and the mitochondrial membrane potential in 6 h **(b)** in AML12 cells. Mean and SD are indicated ($n = 3$). *$p < 0.05$, **$p < 0.01$, ***$p < 0.001$, ****$p < 0.0001$ by one-way ANOVA followed by Dunnett's posthoc test.

We searched for the optimal protocol of ELF-WMF by changing the electromagnetic fields from 30 mG to 3000 mG, the pulse widths from 1 ms to 16 ms, and variable frequency fluctuations and by observing mitochondrial mass in AML12 cells. We found that the specific condition that minimized the temperature hysteresis of modified Ringer solution stated above most efficiently reduced the amount of mitochondria. We also observed similar mitochondria-reducing activities in mouse muscle-derived C2C12 cells, mouse neuron-derived Neuro2a cells, human iPS cells, human kidney-derived HEK293 cells, and human cervical cancer-derived HeLa cells.

Exposure of ELF-WMF to the homogenates of AML12 cells for 8 min reduced only the mitochondrial ETC II activity to 84% **(Figure 2).** Mitochondrial ETC II is comprised of four subunits of SDHA, SDHB, SDHC, and SDHD. Electron transport activities of (i) SDHA, (ii) SDHA-SDHB, (iii) SHDA-SDHB-SDHC-SDHD, (iii) SHDA-SDHB-SDHC-SDHD-CoQ-CytC showed that ELF-WMF reduced these activities to 85-95% in 8 min.

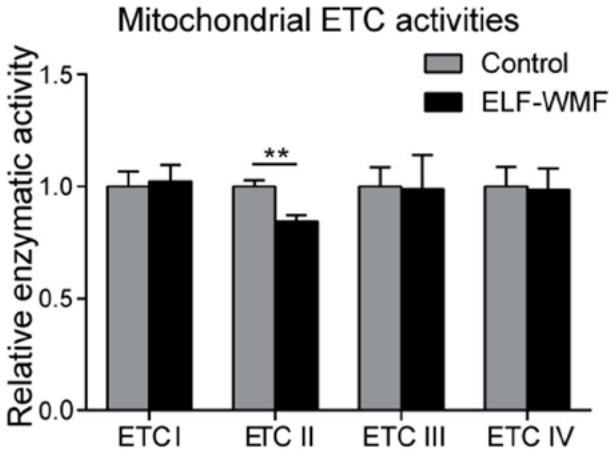

Figure 2. Mitochondrial ELC activities of the homogenates of AML12 cells that were exposed to ELF-WMF for 8 min. Mean and SD are indicated ($n = 3$~6). **$q < 0.01$ by multiple Student's t-test.

ELF-WMF induced PINK1 in 1.5 h, mitochondrial Parkin in 2 h, and LC3-II in 2.5 h in AML12 cells, indicated that mitophagy was indeed induced by ELF-WMF. Indeed, 3 h exposure of ELF-WMF on AML12 cells reduced seven representative mitochondrial ETC proteins, as well as mitochondrial outer membrane protein, VDAC1.

At 12 h after starting exposure of AML12 cells to ELF-WMF, the expression of PGC-1α, PPARα, and TFAM were induced, indicating that mitochondrial neogenesis was activated.

Wild-type C57BL/6J mice were kept under ELF-WMF for 4 weeks. We observed that basal mitochondrial oxygen consumption, mitochondrial membrane potential, and mitochondrial ETC activities in the liver were elevated **(Figure 3)**.

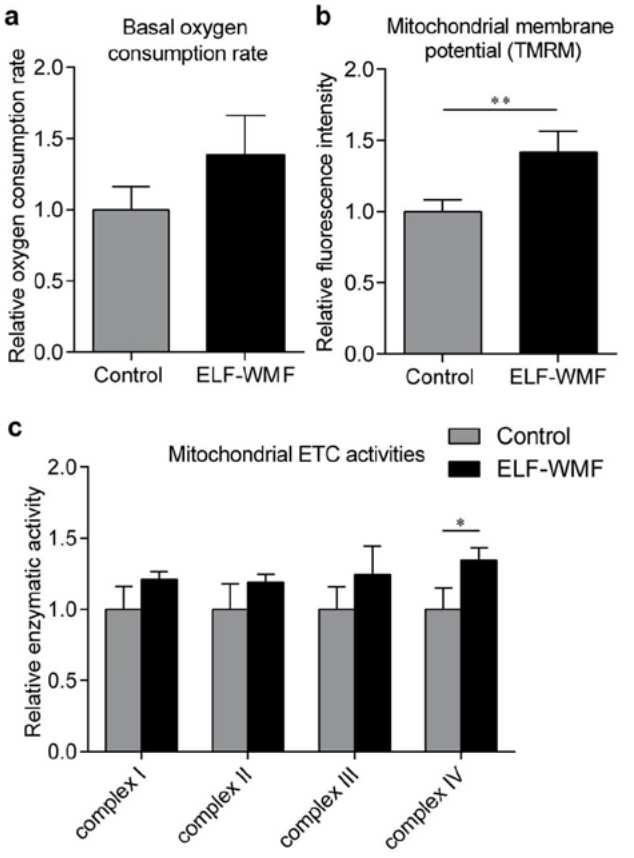

Figure 3. Wild-type C57BL/6J mice were kept under ELF-WMF for 4 weeks. **(a)** Basal mitochondrial oxygen consumption, **(b)** mitochondrial membrane potential, and **(c)** mitochondrial electron transport complex (ETC) activities were evaluated. Mean and SD are indicated ($n = 4$)。 **(b)** $^{**}p < 0.01$ by Student's *t* test. **(c)** $^{*}q < 0.05$ by multiple Student's *t*-test.

4. DISCUSSION

We observed that extremely weak magnetic field, which was about 1/4.5 of the geomagnetic field in Japan and 1/100 of the upper limit of the occupational exposure to electromagnetic fields[2], exerted prominent mitophagy in cultured cells. This study has been published in a scientific journal[3]. We observed the effects of ELF-WMF on mitochondrial ETC II in cell homogenate, where no signal transduction system should be operational, which indicated that the direct target of ELF-WMF resides in ETC II. We are currently dissecting the quantal target of ELF-WMF. Our study also indicates that ELF-WMF would be effective for multiple diseases where mitochondrial dysfunctions are key disease features. Studies on disease models are also currently under progress.

ACKNOWLEDGEMENTS

I would like to acknowledge the Watanabe Foundation for financially supporting this study.

REFERENCES

1) Mohri K, Fukushima M: Gradual decreasing characteristics and temperature stability of electric resistivity in water triggered with milligauss AC field. *Ieee Transactions on Magnetics* 38: 3353-3355 (2002).
2) International Commission on Non-Ionizing Radiation P: Guidelines for limiting exposure to time-varying electric and magnetic fields (1 Hz to 100 kHz). *Health Phys* 99: 818-836 (2010).
3) Toda T, Ito M, Takeda JI, Masuda A, Mino H, Hattori N, Mohri K, Ohno K: Extremely low-frequency pulses of faint magnetic field induce mitophagy to rejuvenate mitochondria. *Commun Biol* 5: 453 (2022).

Fabrication of artificial bone substitute applied to cell orientation characteristics by magnetic stimulation

Takaaki Arahira*

*Faculty of Management and Information Sciences, Kyushu Institute of Information Sciences
6-3-1, Saifu, Dazaifu, Fukuoka 818-0117 Japan

Abstract

We developed a magnetic field stimulation device for constructing artificial bone-like tissue in previous Watanabe Foundation. In this study, we fabricated the scaffold material using a 3D printer and fabricated the scaffold material using the molds. The fabricated scaffolds were evaluated by cell experiments to see whether the scaffolds have any effect on cells or not.

Keywords: magnetic stimulus, 3D printer, scaffold, osteoblast

1. Introduction

Recently, in the field of bone and cartilage regeneration, artificial tissues are constructed ex vivo using scaffolds and cells, and regenerative therapy using regenerated bone and cartilage tissue has been clinically applied[1),2)]. However, it still takes time to construct artificial tissues in vitro, and it is important to construct artificial tissues in a short period of time. Although there are reports on regenerated bone and cartilage tissue transplantation in previous studies, it is difficult to construct an artificial tissue that has the same mechanical properties as the surrounding tissue, and the construction of an artificial tissue with mechanical compatibility with the surrounding tissue. In order to solve these two problems, approaches to the three elements in tissue engineering, "scaffold material", "cells", and "growth factors", are considered. In particular, there have been many studies on the improvement of scaffold materials and the activation of cells, while the history of research on growth factors is short. In recent years, studies on the stimulation of scaffold materials and cells have been conducted actively.

In this study, we focused on this "stimulus". Mechanical stimuli such as compression and tension have been shown to be useful for activating bone and cartilage cells. However, it is difficult to apply mechanical stimuli uniformly to scaffold materials and cells, and the uniformity of constructed tissues is a concern. In addition, the scaffold material may be destroyed by mechanical stimulation. Therefore, we proposed magnetic field stimulation and developed a magnetic field stimulator for the construction of artificial bone-cartilage tissue when we applied to your foundation in 2015. In previous study in 2015, we found that the magnetic field stimulation activated osteoblasts for the construction of artificial bone tissue, and that osteoblasts oriented themselves in the direction of the magnetic field and proliferated. This phenomenon has been reported for neurons in previous studies by other researchers, but this is a new finding for osteoblasts. We will fabricate more oriented artificial bone tissues

by using the orientation property of osteoblasts in the direction of the magnetic field to realize high functionality of artificial bone tissues. Therefore, in this paper, we fabricated the scaffold material using a 3D printer and fabricated the scaffold material using the molds. The fabricated scaffolds were evaluated by cell experiments to see whether the scaffolds have any effect on cells or not.

2. Materials and Methods

The mold was fabricated using a 3D printer da Vinci 1.0pro (XYZ Printing). The size of the mold is a cylinder of about 15 mm in diameter, and a cylinder of about 2 mm in diameter is placed in the center (Fig. 1). Collagen scaffolds were prepared by lyophilization using the prepared molds[3] . The collagen solution was loaded into the template, frozen at -60°C, freeze-dried at -50°C, chemically cross-linked under saturated glutaraldehyde vapor for 4 hours, and blocked with a glycine solution.

Collagen scaffold was immersed in 50ml of culture medium for 24h (test medium), and the osteoblast-like cells, MC3T3-E1, were cultured in a 24-well plate for 24h using the test medium and usual medium. After culturing, absorbance at 450 nm was measured by a plate reader.

Magnetic field stimulation experiments were carried out using columnar collagen scaffolds prepared without using a mold. The magnetic field stimulator was used in previous study[4] . MC3T3-E1 was seeded in 100,000 cells per scaffold and pre-cultured for 24h before magnetic field stimulation. Stimulation conditions were 1 mT for 30 s followed by a 30-min pause cycle. Cell number was measured on day 7.

3. Results and discussion

Figure 2 shows an image of the collagen scaffold fabricated using the mold. The shape of the scaffold reflected the shape of the template. In this study, we confirmed whether the mold used for the scaffold material preparation had any negative effects on the cells by cell experiments. Figure 3 shows the absorbance of cell viability assay cultured in two-dimensional culture. Both groups showed similar absorbance, and it is considered that there is no toxicity in the cells. Therefore, it is expected that the collagen scaffolds prepared using this template will function as scaffolds with cell orientation characteristics.

Figure 4 shows the absorbance of the cell proliferation assay when cells were cultured on the columnar collagen scaffold without using a mold. The cell proliferation was better when the magnetic field was applied perpendicular to the scaffold than when the field was applied horizontally. Therefore, when the scaffold material shown in Fig. 2, which was successfully fabricated in this study, is subjected to magnetic field stimulation, it is expected that cells will enter the central hollow space and organize themselves.

Acknowledgments

This work was supported by Watanabe Foundation.

参考文献

1) Morishita T et al.: Tissue engineering approach to the treatment of bone tumors: Three cases of cultured bone grafts derived from patients' mesenchymal stem cells. Artif Organs 30: 115-118, 2006.
2) Ichinose S et al.: Comparative sequential morphological analyses during in vitro chondrogenesis and osteogenesis of mesenchymal stem cells embedded in collagen gels. Medical Molecular Morphology 46: 24-33, 2013.
3) Arahira T et al: Effects of proliferation and differentiation of mesenchymal stem cells on compressive mechanical behavior of collagen/β-TCP composite scaffold. J Mech Behav Biomed Mater 39: 218-230, 2014.
4) Takaaki Arahira et al. : Clinical Biomechanics 41(2020). (in Japnese)

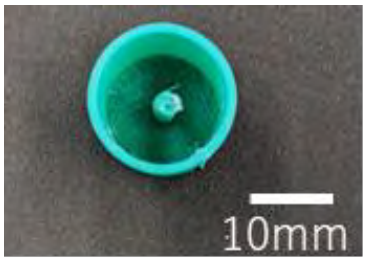

Fig.1 Photograph of mold by 3D printer.

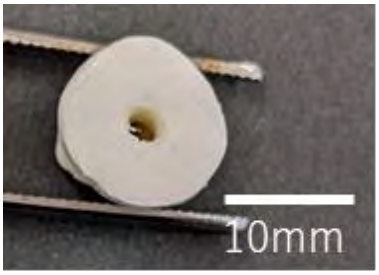

Fig.2 Image of collagen scaffold.

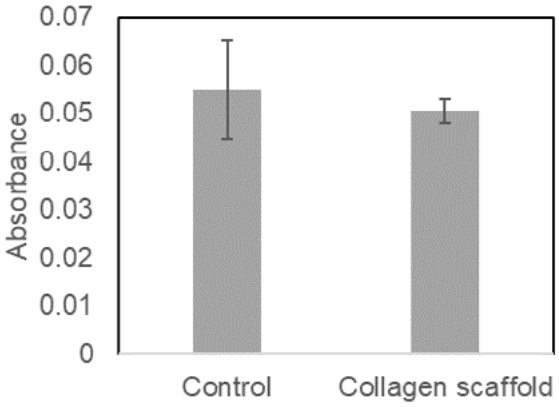

Fig.3 Cell proliferation assay of 2D culture.

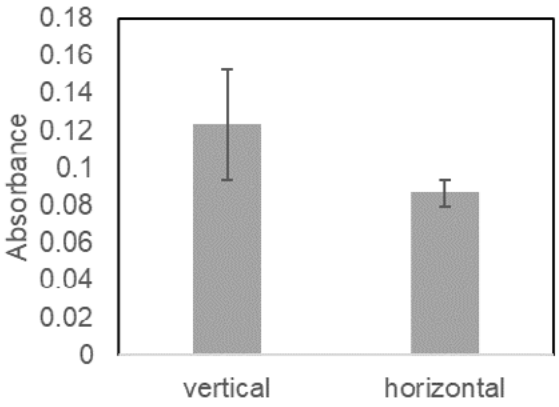

Fig.4 Cell proliferation assay of 3D culture.

Morphological and metabolic characteristics of browning of white adipose tissue in inguinal and epididymal adipose tissues

Madoka Ogawa* Yuki Tamura** Junichi Hata***

** Kyoto Sangyo University, Motoyama, Kamigamo, Kita-ku, Kyoto 603-8555, Japan
** Nippon Sport Science University, 7-1-1, Fukazawa, Setagaya-ku, Tokyo 158-0081, Japan
*** Tokyo Metropolitan University 7-2-10, Higashiogu, Arakawa-ku, Tokyo 116-8551, Japan

Abstract

The aim of this study was to clarify the morphological characteristics by T2* and diffusion tensor image (DTI) and metabolism products by ^{1}H-MRS in inguinal adipose tissue (iWAT) and epididymal adipose tissue (epiWAT) of the mice, that with and without β3-adrenoceptor agonist. We confirmed the anatomical location and position in relation to other organs and iWAT and epiWAT in vivo were identified from T2* and DTI images. ^{1}H-MRS were 1) more spectral peaks were observed in epiWAT than in iWAT; 2) the administration of β3-adrenoceptor agonists increased the spectral peaks observed in iWAT, whereas not observed that in epiWAT.

Keywords: browning, adipose tissue, inguinal, epididymal, T2*, DTI, ^{1}H-MRS

1. PURPOSE

Adipose tissues are mainly distributed subcutaneous and around organs. Differences in developmental processes and gene expression patterns have been shown depending on the distribution position of adipose tissue.[1] This previous study could indicate functional differences between adipose tissues, but the details remain unclear.

Adipose tissue is mainly composed of adipocytes. Typical adipocytes are white adipocytes, while other adipocytes are brown adipocytes and beige adipocytes.[2] Brown and beige adipocytes are rich in small lipid droplets and mitochondria, uncoupling protein 1 (UCP1)-expressing, expansible for energy homeostasis through thermogenesis.[3] Brown adipocytes are within brown adipose tissue (BAT). On the other hand, beige adipocytes are expressed within white adipose tissue (WAT) of the mice in response to environmental conditions or external stimuli such as cold, exercise and drugs (e.g., β3 adrenergic agonists). [4] Those phenomena are known as browning of WAT and have attracted attention as a promising therapeutic strategy for obesity and its related metabolic complications.

Brown/beige adipose tissue in vivo has been assessed by FDG-PET, MRI and ^{1}H-MRS.[5-6] On the other hand, method has not established to imaging for browning of WAT,[7] which is one of the factors hindering the elucidation of the functional regulation mechanisms of beige adipocyte in vivo in response to physiological stimuli. Clarification of MRI and ^{1}H-MRS characteristics between the WAT and adipose tissue, including beige adipocyte, produced by β3-adrenergic stimulants would provide useful information for the establishment of imaging methods for browning of WAT in vivo. Therefore, we aimed to 1) clarify the morphological characteristics by T2* and DTI and those of metabolism products by ^{1}H-MRS in iWAT and epiWAT, 2) clarify the imaging and spectrum characteristics of browning by β3-adrenoceptor agonist in iWAT and epiWAT. As our experiments has been completed but the image analysis is in progress, a representative example of the data is presented in this report.

2. METHODS

The experiments were approved by the Animal Experimental Committee of Kyoto Sangyo University (No. 2021-45).

2.1 Animals

Seven-week-old male wild-type mice (C57BL/6J) were separated each six animals in the control and β3 groups.

2.2 Experimental models

After a 3-day pre-rearing period, the mice were reared for 7 days at 22°C of room temperature. Mice in both groups were fed ad libitum with food and water, and solid food (CREA Rodent Diet CE-2) was used. β3 group were injected with 1 mg・kg^{-1} of β3-adrenoceptor agonist (CL316,243) for 7 days based on previous study.[4] N=1 in the β3 group died on day 1 of treatment.

2.3. Imaging methods

Mice inhaled anaesthetic gas (isoflurane 1.5-3%) 10 min before imaging and were fixed to a 9.4 T MR system (Bruker Bio Spec) equipped with an 86 mm transmitter coil and an 18 mm bore 4 ch receiving cryoprobe coil placed at 20°C of room temperature. The researcher, who had experience in collected adipose tissues from mice, and the clinical radiologists in charge of imaging, the anatomical location and position in relation to other organs were confirmed and iWAT and epiWAT were identified.

^{1}H-MRS

The PRESS method was used. The detailed sequence is shown below, with TE = 16.5 ms, TR = 2000 ms, volume of interest = 2 mm × 5 mm × 8 mm, average = 128, number of samplings = 2048, acquisition bandwidth = 4401 Hz. The water signal suppression was deactivated.

T2*

The detailed sequence is shown below, with TE= 1.63 ms, 2.96 ms, 4.29 ms, 5.62 ms, 6.95 ms, 8.28 ms, 9.61 ms, 10.94 ms, 12.27 ms, 13.60 ms, 14.93 ms, TR=800 ms, slice thickness=1 mm, gap=0.2 mm, matrix 214 × 160, number of signal averages=8, acceleration factor=1.6, flip angle=45°, field of view=32 mm×24 mm, number of slices=25.

DTI

The detailed sequence is shown below, with TE = 20.583 ms, TR = 800 ms, δ/Δ = 5.0/10.5 ms, b-value = 3000 s/mm^2, average = 4, field of view = 32 × 24 mm^2, matrix size = 128 × 96, number of slices = 25, slice thickness = 1.0 mm, slice gap =0.2 mm, motion probing gradient moment = six directions (xy, xz, yz, -xy, -xz, -yz).

2.4. Imaging analysis

^{1}H-MRS

LC Model (ver. 6.3-1R) lipid-8 was used to calculate each spectrum.

T2* and DTI

T2*maps and eigenvectors e1, e2 and e3 images were created from the images. The T2* value and the apparent diffusion coefficient (ADC) in the e1, e2 and e3 directions for each adipose tissue will be calculated.

3. RESULTS

Body weight and food intake during the period did not differ significantly between the two groups.

Examples of T2* maps of each adipose tissues in both groups are shown in Fig. 1.

Fig. 2 are shown examples of ^{1}H-MRS of iWAT and epiWAT in both groups. Peaks of methylene groups (1.3 ppm), α-methylene to carboxylic acid group (2.25 ppm) and olefin groups (5.3 ppm) were identified in both groups of epiWAT. The methylene group (1.3 ppm) and water (4.7 ppm) peaks were identified in the iWAT of both groups. In addition, the β-methylene to carboxylic acid group (1.5 ppm), glycerol backbone (4.2 ppm) and olefinic groups (5.3 ppm) were identified in the iWAT of β3 group.

4. DISCUSSION

The aim of this study was to clarify the morphological characteristics by T2* and DT and metabolism products by ^{1}H-MRS in iWAT and epiWAT of the mice, that with and without β3-adrenoceptor agonist. Although the image analysis is in progress, the characteristics of the metabolism products by ^{1}H-MRS are 1) more spectral peaks were observed in epiWAT than in iWAT; 2) the administration of β3-adrenoceptor agonists increased the spectral peaks observed in iWAT, whereas not observed that in epiWAT.

There are differences in fatty acid composition within adipose tissue at the site of accumulation,[8] and these differences could be indicated differences in metabolism activity.[9] In the present study, administration of β3-adrenoceptor agonists increased the spectral peaks observed in iWAT, but there were no differences in those in epiWAT. These results may support results of previous study by biochemical analysis[10] that β3-adrenoceptor agonist-induced browning of WAT was more extensively confirmed in iWAT than in epiWAT.

T2* and DTI images analysis are in progress. We continue to confirm whether there is a difference in the morphology of iWAT and epiWAT in with and without β3-adrenoceptor agonist.

ACKNOWLEDGEMENTS

This study was supported by a research grant from the Watanabe Foundation. We thank RIKEN and Hinako Oshiro (Tokyo Metropolitan University Graduate School).

REFERENCES

1) Chanclón, B. et al., Peripancreatic adipose tissue protects against high-fat-diet-induced hepatic steatosis and insulin resistance in mice. Int J Obes, 44, 2323-2334 (2020).
2) Wang, W. et al., Control of brown and beige fat development. Nat Rev Mol Cell Biol, 17, 691-702 (2016).
3) Giralt, M. et al., White, brown, beige/brite: different adipose cells for different functions? Endocrinology, 154, 2992-3000 (2013).
4) Altshuler-Keylin, S. et al., Beige adipocyte maintenance is regulated by autophagy-induced mitochondrial clearance. Cell Metab, 24, 402-419 (2016).
5) Holstila, M. et al., MR signal-fat-fraction analysis and T2* weighted imaging measure BAT reliably on humans without cold exposure. Metabolism, 70, 23-30 (2017).
6) Koskensalo, K. et al., Human brown adipose tissue temperature and fat fraction are related to its metabolic activity. J Clin Endocrinol Metab, 102, 1200-1207 (2017).
7) Hu, H. H., Magnetic resonance of brown adipose tissue: a review of current techniques. Crit Rev Biomed Eng, 43, 161-181 (2015).
8) Machann, J. et al., Intra- and interindividual variability of fatty acid unsaturation in six different human adipose tissue compartments assessed by (1) H-MRS in vivo at 3 T. NMR Biomed, 30, (2017).
9) Hamilton, G. et al., In vivo triglyceride composition of abdominal adipose tissue measured by (1) H MRS at 3T. JMRI, 45, 1455-1463 (2017).
10) Labbé, S. M. et al., Metabolic activity of brown, "beige," and white adipose tissues in response to chronic adrenergic stimulation in male mice. Am J Physiol Endocrinol Metab, 311, E260-268 (2016).

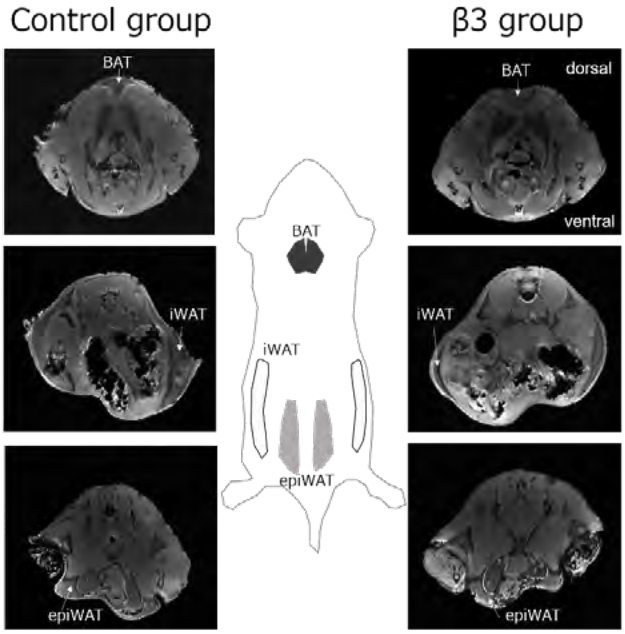

Fig. 1. T2* map in brown adipose tissue (BAT), inguinal adipose tissue (iWAT) and epididymal adipose tissue (epiWAT) in both groups.

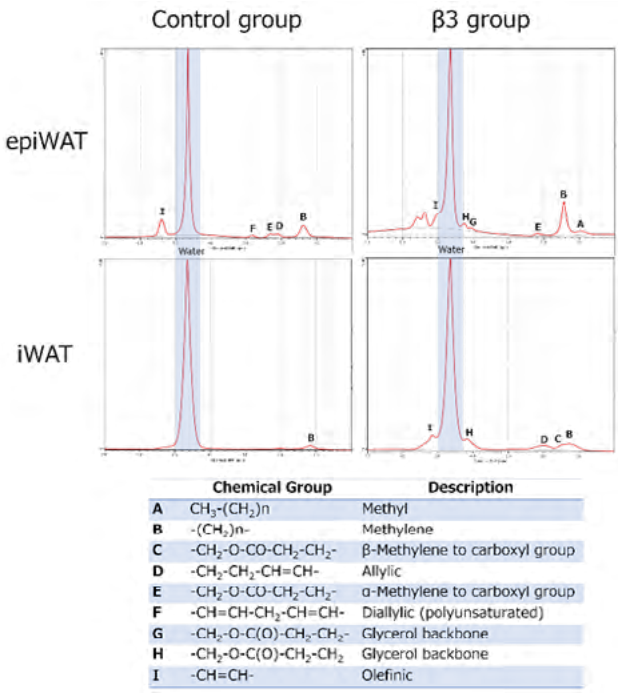

	Chemical Group	Description
A	CH_3-$(CH_2)n$	Methyl
B	-$(CH_2)n$-	Methylene
C	-CH_2-O-CO-CH_2-CH_2-	β-Methylene to carboxyl group
D	-CH_2-CH_2-CH=CH-	Allylic
E	-CH_2-O-CO-CH_2-CH_2-	α-Methylene to carboxyl group
F	-CH=CH-CH_2-CH=CH-	Diallylic (polyunsaturated)
G	-CH_2-O-C(O)-CH_2-CH_2-	Glycerol backbone
H	-CH_2-O-C(O)-CH_2-CH_2	Glycerol backbone
I	-CH=CH-	Olefinic

Fig. 2. ^{1}H-MRS in inguinal adipose tissue (iWAT) and epididymal adipose tissue (epiWAT) in both groups

Application of TMS-EEG as a novel biomarker of epilepsy

Satoshi Kodama

Department of Neurology, The University of Tokyo Hospital
7-3-1 Hongo, Bunkyo-ku, Tokyo 102-0073 Japan

Abstract

TMS (transcranial magnetic stimulation) may be a good candidate for a new diagnostic tool for epilepsy because it can reflect hyperexcitability of the neural cells in brain. TMS-EEG (TMS-electroencephalogram) is a newly developed technique measuring EEG while performing TMS. TMS-EEG may be superior to classic TMS using electromyogram as an indicator of brain function, because it can reflect pure cerebral activity. We evaluated the efficacy of TMS-EEG as a diagnostic measure for epilepsy. Amplitudes of TMS-evoked potentials in myoclonus epilepsy patients tended to be higher in N45, P60, and N100 than in normal subjects, although the sample size was small and the differences were not significant.

Keywords: cortical excitability, TMS-evoked potentials

1. Introduction

We performed a study of TMS-EEG (transcranial magnetic stimulation-electroencephalogram) (Ref 1, Ref 2) for epilepsy patients. TMS-EEG is a method to measure EEG response to TMS. The advantage of TMS-EEG compared to conventional TMS-EMG (electromyogram) is that it can record direct brain responses, and it is not affected by motor pathways in the spinal cord, peripheral nerves, or muscles (Ref 2). The late component of TMS-evoked potentials (TEP) is increased by GABAergic drugs and antiepileptic drugs such as levetiracetam and lamotrigine, suggesting that it may reflect some inhibitory mechanism.

2. Method

We retrospectively collected the results of TMS-EEG recordings in patients with epilepsy at the University of Tokyo Hospital.

Stimulation and surface EMG recording

TMS was performed by connecting a Magstim 200 Square (Magstim Co., Ltd.) to a figure-of-eight coil (Magstim Co., Ltd.) with a diameter of 7 cm, and the stimulation site was the left M1 corresponding to the right FDI muscle.

To avoid auditory evoked potentials caused by the TMS stimulus clicks, patients wore earplugs. The TMS coil was placed on the head through a silicon sheet to reduce the click sounds, which were perceived not only by air conduction but also by bone conduction from the TMS coil in contact with the head. Stimulus interval was 3.5 s on average, with a variation of ±500 ms to avoid anticipation to the stimuli, for a total of 150 stimulations.

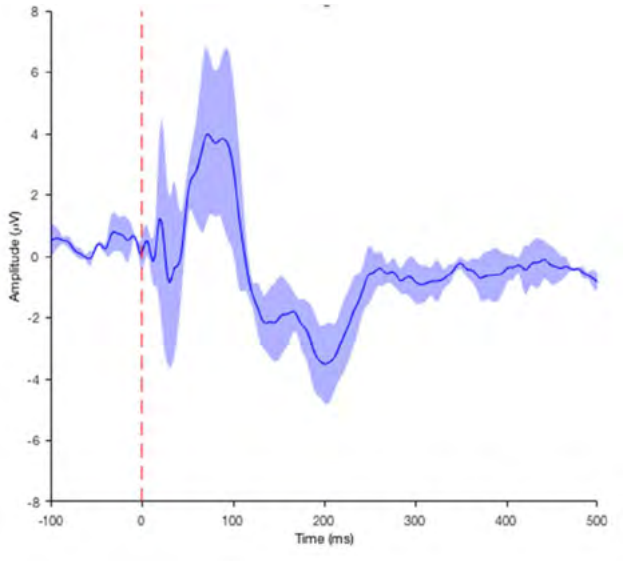

Figure 1A Average TEP of healthy subjects

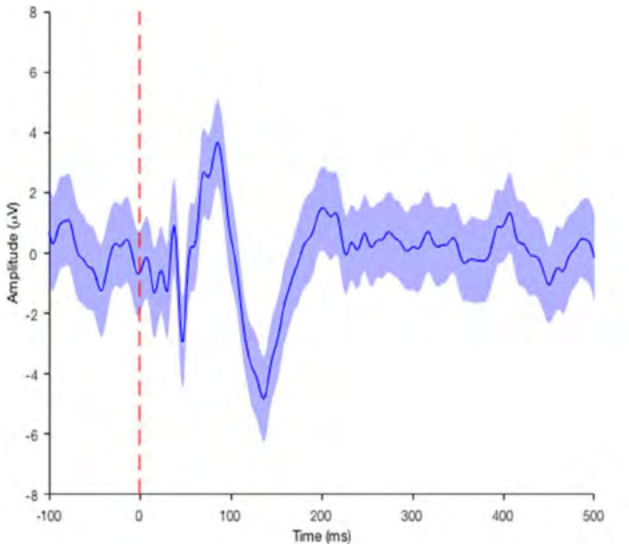

Figure 1B Mean TEP of patients with myoclonus epilepsy

Table 1 Latency and amplitude of TEP

	Control		myoclonus epilepsy patients	
	latency (ms)	amplitude (μV)	latency (ms)	amplitude (μV)
N45	31.8	3.5	33.3	7.5
P60	80.0	5.6	92.4	9.7
N100	136.4	3.4	133.0	6.6
P180	166.7	2.2	197.0	1.3

EEG recordings

EEG recordings were made via TruScanRE (Deymed Diagnostic, Co., Ltd.), which can avoid saturation of the EEG amplifier due to stimulation artifacts from TMS. The electrodes were 32-channel cap-type EEG electrodes. The signals were bandpass filtered with a passband of 0.16 Hz to 1 kHz and recorded at a sampling frequency of 3 kHz, using the right auricular electrode which was distant from the TMS stimulation site (left M1) as reference. All electrode impedances were set to less than 5 kΩ.

EEG post-processing

EEG was analyzed offline using MATLAB (ver. R2017b) with the following pipeline: 1) Epocking was performed 1 s before and after TMS. 2) TMS artifacts were removed from 2 ms before stimulation to 10 ms after stimulation. 3) Trials with obvious EMG, body movement or eye movement artifacts were excluded. 4) Bandpass filter was set from 1 to 500 Hz, and notch filter was applied. 5) Downsampling to 500 Hz was applied. 6) Re-reference to the average potential of all the electrodes. 7) Perform independent component analysis using FastICA, a toolbox that functions in MATLAB, and exclude independent components considered as artifacts. 8) The average of the EEG responses of the region of interest (C3, C4, FC5, FC1, FC2, FC6, CP5, CP1, CP2, and CP6) were set as TEP. In this study, the negative peak appearing between 30-50 ms is designated as N45, the positive peak between 50-90 ms as P55, the negative peak between 90-150 ms as N100, and the positive peak between 150-300 ms as P180. The amplitude of each peak was the mean of the amplitudes from the two opposite peaks before and after it.

3. Results

Three patients with myoclonus epilepsy who underwent TMS-EEG at the University of Tokyo Hospital were included. None of the patients had undergone epilepsy surgery, and none had adverse events during or after the examination.

Figure 1 shows the averaged TEPs for each healthy subject and patient group. Table 1 shows the latency and

amplitude of each component of the averaged TEPs. In patients with myoclonus epilepsy, the latencies of the TEPs were generally consistent with those of normal subjects, but the amplitudes tended to be higher than those of normal subjects at N45, P60, and N100. However, the sample size was small, and the differences were not significant.

4. Discussion

In myoclonus epilepsy, the amplitudes of N45, P60, and N100 tended to increase in this study, although the number of cases was small and not accompanied by significant differences.

Previous studies have suggested that the amplitude of each component of TEP reflects the neurotransmission mechanism in the cerebrum, and that $GABA_A$ receptor-mediated neurotransmission is involved in N45, which was found to be increased in healthy subjects after treatment with a $GABA_A$ receptor agonist (Ref 3). Similar studies have suggested that the amplitude of N100 is related to the inhibitory mechanism of $GABA_B$ receptors (Ref 3, Ref 4). In a previous study using paired-pulse stimulation TMS-EMG for myoclonic epilepsy, short-interval inter cortical inhibition (SICI) was attenuated, suggesting the impaired inhibitory cerebral neurons (Ref 5). The amplitude increases of N45 and N100 in the our study suggested that these GABA-mediated neural mechanisms are abnormal in myoclonic epilepsy.

Acknowledgement

This research was supported by the 27th Grant-in-Aid for Magnetic Research and Osamu Okai Special Grant from the Watanabe Foundation.

References

1) Ilmoniemi RJ, Virtanen J, Ruohonen J, Karhu J, Aronen HJ, Naatanen R, et al: Neuroreport 8(16)3537-40 (1997).

2) Tremblay S, Rogasch NC, Premoli I, Blumberger DM, Casarotto S, Chen R, et al: Clin Neurophysiol 130(5):802-44 (2019).

3) Premoli I, Castellanos N, Rivolta D, Belardinelli P, Bajo R, Zipser C, et al: J Neurosci. 34(16):5603-12 (2014).

4) Casula EP, Tarantino V, Basso D, Arcara G, Marino G, Toffolo GM, et al: Neuroimage 98:225-32 (2014).

5) Hanajima R, Ugawa Y, Terao Y, Ogata K, Kanazawa I: J Neurol Sci 140(1-2):109-16 (1996).

Optimization of magnet shape for compact magnetic probe with nitrogen-vacancy center

Akihiro Kuwahata

Graduate School of Engineering, Tohoku University
6-6-05, Aramaki Aza-Aoba, Aoba-ku, Sendai 980-8579 Japan

Abstract

Cancer cells metastasize through the lymphatic system, so it is necessary to identify and examine the lymph nodes that lymphatic fluid and cancer cells first reach to diagnose metastasis status. A magnetic probe with diamond NV (nitrogen-vacancy) was developed for the detection of sentinel lymph nodes. In order to optimize the performance of diamond NV, in this research, an optimized permanent magnet is developed by the innovative idea (inverse solution), and to be mounted on a compact magnetic probe head to generate a spatially uniform magnetic field, leading to the highly-sensitive magnetic detection.

Keywords: Permanent magnet, diamond nitrogen-vacancy center, inverse problem, optimization

1. Introduction

Cancer is the leading cause of death in Japan, and the annual mortality rate is increasing monotonically. Breast cancer is the most common cancer that affects Japanese women. When treating breast cancer, it is essential to make an accurate diagnosis of cancer metastasis because the treatment method changes depending on the presence or absence of cancer metastasis and the number of metastasized cancers.

The magnetic sensor equipped with the diamond nitrogen-vacancy (NV) center is capable of highly sensitive detection of magnetic nanoparticles, and is expected to be applied to the medical field such as cancer metastasis diagnosis using the magnetic nanoparticles method[1,2].

In this study, to improve the magnetic sensitivity of the diamond NV center, a uniform magnetic field specialized for the diamond NV center is applied by an inverse problematic approach of determining the shape of the magnet from the desired magnetic field uniformity. We develop a novel method for optimizing the shape of unique magnets. By determining the shape by an inverse problem approach that optimizes the shape of the model, we aim to develop a magnet shape with a unique shape that cannot be found in the conventional forward problem method.

2. Method

The conventional magnet shape design is based on the idea of the forward problem, and the first step is to determine the magnet shape and verify that its magnetic field distribution is uniform. If the magnetic field distribution is not desirable, we need to repeat the above process until the desired magnetic field distribution is achieved. With such a forward-problem design method, only magnet shapes based on existing knowledge can be designed, and it is difficult to create innovative magnet shapes. Therefore, we establish the idea and develop an inverse problematic method to determine the shape of the magnet from the desired magnetic field distribution.

The value of each magnetic moment is obtained from the magnetic field distribution in the diamond NV center region, which is the target area, and the magnet shape is determined from the magnetic moment. The size of the entire magnet that can be mounted in the magnetic probe was determined, and a diamond (3.9 mm × 3.9 mm × 1 mm) was placed 5 mm above the magnet. The region where the spatial uniformity of the magnetic field is required is the diamond surface. 45 magnetic moments inside the magnet were placed on the XY plane at intervals of 5 mm and at intervals of 6 mm in the Z direction. Regarding the optimization of the inverse problem, Tychonoff's regularization has the feature that it can calculate an approximate solution with a regular parameter even for an inappropriate problem. In addition, the L-Curve Method was used as a regularization parameter determination method that satisfies Morozoff's principle as the judgment condition for the optimum regularization parameter.

3. Results and Discussion

Figure 1 shows the magnet shape obtained from the result of solving the optimization problem. The target area is the optimization result in which a total of 125,000 uniform magnetic field data are input, divided into 50 * 50 * 50 in the XYZ directions. As shown in Fig. 1, we succeeded in obtaining an innovative magnet shape that cannot be found by the conventional

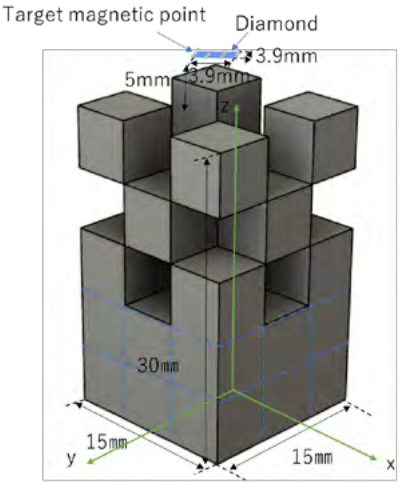

Fig. 1. Optimized magnet geometry. The top row has a cross-shaped cutout, and the second row has a cross-shaped magnetic moment block. The third row has the same shape as the top row.

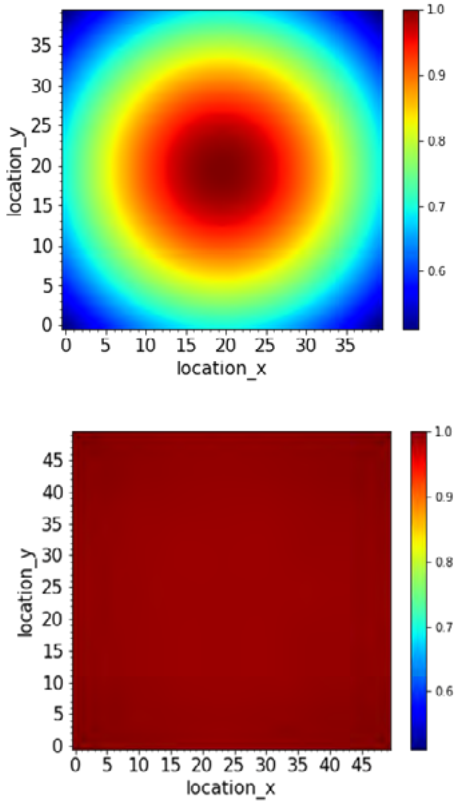

Fig. 2. Evaluation of magnetic field uniformity of (top) a conventional magnet and (bottom) a magnet solved by our optimization method.

Fig. 3 Development of optimized magnet shape by combination of small magnets. The part where magnetic moment exists is formed by permanent magnets, and the part where magnetic moment does not exist is formed by acrylic.

forward solution. The ratio of the maximum strength of the magnetic field to the minimum strength of the magnetic field in the entire diamond region was calculated and the magnetic field uniformity was evaluated (Fig. 2). With conventional magnets, the magnetic field uniformity is low at approximately 48.1%. On the other hand, in the optimized magnet shape, the magnetic field uniformity was 99.7%, indicating that the magnetic uniformity was significantly improved.

By combining about 100 small magnets and acrylic processed products, we fabricated the prototype magnet that was found by the optimization problem smethod (Fig. 3). As a result of measurement of the magnetic field distribution of the prototype magnet, the magnetic field space uniformity was 99.6%, which was equivalent to the numerical calculation.

We constructed a diamond magnetic probe system using an optimized magnet shape and conducted magnetic nanoparticle detection experiments using a biological phantom simulating a mouse animal. A magnetic coil system and microwave antenna system were constructed, and a tiny amount of magnetic nanoparticles were successfully detected.

4. Conclusion

We found a new optimized magnet shape by an inverse problem analysis method based on the magnetic moment. The magnetic field uniformity was as high as 99.7%, and we succeeded in detecting magnetic nanoparticles using a biomedical phantom. It is expected that this study will improve the accuracy of cancer diagnosis and detect smaller cancers in future biomedical applications.

Acknowledgement

This study was supported by the Watanabe Foundation (2021).

This study was presented at the annual conference of the Institute of Electrical Engineers of Japan on March 2022. In addition, This study was submitted to Japan Patent Office on 25th February 2022.

Reference

1) M. Sekino, A. Kuwahata, *et al.*, Scientific Reports 8 (2018).
2) A. Kuwahata *et al.*, Scientific Reports 10 (2020).
3) 桑波田晃弘，田中治樹，「磁石形状設計方法および最適化設計プログラム」，特開 P202110284（2022 年 2 月 25 日）

Elucidation of Sodium Metabolism Disorders in Systemic Sclerosis using Na-MRI

Kaoru Minegishi

Department of Stem Cell and Immune Regulation,
Yokohama City University Graduate School of Medicine
3-9 Fukuura, Kanazawa-Ku, Yokohama, 236-0004, Japan

Abstract

Systemic sclerosis is an intractable disease of unknown cause that involves progressive fibrosis of the skin and internal organs. Maintaining the homeostasis of water-soluble electrolytes is indispensable to life, and it has been believed that this is maintained by the kidneys. However, it has become clear that metabolism of sodium in our body is controlled in collaboration with the skin, and that abnormal sodium metabolism causes various diseases. Here, we introduced Na-MRI that can measure sodium levels in tissue, in order to elucidate abnormal sodium metabolism in systemic sclerosis as well as its pathology and mechanisms.

Keywords: Na-MRI, sodium metabolism, systemic sclerosis

1. PURPOSE

Sodium (Na) metabolism is particularly important because it is directly related to various diseases such as brain, cardiovascular, and renal diseases. However, it has recently been revealed that sodium is regulated by multiple organs, including the skin, liver, and muscles, and that abnormalities in sodium metabolism can lead to a variety of diseases.

Systemic sclerosis is characterized by progressive fibrosis of the skin, lungs, and other internal organs against a background of autoimmune phenomena. It has been shown that localized sodium accumulation in the skin and other tissues due to excessive salt intake leads to an increase in autoimmune disease due to polarization of T cells toward pathogenic Th17 cells via the p38/MAP kinase pathway. Skin sodium accumulation is shown that a predictor of the progression of skin thickness in patients with systemic sclerosis.

The etiology of systemic sclerosis is known to include fibroblast activation, vascular damage, and immune abnormalities. Skin hardening progresses through an edematous, sclerotic, and atrophic phase, and corticosteroids may be administered during the edematous phase, but the therapeutic effect is limited and local electrolyte dynamics have not been verified. The aim of this study is to elucidate the mechanism by which sodium accumulated in the skin causes the development and exacerbation of systemic sclerosis, and to develop a novel treatment targeting this regulatory mechanism. In order to carry out this research, ^{23}Sodium-magnetic resonance imaging (Na-MRI), which was developed as a tool to evaluate tissue Na levels, was introduced for the first time in Japan.

2. METHOD

Clinically used MRI systems cannot detect 23Na atoms. Since the Japan Institute of Sports Sciences (Tokyo, Japan) owns a Siemens high-field MRI system with the Multinuclear Option, which is the basis for Na-MRI. This study was conducted at the Japan Institute of Sports Sciences using a Siemens MAGNETOM Skyra.

3. RESULTS

A 3.0 tesla MRI (MAGNETOM Skyra, Siemens) was equipped with a custom-made coil (Stark-Contrast, Erlangen, Germany) that can measure the amount of Na, and the coil file was installed, set, and the parameters of the imaging sequence were registered. Next, a test scan was performed using a phantom containing NaCl to confirm that imaging was possible (Figure 1). In the test scan, the signal-to-noise ratio and RF noise spectrum of the images were verified, and it was confirmed that the quality of the captured images was of good quality (Figure 2).

Furthermore, Na-MRI was performed on the left lower leg of a healthy subject using the imaging conditions set in the test scan. In this imaging, calibration tubes filled with NaCl solutions of different concentrations (10, 20, 30, and 40 mmol/L) were simultaneously imaged to quantify the tissue Na content. In two cases, a 50-year-old man and a 45-year-old man, the Na content was 16.6 mmol/L in skin and 16.8 mmol/L in muscle, and 13.9 mmol/L in skin and 16.3 mmol/L in muscle, respectively (Figure 3).

4. DISCUSSION

The results of this study represent a breakthrough in the field of sodium regulation in tissues, contrary to the conventional theory that the amount of sodium in the body is maintained constant by the kidneys. However, previous studies have not taken local tissue sodium accumulation into consideration, and it is impossible to detect abnormal tissue sodium levels in routine clinical examinations, potentially missing abnormal tissue sodium and fluid balance in patients with diseases.

Clinical studies conducted overseas using Na-MRI have shown that there are differences in skin and muscle Na levels between men and women, and that Na levels are higher in older patients[1]. It has also been found that skin and muscle Na levels are higher in hypertensive patients than in normal subjects[2]. In the present study, skin Na levels were higher in patients aged 50 years than in those aged 45 years. We plan to use this technique in clinical research to elucidate the pathophysiology of systemic sclerosis and to develop new treatment methods. Furthermore, the Na-MRI technique can be applied directly to other diseases.

Serum Na concentration does not indicate the total Na in the body, and research using Na-MRI has the potential to detect abnormalities in diseases that have been considered off-limits to diagnostic imaging, and has the potential to contribute to the creation of new technologies and industries in Japan. The development of such technology is expected to further advance the development of drugs to treat intractable diseases.

5. ACKNOWLEDGMENT

I would like to thank the Watanabe Foundation and the Japan Institute of Sports Sciences for their research assistance and helpful suggestions.

REFERENCES

1) Kopp C, et al. 23Na magnetic resonance imaging-determined tissue sodium in healthy subjects and hypertensive patients. Hypertension. 2013;61:635-40.
2) Kopp C, et al. (23)Na magnetic resonance imaging of tissue sodium. Hypertension. 2012; 59:167-72.

(図 1)

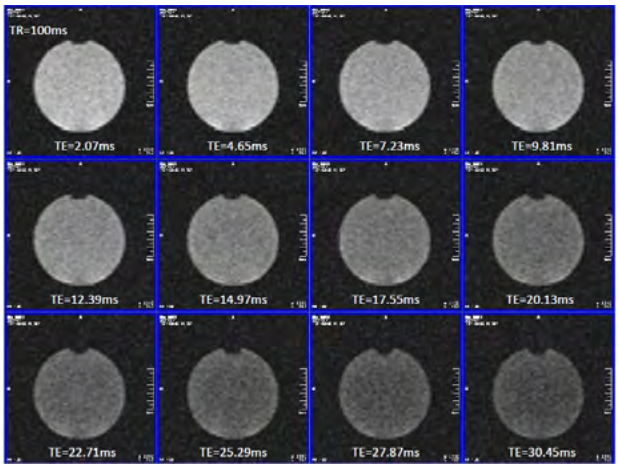
TR=100ms
TE=2.07ms
TE=4.65ms
TE=7.23ms
TE=9.81ms
TE=12.39ms
TE=14.97ms
TE=17.55ms
TE=20.13ms
TE=22.71ms
TE=25.29ms
TE=27.87ms
TE=30.45ms

(図 2)

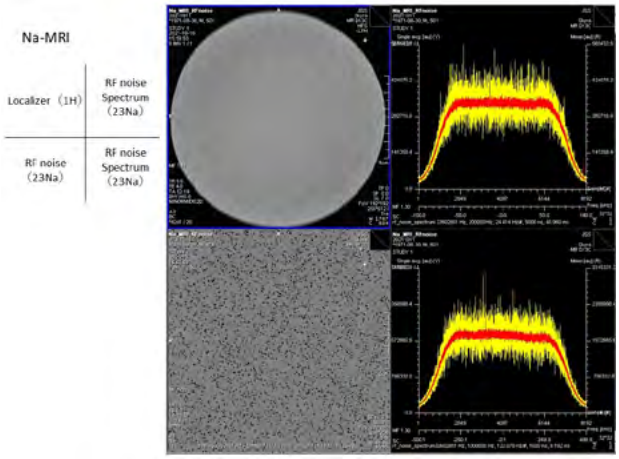
Na-MRI
Localizer (1H)
RF noise Spectrum (23Na)
RF noise (23Na)
RF noise Spectrum (23Na)

(図 3)

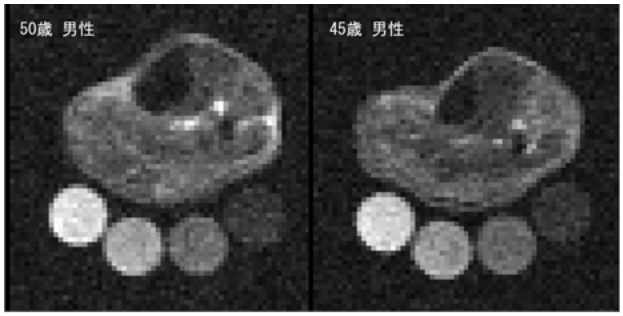
50歳 男性
45歳 男性
Skin Na+= 16.6 mmol/L
Muscle Na+= 16.8 mmol/L
Skin Na+= 13.9 mmol/L
Muscle Na+= 16.3 mmol/L

Investigation of stimulation parameters for plastic changes in the central nervous system by paired associative stimulation of magnetic stimulation and transcutaneous spinal cord stimulation

Naotsugu Kaneko*,**, Atsushi Sasaki*,**, Yohei Masugi*,***, and Kimitaka Nakazawa*

*Department of Life Sciences, Graduate School of Arts and Sciences, The University of Tokyo
3-8-1 Komaba, Meguro-ku Tokyo 153-8902, Japan
**Japan Society for the Promotion of Science
5-3-1 Kojimachi, Chiyoda-ku, Tokyo 102-0083, Japan
***School of Health Sciences, Tokyo International University
1-13-1 Matobakita, Kawagoe-shi Saitama 350-1197, Japan

Abstract

Paired associative stimulation (PAS) method for inducing neural plastic changes involves pairing of peripheral nerve stimulation and transcranial magnetic stimulation (TMS) over the primary motor cortex. The present study aimed to investigate the effect of transcutaneous spinal cord stimulation (TSCS) with TMS for PAS (TSCS-PAS) with different stimulus timings on corticospinal excitability. Our results showed that PAS timed to coincide with the TMS-induced signal arriving at the motor cortex shortly after the TSCS-induced signal, increased corticospinal excitability. We concluded that regulation of stimulus timing is important to induce plastic changes by TSCS-PAS.

Keywords: Paired Associative Stimulation, Transcutaneous Spinal Cord Stimulation, Transcranial Magnetic Stimulation, Corticospinal Excitability.

1. PURPOSE

Neuro plasticity is the ability of neural networks in the brain to functionally reorganize owing to adaptation to the environment or long-term training. For example, the cortical networks in stroke patients differ from those in healthy individuals.[1)] Motor dysfunction in these patients can be restored by reorganizing the neural networks through long-term rehabilitation. If such plastic changes in the brain can be induced noninvasively and artificially, it would be possible to efficiently restore patients' motor functions.

Paired associative stimulation (PAS) is a method for inducing plastic changes in the brain. It involves the combination of electrical stimulation of sensory nerves and transcranial magnetic stimulation (TMS) over the primary motor cortex (M1), synchronizing these stimuli at specific times.[2)] The plastic changes induced by PAS occur specifically in the M1 regions associated with electrically stimulated sensory nerves. Therefore, we hypothesized that TSCS-PAS, combining TMS with transcutaneous spinal cord stimulation (TSCS),[3)] which allows simultaneous electrical stimulation of multiple sensory nerves, could induce plastic changes in a wider range of M1 regions.

In this study, we focused on stimulus timing, an important parameter of PAS. In conventional PAS, it has been reported that changes in corticospinal excitability (increases or decreases) can be manipulated by slightly adjusting the timing of electrical stimulation and TMS.[4)] Therefore, the purpose of the present study was to determine the effects of each TSCS-PAS intervention using different

stimulus timings on corticospinal excitability.

2. METHODS

Eighteen non-disabled men, with no history of neurological disorders, were enrolled in the study. The participants were instructed to keep their bodies still and relaxed in a semi-sitting position (knee extension angle of 0° and hip flexion angle of 60°) during intervention of TSCS-PAS and evaluation.

TSCS-PAS consists of TSCS to the posterior root, stimulating the sensory nerves of multiple lower-limb muscles, with TMS applied over the lower-limb M1. For TSCS, the cathode was placed on the skin in the midline between the spinous processes of the two highest lumbar vertebrae (L1-L2), and the anode was placed over the abdomen. The intervention consisted of 120 sessions of these paired stimuli.

In this study, we investigated the relationship between stimulus timing and excitability changes by adjusting the timing of TSCS-induced and TMS-induced inputs reaching the M1. The following three different stimulus timings were used in the TSCS-PAS intervention.

i. TSCS→TMS condition: TMS was performed immediately after the TSCS-induced sensory input reached the M1 (12 participants)

ii. TMS→TSCS condition: TSCS-induced sensory input reached the M1 immediately after TMS (9 participants)

iii. Control condition: TSCS-induced and TMS-induced inputs reach the M1 at distinctly different times (12 participants).

We used TMS to evaluate corticospinal excitability from the five lower-limb muscles: tibialis anterior (TA), soleus (SOL), medial head of gastrocnemius (MG), vastus medialis (VM), and long head of biceps femoris (BF) muscles. The peak-to-peak amplitude of motor evoked potentials (MEPs) reflects the corticospinal excitability. We investigated the effect of TSCS-PAS intervention on corticospinal excitability.

3. RESULTS

Figure 1 shows the changes in MEPs for each condition. Compared to pre-intervention, MEPs of the TA, SOL, MG, and BF muscles increased 30 minutes after the TSCS-PAS intervention in the TSCS→TMS condition (Friedman and Wilcoxon signed rank tests, $p<0.05$). There were no significant changes in MEP in the TMS→TSCS and Control conditions (Friedman test, $p>0.05$).

4. DISCUSSION

Intervention in the TSCS→TMS condition increased the corticospinal excitability in multiple lower-limb muscles, suggesting that the intervention widely facilitated the excitability in the lower-limb M1. Since there were no significant MEP changes in the Control and TSCS→TMS conditions, adjusting the timing of TSCS and TMS is essential in inducing plastic changes in the M1. Conventional PAS can reduce corticospinal excitability by adjusting stimulus timing.[4] In further studies, we will explore the stimulus parameters of TSCS-PAS that reduce the corticospinal excitability.

ACKNOWLEDGEMENTS

This research was supported by the 27th Magnetic Research Grant from the Watanabe Foundation.

Part of the present study was presented at the 76th Annual Meeting of the Japanese Society of Physical Fitness Medicine held in September 2021. Furthermore, part of the present study has been published in *Neuroscience*.[5]

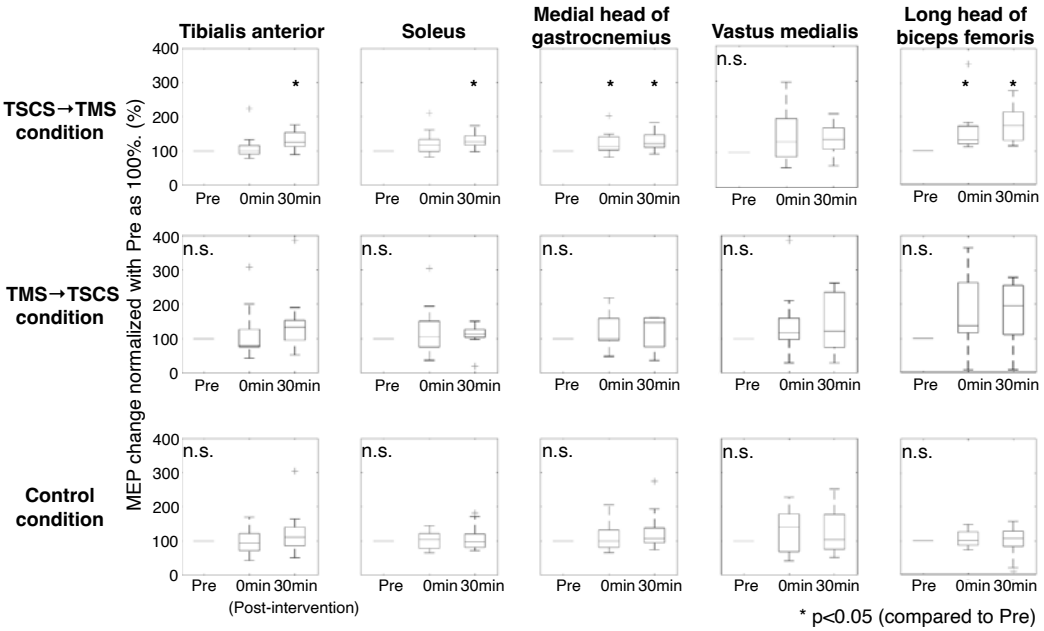

Figure 1: Changes in MEP after TSCS-PAS intervention

TSCS, transcutaneous spinal cord stimulation; TMS, transcranial magnetic stimulation; MEP, motor evoked potential.

REFERENCES

1) Jones, T.A. Motor compensation and its effects on neural reorganization after stroke. *Nat. Rev. Neurosci.* **18**, 267–280 (2017).
2) Stefan, K. et al. Induction of plasticity in the human motor cortex by paired associative stimulation. *Brain* **123**, 572–584 (2000).
3) Courtine, G. et al. Modulation of multisegmental monosynaptic responses in a variety of leg muscles during walking and running in humans. *J. Physiol.* **582**, 1125–1139 (2007).
4) Wolters, A. et al. A temporally asymmetric Hebbian rule governing plasticity in the human motor cortex. *J. Neurophysiol.* **89**, 2339–2345 (2003).
5) Kaneko, N. et al. The Effects of Paired Associative Stimulation with Transcutaneous Spinal Cord Stimulation on Corticospinal Excitability in Multiple Lower-limb Muscles. *Neuroscience.* **476**, 45–59 (2021).

Inhibitory effects of magnetic stimulation on the onset of psychiatric symptoms and elucidation of the mechanism

Minori Koga*, Hiroyuki Toda*, Masanori Nagamine**, Fumiho Asai* and Aihide Yoshino*

*Department of Psychiatry, National Defense Medical College
3-2 Namiki, Tokorozawa, Saitama 359-8513 Japan
** Division of Behavioral Science, National Defense Medical College Research Institute,
3-2 Namiki, Tokorozawa, Saitama 359-8513 Japan

Abstract

The effectiveness of repetitive transcranial magnetic stimulation (rTMS) has not been fully proven. For example, it is still unclear whether rTMS effectively prevents recurrence and relapse in depression. In addition, the molecular mechanism of the effect of rTMS has been poorly understood. We investigated behavioral changes and gene expression changes in mice subjected to water immersion restraint stress, which induces depressive symptom-like behavior, when treated with rTMS. We found that rTMS increased the amount of spontaneous behavior. The gene expression analysis suggested that the Myd88 gene, which is involved in signaling innate immune responses, is the mechanism of the antidepressant effect of rTMS therapy.

Keywords: Repetitive transcranial magnetic stimulation, depression, microglia, inflammation

1. PURPOSE

The biological pathogenesis of depression is still unknown, and the development of treatment and prevention methods and drug discovery lag behind that of other physical diseases. Several recent studies have shown a significant correlation between abnormal inflammation in the brain and the pathophysiology of psychiatric symptoms, making the brain immune system a potential target for treatment and prevention. Repetitive transcranial magnetic stimulation (rTMS), which has long been expected to have antidepressant effects, has recently been covered by insurance. However, the impact of rTMS on mental disorders has not been fully proven so far. For example, it is still unclear whether rTMS effectively prevents recurrence and relapse in depression. The mechanism of biological effects has also been poorly evidenced. Previous studies have reported suppressing inflammatory cytokine expression by rTMS[1], suggesting that the anti-inflammatory effect of magnetic stimulation is one of the effects of rTMS. Although the brain immune system is suggested to be the point of action of rTMS, it is still unclear what pathological conditions magnetic stimulation is effective for and how it works. In the present study, we used a mouse model of depression to search for symptoms ameliorated by rTMS and molecules involved in the effects of stimulation.

2. METHODS

Behavior analyses in mice treated with a water immersion restraint stress

After acclimation, C57BL/6 mice (8 weeks old, male) were placed in a 25-mL plastic conical tube with

holes and placed in a container filled with water at a depth not exceeding the face and subjected to three hours per day of water immersion and restraint stress for two weeks. An open field test and a forced swim test were performed five days after the last stress administered (Fig. 1A). To assess anxiety and locomotor behaviors, we used a square acrylic apparatus (43 cm × 43 cm) equipped with a panel of 16 horizontal infrared beams per axis. Data recorded for 5-min spontaneous activity in the field for each mouse was collected and analyzed. For the forced swimming test, mice were placed in a container filled with water to a depth of 12.5 cm in a cylinder 11 cm in diameter and 18 cm in height, and their behavior of struggling to escape was recorded for 6 minutes. The recorded data during the last 5 minutes was used for analysis.

Analysis of the relationship between microglia and depressive-like behaviors induced by water immersion stress

C57BL/6 mice (6 weeks old, male) were administered with PLX3397 for three weeks to eliminate microglia in the mouse brain according to the method by Elmore et al[2]. Then, the open field test and the forced swim test were then conducted after subjecting them to water-immersion restraint stress (Fig. 2A). After three weeks of PLX3397 administration, Brains were removed, and the tissues were fixed with 4% paraformaldehyde. Frozen sections were prepared from fixed brains, and microglial marker (IBA1) and astrocyte marker (GFAP) were detected by immunohistofluorescence staining to confirm that microglia were specifically eliminated.

Antidepressant effect of rTMS

After acclimation, C57BL/6 mice (8 weeks old, male) were subjected to water immersion restraint stress, and then the Magstim Rapid System MRS1000/50 was used to deliver three sets of stimuli (each stimulus interval was 36.5 seconds), each set consisting of 150 pulses at 15 Hz to the frontal portion of the mice at 57% output for five consecutive days. After magnetic stimulation, an open field test and a forced swimming test were conducted (Fig. 3). Then, after behavioral experiments, the brains of mice were removed, the hippocampus was dissected, and the total RNA was extracted. Total RNA was also extracted from control mice. Real-time PCR was performed using cDNA synthesized by reverse transcription from the total RNA as a template and primer sets of the target genes to compare gene expression levels among the experimental groups.

The animal experiments in the present study were properly performed under the approval of the Ethics Committee for Animal Experiments of the National Defense Medical College.

3. RESULTS

No difference was observed in the amount of spontaneous or exploratory behavior of mice subjected to water immersion restraint stress load compared to controls (Fig. 1C). The mice subjected to water immersion restraint stress significantly increased immobility time in the forced swimming test (Fig. 1D). To confirm whether microglia is necessary for the increase in immobility time, we performed a forced swimming test in mice with microglia-eliminated conditions (decrease in IBA1-positive cells, shown in Fig. 2B). The immobility time was not increased even after water immersion restraint stress was administered (Fig. 2C). Next, we administered rTMS to the mice subjected to water immersion restraint stress. As a result, it did not prevent the increase in immobility time in the forced swimming test (Fig. 3D). However, it did increase spontaneous activity (Fig. 3B). No significant change was shown in rearing behavior (Fig. 3C). Comparisons of gene expression levels showed no differences in *Il-1β*, *Tnf-α*, and *Tspo1* genes among control, stress, and rTMS groups (Fig. 4A, B, E). *Iba1*, *Gfap*, *Myd88*, and *Tlr4* genes were significantly downregulated in response to water immersion restraint stress compared to controls (Fig. 4C, D, F, G). Of these genes, the *Myd88* gene, which significantly decreased expression by stress administration, was

rescued to the same expression level as the control group by magnetic stimulation.

4. DISCUSSION

No improvement in depressive symptom-like behavior induced by water immersion stress was indicated by rTMS. This result might be because the duration of rTMS treatment was short and did not reflect biochemical changes. However, magnetic stimulation significantly increased spontaneous behavior, suggesting that magnetic stimulation is effective, although only partially, in treating some symptoms of depression. Biochemical analysis revealed that the *Myd88* gene, of which genetically deficient mice have been reported to demonstrate depressive-like behavior[3], was down-regulated by water immersion restraint stress and rescued by rTMS, suggesting that MyD88 is the action point of rTMS therapy for depressive symptoms. MyD88, an essential downstream adaptor protein of TLRs, has a role in signaling in the innate immune system. Since recent studies have indicated that abnormalities in the brain immune system are involved in the pathogenesis of depressive and other psychiatric symptoms, maintenance of the brain immune system might be a mechanism for the antidepressant effect of rTMS. Further investigations, such as the dynamics of downstream molecules in the MyD88-mediated signaling pathway, are needed to elucidate the mechanisms of beneficial effects of rTMS.

ACKNOWLEDGEMENT

The present study was supported by the 27th research grant from the Watanabe Foundation (Grant No. 02302).

REFERENCES

1. Tateishi H, Mizoguchi Y, Kawaguchi A, Imamura Y, Matsushima J, Kunitake H, Murakawa T, Haraguchi Y, Kunitake Y, Maekawa T, Kato TA, Asami T, Monji A. Changes in interleukin-1 beta induced by rTMS are significantly correlated with partial improvement of cognitive dysfunction in treatment-resistant depression: a pilot study. Psychiatry Res. 2020 Jul; 289:112995.
2. Elmore MR, Najafi AR, Koike MA, Dagher NN, Spangenberg EE, Rice RA, Kitazawa M, Matusow B, Nguyen H, West BL, Green KN. Colony-stimulating factor 1 receptor signaling is necessary for microglia viability, unmasking a microglia progenitor cell in the adult brain. Neuron. 2014 Apr 16;82(2):380-97.
3. Choudhury ME, Mikami K, Nakanishi Y, Matsuura T, Utsunomiya R, Yano H, Kubo M, Ando R, Iwanami J, Yamashita M, Nagai M, Tanaka J. Insomnia and depressive behavior of MyD88-deficient mice: Relationships with altered microglial functions. J Neuroimmunol. 2022 Feb 15;363:577794.

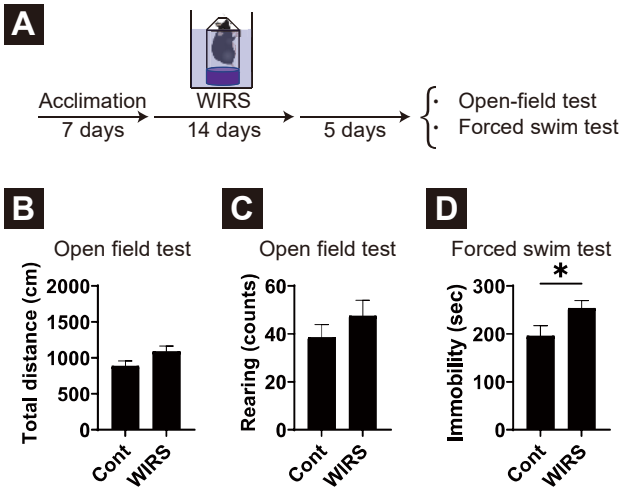

Fig. 1. Behavior of mice subjected to water immersion restraint stress
Experimental design (A). Total distance traveled by open field test (B) and rearing counts. Immobility time by forced swim test (D). * ($p<0.05$) indicates a significant difference as determined by t-test.

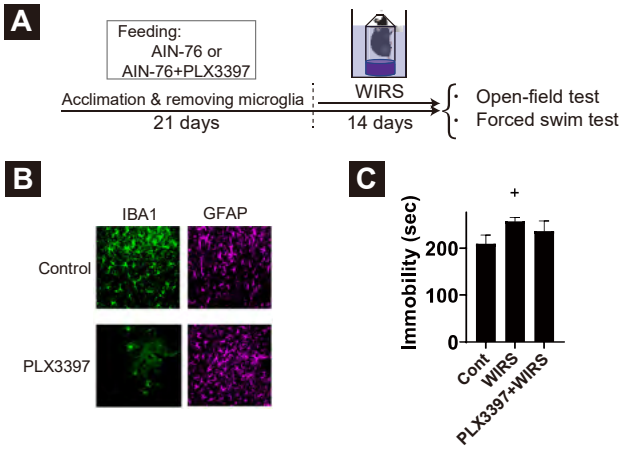

Fig. 2. Behavioral changes in response to stress in mice with erased microglia
Experimental design (A). Results of immunohistofluorescence staining of microglial marker (IBA1) and astrocyte marker (GFAP) (B). Immobility time from forced swim test (C). + ($p<0.1$) indicates a trend difference compared to control (Cont) as determined by a Dunnett test.

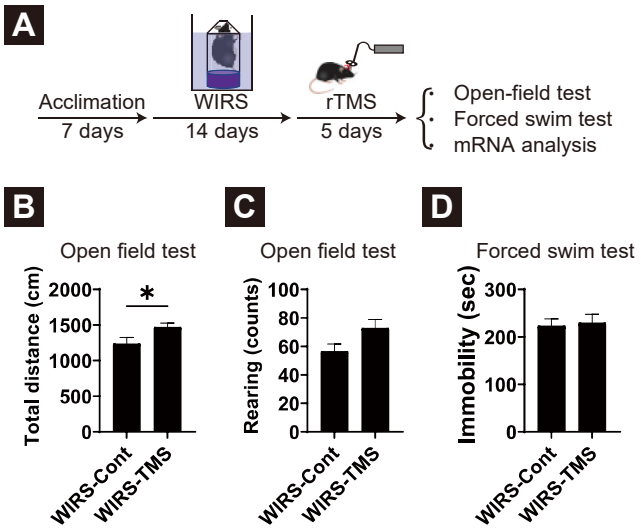

Fig. 3. Effects of repetitive transcranial magnetic stimulation on depressive-like Behaviors
Experimental design (A). Total distance traveled by open field test (B) and rearing counts. Immobility time by forced swim test (D). * ($p<0.05$) indicates significant differences as determined by t-test.

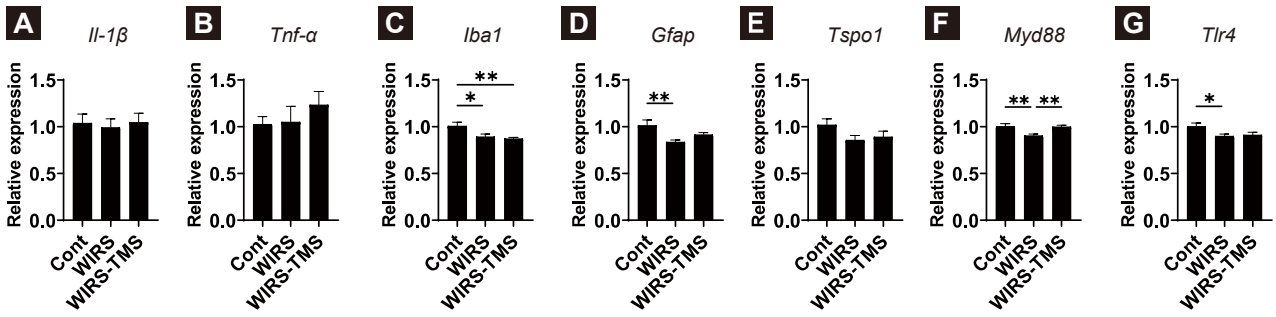

Fig. 4. Comparison of gene expressions among the experimental groups by real-time PCR
Fold changes of genes encoding the inflammatory cytokines IL-1β (A) and TNF-α (B), the markers of microglia IBA1 (C), astrocytes GFAP (D), activated glia TSPO1 (E), and the signaling molecules MyD88 (F) and TLR4 (G) involved in immune responses are indicated. *($p<0.05$), **($p<0.01$) indicate significant differences as determined by a Tukey's test.

Nerve block effect with low-frequency magnetic stimulation

Eri Kaneda

Department of Cardiovascular Surgery, Graduate of Medicine, Osaka University
2-2 Yamadaoka, Suita-shi, Osaka 565-871 Japan

Abstract

Stellate ganglion block injections for the relief of neuropathic pain and autonomic abnormalities are associated with risks. To ameliorate these problems, there is an attempt to obtain therapeutic effects by applying low-frequency magnetic stimulation to the ganglion and suppressing its function. Using a neodymium magnet, a large magnetic field gradient of 7-9 mT/mm was applied to a rat ganglion for a short time, and the increase in sympathetic nervous system parameters of blood pressure was suppressed. This study confirmed the nerve blocking effect of low-frequency magnetic stimulation.

Keywords: low-frequency magnetic stimulation, sympathetic nervous system

1. PURPOSE

Stellate ganglion block injection is a treatment used in anesthesiology and pain clinics to relieve neuropathic pain and autonomic nervous system abnormalities. This is an invasive procedure in which a local anesthetic is injected near the stellate ganglion, one of the ganglia in the neck, to suppress stellate ganglion activity. This procedure is undesirable for patients because of the risk of needling near the carotid artery and the high incidence of Horner's syndrome, which is represented by droopy eyelids. In addition, the fact that patients must visit the hospital to undergo this procedure is a barrier to continued treatment.

On the other hand, it has recently been reported that low-frequency magnetic stimulation of the same region may produce effects like those of stellate ganglion block injection (hereafter referred to as the blocking effect[1]). In one study, long-term magnetic stimulation of a rat ganglion suppressed the increase in sympathetic nervous system parameters when an adrenergic agonist was administered[2].

Therefore, with the aim of establishing a noninvasive method and apparatus for stellate ganglion blockade, we decided to demonstrate the blocking effect of short-term low-frequency magnetic stimulation in rats.

2. METHOD

2-1. Selection of suitable magnets for animals

Based on the results of a magnetic field simulation analysis using the anatomy of a 10-week-old male nude rat (220 ± 10 g body weight) as a reference, a neodymium magnet was selected with a shape that generates a magnetic field gradient of 7-9 mT/mm at the position behind the carotid artery at the first cervical vertebra level. A metal magnet with a similar shape but without magnetic properties was prepared as the Sham magnet.

2-2. Adrenergic agonist dosage determination

To induce a sympathetic hyperactivity-like state, we administered intraperitoneally an adrenergic agonist that raises blood pressure. The dose that maintained stable blood pressure in the range of 30-60% for 60 minutes was determined in a previous study.

2-3. Magnet attachment to rats and blocking effect

After induction of anesthesia, we first confirm that the blood pressure has been stable for at least 5 minutes in

a non-intensive systolic blood pressure measurement in the tail vein. The blood pressure currently is the Pre value. After that, an adrenergic agonist is administered intraperitoneally, and a magnet or a Sham magnet is applied when the blood pressure reaches 130% of the Pre value, and observation of blood pressure changes begins for 45 minutes. After 45 minutes of observation, the magnets are removed and observation continues for another 15 minutes, for a total of 60 minutes.

3. RESULTS

3-1. Case with sham magnet

Under anesthesia, blood pressure pre values were stable at 120 mmHg. After intraperitoneal administration of adrenergic agonists at the dose determined in 2-2, blood pressure began to rise immediately. When a 130% increase in blood pressure was reached, the Sham magnet shown in 2-1 was placed at the appropriate site. The blood pressure remained above 160 mmHg (133%) for more than 30 minutes. Even after the Sham magnet was removed 45 minutes after the start of observation, the blood pressure remained at 140 mmHg (117%), and there was no tendency for the blood pressure to approach the Pre value even after the end of observation.

3-2. Case with Neodymium magnet

Under anesthesia, blood pressure Pre remained stable at 90 mmHg. After intraperitoneal administration of an adrenergic agonist, blood pressure rose immediately and reached 140 mmHg (156%), as in the case of the individual with the Sham magnet. Blood pressure began to decrease gradually after 7 minutes after the neodymium magnet was applied to the appropriate site. At 30 minutes after application, the blood pressure was 110 mmHg (122%), and at 45 minutes after application, the blood pressure recorded 90 mmHg. Even after the observation was terminated and the neodymium magnet was removed, the slight downward trend of blood pressure did not stop, and the systolic blood pressure of the rats at the end of the observation was 85 mmHg (94%), which was lower than the Pre value.

4. DISCUSSION

Low-frequency magnetic stimulation using a neodymium magnet in rats clearly suppressed the increase in blood pressure, one of the sympathetic hyperactivity-like states produced by the administration of adrenergic agonists. It is suggested that this is due to the mechanism that the change in potential brought about by the action of low-frequency magnetic stimulation on neurons alters the orientation of ion channels and suppresses neuronal activity.

In the present study, a relatively large magnetic field gradient was applied to the ganglion to act on the living body, and a neuroinhibitory effect was obtained in a short time. As a result, the increase in systolic blood pressure was strongly suppressed. To the best of my knowledge, there is no report of a brief neuroinhibitory effect of low-frequency magnetic stimulation, and this practical finding is a great achievement.

On the other hand, when considering the application to medical devices, it is essential to find a threshold value that guarantees safety and effectiveness. For example, it has been reported that a static magnetic field with a flux density of 37.9 mT suppresses the activity of sensory nerves by 80%[3]. However, it is unknown how much suppression of neuronal activity leads to overall neuronal suppression and what range of magnetic field gradients can safely suppress the nerves. We are planning to conduct future research using pigs that are similar in size to the human body, and to verify the effects of low-frequency magnetic stimulation on sympathetic nerve suppression in conjunction with magnetic field simulations.

ACKNOWLEDGEMENT

This research was supported by the 27th Osamu Okai Special Research Grant from the Watanabe Foundation.

REFERENCES

1) Timothy M. Markman, Roy H. Hamilton, Francis E. Marchlinski, Saman Nazarian. Case series of transcutaneous magnetic stimulation for

ventricular tachycardia storm. JAMA 2;323(21):2200-2202 (2020).
2) Hideyuki Okano, Chiyoji Okubo. Effects of 12mT static magnetic field on sympathetic agonist -induced hypertension in wistar rats. Bioelectromagnetics 28:369-378 (2007).
3) Arthur D. Rosen. Thereshold and limits of magnetic field action at the presynaptic membrane. Biochemica et Biophysica Acta, 1193.62-66(1994).

Understanding of multisensory integration of brain by magnetoencephalography and application to multisensory brain-machine interface

Kiyoshi Kotani*

*Research Center for Advanced Science and Technology, The University of Tokyo
4-6-1 Komaba, Meguro-ku, Tokyo 153-8904 Japan

Abstract

Brain machine interface (BMI) is an interface that reads the user's intention from the brain activity in real time. In spite of its potential to alter the human interface and communications, there is a disadvantage that the speed of BMI is still slower than other types of interface. In this research, we obtain the brain activity by magnetoencephalograms and investigate the fundamental properties of integrating multi-sensory information in the brain. Then we propose a feasible BMI system with multi-sensory augmented reality technology.

Keywords: Multisensory Integration, Brain Machine Interaction

1. PURPOSE

Brain-machine interface (BMI) is a system that measures the neural activity of a human's brain and converts it into a signal for controlling a machine and is expected to support a disabled person's life[1]. For real life support, BMIs using augmented reality (AR) were developed[2]. It provides multisensory stimuli to improve an information transfer rate. However, a large part of multisensory integration remains to be studied. In addition, non-cryogenic quantum-enabled sensors, called optically pumped atomic magnetometer (OPM) was developed[3]. An OPM sensor can be put in arbitrary place without a paste, and its sensitivity is higher than superconducting quantum interference device (SQUID), so there is a possibility that OPM sensors improve a BMI's performance.

In this study, as basic research, we measured responses to audiovisual stimuli by magnetoencephalography (MEG), which has high spatiotemporal resolution and evaluated strength and spatiotemporal locality. We also verified the feasibility of BMI using OPM-MEG. Furthermore, as applied research, we developed a wheelchair AR-BMI that enables movement and rotation, and a BMI that allows to choose objects after environment recognitions.

2. Evaluation of brain activity by using index of spatiotemporal locality of MEG

2.1. METHOD

In this section, the brain response was recorded by a magnetoencephalographic system (RICOH160-1, RICOH). Participants performed 2 tasks that had different number of auditory and visual choices. Visual stimuli were flashes of the marker on the screen, and auditory stimuli were 440 Hz pure tone (Fig 1). Participants were told to push a button when the location of the flashed marker and the presented sound were the same as the instruction which was told before the measurement.

The stimuli were labeled "target", "visually true stimuli", "auditory true stimuli" and "both false stimuli" and the responses of each label were averaged. We calculated the root mean square of

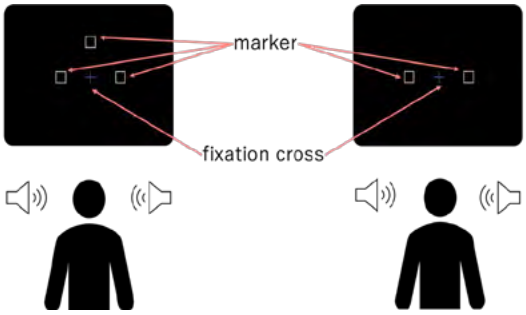

Fig1. The image of presenting audiovisual stimuli. Left: Task1, in which there were 3 visual choices. Right: Task2, in which there were 2 visual choices.

the amplitude of 160 channels and named the time-averaged value "strength". We also calculated kurtosis of squared value of each channel.

2.2. RESULTS and DISCUSSION

In Task1, 16 measurements were conducted, and the highest strength of the target and the visually true stimuli was 5 and 9 measurements, respectively. There was significant difference as shown in Fig2.

In Task2, 10 measurements were conducted, and the highest strength of the target, the visually true stimuli, and the auditory true stimuli was 6, 1 and 2 measurements, respectively. There was no significance in both strength and kurtosis.

In Task1 the strength of not only the target but also the visually true stimuli tended to be high. On the other hand, in Task2, in which there were only 2 visual choices, the tendency of Task1 was not observed. Therefore, visual dominance may affect the response. In both tasks, there were no significance in kurtosis.

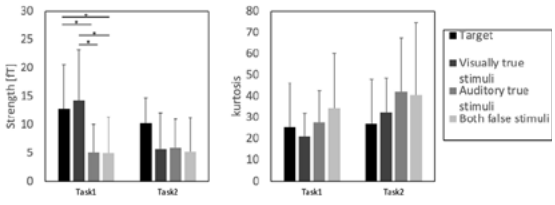

Fig2. The strength and the kurtosis of the amplitudes. *p < 0.05

In previous studies, psychological tasks were conducted, and visual dominance was indicated based on the correct answer rate to audiovisual stimuli[4,5]. In our study, visual dominance like the previous studies was indicated by direct brain activities.

3. Measurement of brain activity by OPM sensors

3.1. METHOD

In this section, the brain response was recorded by 2 OPM sensors (QZFM Gen-2, QUSPIN). In the first experiment, the task was conducted to induce alpha waves. The OPM sensors were put on the scalp near the visual cortex. A participant repeatedly opened and closed his eyes to an auditory cue.

In the second experiment, the task was conducted to induce N100m. The OPM sensors were put on the scalp near the auditory cortex. 400 Hz pure tone was presented to a participant. The participant participated in the same task with SQUID sensors.

3.2. RESULTS and DISCUSSION

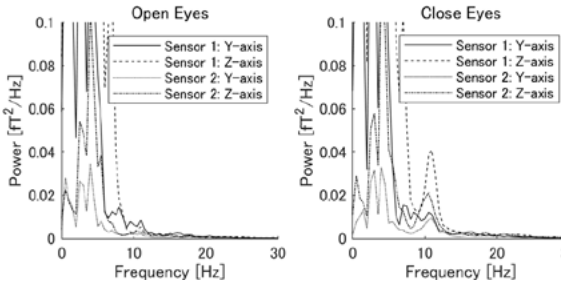

Fig3. The frequency spectrum during opening and closing eyes.

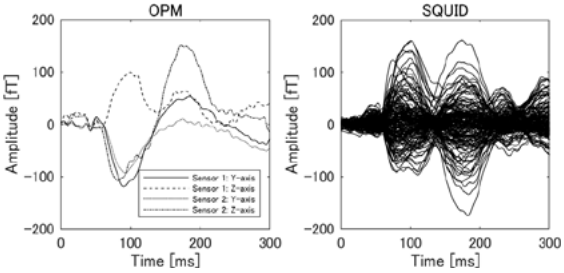

Fig4. The waves of N100m measured by OPM-MEG and SQUID-MEG.

In the task that induced alpha waves, when the participant closed his eyes, the power spectrum around 10 Hz increased (Fig3), so it is possible to use a OPM sensor for operating BMI by steady state visual evoked fields.

In the task that induced N100m, N100m, which has a peak about 100 ms after presenting a stimulus, was found by both OPM and SQUID (Fig 4). Therefore, it is possible to use OPM sensors for operating BMI that uses evoked responses.

4. Development of wheelchair BMI by multisensory stimuli

4.1. METHOD

In this section, the audiovisual stimuli were presented through AR goggles (HoloLens, Microsoft). By using the HoloLens, the spatial information of the real word was acquired, and virtual markers and sound sources were put around the user (Fig 5). A visual stimulus was a flash of the virtual markers. The participant put on a wheelchair and wore an electroencephalograph and the HoloLens.

In the task to move the wheelchair forward, the participants counted the number of flashing the target marker. In the task to turn the wheelchair, the participants counted the number of presenting the sound from the target location.

4.2. RESULTS and DISCUSSION

Classifiers were trained by linear discriminant analysis and leave-one-out cross-validation was applied. The average accuracy of 4 participants was 62.5%. The chance level was 4% because there are 25 virtual markers and sound sources in total. All participants' accuracy were better than the chance level. By acquiring the spatial information and putting virtual markers and sound sources, we confirmed the feasibility of a BMI that allows to move and turn to any location.

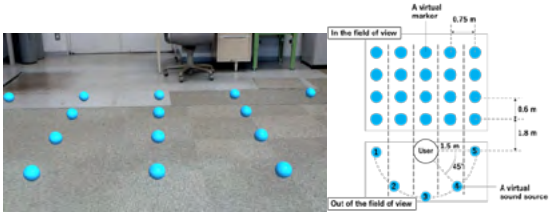

Fig5. The image of virtual markers and the sound sources. Left: The scenery through the AR goggles. Right: The location of the virtual markers and the sound sources.

5. Development of AR-BMI using object detection and environmental awareness

5.1. METHOD

In this section, objects were detected using the Single Shot Multi-box Detector (SSD) from images captured by the camera of AR goggles (Microsoft Hololens2) and combined with information by the depth sensor to calculate their position in real space. The markers were displayed as spherical objects at the corresponding coordinates in the virtual space. The intensity of steady-state visual evoked potentials (SSVEPs) was calculated when each option was simultaneously flickering at 8-14 Hz for four seconds to estimate which option the user focused on.

5.2. RESULTS and DISCUSSION

Estimation accuracy exceeded 25% of chance level for all participants. The duration from the start of object detection to the end of object

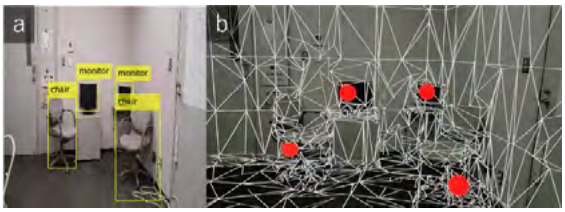

Figure 6. (a) Object detection in real space. (b) Spatial recognition and choice placement on AR space.

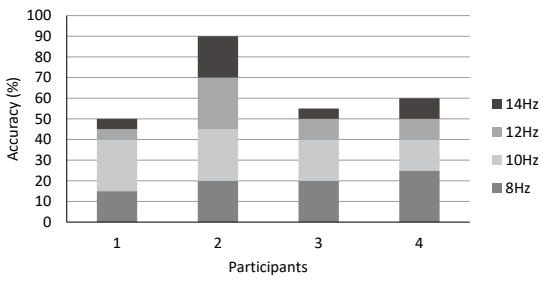

Fig7. The accuracy of each participant.

estimation was within 7 seconds.

Although the use of a see-through display reduced estimation accuracy and individual differences to some extent, the potential of BCI systems using both machine learning and environmental awareness was confirmed.

ACKNOWLEDGENEMTS

This study was supported by Watanabe Foundation. Part of this study was reported at the "43rd Annual International Conference of the IEEE Engineering in Medicine and Biology Society" held online from November 1st to 5th, 2021, "2021 Annual Conference on Electronics, Information and Systems Institute of Electrical and Engineering of Japan (IEEJ)" held online from September 15th to 17th, 2021 and IEEJ Transactions on Electronics, Information and Systems, Vol. 140, No.7, 2020.

REFERENCES

1) J. Wolpaw et al. Brain-computer interfaces for communication and control, *Clinical Neurophysiology*, Vol.113, No.6, pp.767-791 (2002).
2) K. Takano et al. Towards intelligent environments: an augmented reality–brain–machine interface operated with a see-through head-mount display, *Frontiers in neuroscience*, Vol. 5, No. 60 (2011).
3) E. Boto et al. Moving magnetoencephalography towards real-world applications with a wearable system. *Nature*, vol. 555, No. 7698, pp. 657-661 (2018).
4) F.B. Colavita. "Human sensory dominance." *Perception & Psychophysics*, Vol. 16, No. 2, pp. 409-412 (1974):
5) S. Sinnett, et al. "Visual dominance and attention: The Colavita effect revisited." *Perception & Psychophysics*, Vol. 69, No. 5, pp. 673-686, (2007).

The Subjects for the 2021 Research Grants

Here are the subjects (5 Basic Researches, 4 Application Researches, 2 Specific Researches and 1 Special Research 2021) that the 2021 Research Grants are subsidized.

Ⅰ. Basic Research

Ⅰ-1. Prevention of obesity-associated dementia with spleen-derived IL-10 induction by magnetic field
Department of Endocrinology, Metabolism, Rheumatology and Nephrology, Faculty of Medicine, Oita University／Koro Gotoh

Ⅰ-2. Measurement and evaluation of interaction between local electromagnetic field and nuclear spin by gamma photon correlation
The University of Tokyo／Kenji Shimazoe

Ⅰ-3. Investigation for improvement of reflex by the magnetic vestibular stimulation.
Graduate School of Health and Medicine, Gifu University of Medical Science／Kunihiko Tanaka
<This study was selected for OKAI Special Grant>

Ⅰ-4. Development of techniques to create novel neural circuits with magnetic stimulation
Doshisha University／Yoshito Masamizu

Ⅰ-5. Magnetic Nanoparticles for Cancer Thermotherapy and Diagnostics
Yokohama National University／Yuko Ichiyanagi

Ⅱ. Application Research

Ⅱ-1. Verification of cognitive function improvement by cognitive rehabilitation combined with repeated transcranial magnetic stimulation
Dept. of Rehabilitation Medicine, Juntendo University Graduate School of Medicine／Tomokazu Takakura

Ⅱ-2. Development of ultra-small nanocapsules as fluorine MRI contrast agent
Graduate School of Engineering, Osaka University／Masafumi Minoshima

Ⅱ-3. Magnetic stimulation therapy for focal dystonia of the upper limb using a wearable device
Fujita Health University／Kenta Fujimura

Ⅱ-4. Study for the membrane damage of intracellular organelles with magnetic nanoparticle and the release of nanoparticle from the cell
Faculty of Science and Engineering, Iwate university／Yoko Shiba

Ⅲ. Specific Research

Ⅲ-1. Role of AMPA-type glutamate receptor in gamma-band oscillatory deficits in schizophrenia
Kyushu University／Shunsuke Tamura

Ⅲ-2. Development of a novel risk stratification strategy using liver congestion assessed by magnetic resonance elastography in patients with heart failure
Department of Cardiovascular Medicine, Faculty of Medicine and Graduate School of Medicine, Hokkaido University／Toshiyuki Nagai

Ⅳ. Special Reseach Grant 2021

Ⅳ-1. Development of State-of-the-Art Neuromodulation for Treatment-Resistant Schizophrenia
Department. of Neuropsychiatry, School of Medicine, Keio University／Shinichiro Nakajima

Note: Affiliations above are at the time of the grants were subsidized.

THE REPORT OF STUDY RESULT BY SUBSIDY
助 成 研 究 成 果 報 告 書
第27回

発 行 日　令和4年9月1日
発 行 所　公益財団法人 渡邉財団
福岡県福岡市中央区天神1-13-17
TEL 092-724-3605
FAX 092-724-3690
印　　刷　三栄印刷株式会社

より明瞭なカラーデータの図表をご希望の方はサイト(https://watanabe-zaidan.or.jp/)に掲載しておりますのでご覧下さい。

この印刷物は、環境に配慮した
ベジタブルインクを使用しています。